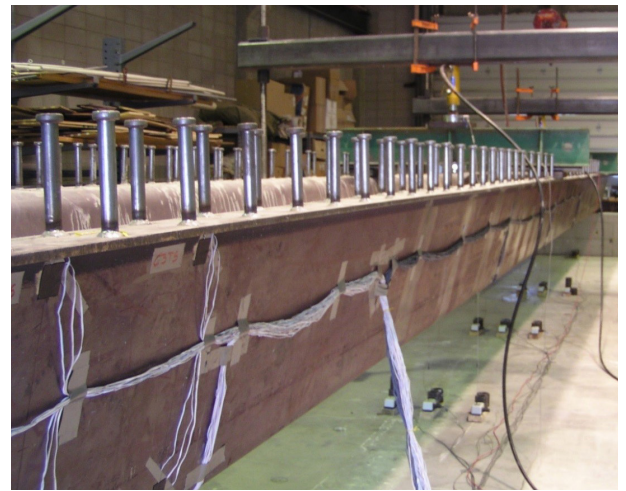


Evaluation of a Folded Plate Girder Bridge System

Final Report
June 2017



IOWA STATE UNIVERSITY
Institute for Transportation

Sponsored by

Iowa Department of Transportation
(InTrans Project 13-458)
Federal Highway Administration
Innovative Bridge Research and
Deployment (IBRD) Program

About the Bridge Engineering Center

The mission of the Bridge Engineering Center (BEC) is to conduct research on bridge technologies to help bridge designers/owners design, build, and maintain long-lasting bridges.

About the Institute for Transportation

The mission of the Institute for Transportation (InTrans) at Iowa State University is to develop and implement innovative methods, materials, and technologies for improving transportation efficiency, safety, reliability, and sustainability while improving the learning environment of students, faculty, and staff in transportation-related fields.

Disclaimer Notice

The contents of this report reflect the views of the authors, who are responsible for the facts and the accuracy of the information presented herein. The opinions, findings and conclusions expressed in this publication are those of the authors and not necessarily those of the sponsors.

The sponsors assume no liability for the contents or use of the information contained in this document. This report does not constitute a standard, specification, or regulation.

The sponsors do not endorse products or manufacturers. Trademarks or manufacturers' names appear in this report only because they are considered essential to the objective of the document.

Iowa State University Non-Discrimination Statement

Iowa State University does not discriminate on the basis of race, color, age, ethnicity, religion, national origin, pregnancy, sexual orientation, gender identity, genetic information, sex, marital status, disability, or status as a U.S. veteran. Inquiries regarding non-discrimination policies may be directed to Office of Equal Opportunity, 3410 Beardshear Hall, 515 Morrill Road, Ames, Iowa 50011, Tel. 515-294-7612, Hotline: 515-294-1222, email eooffice@iastate.edu.

Iowa Department of Transportation Statements

Federal and state laws prohibit employment and/or public accommodation discrimination on the basis of age, color, creed, disability, gender identity, national origin, pregnancy, race, religion, sex, sexual orientation or veteran's status. If you believe you have been discriminated against, please contact the Iowa Civil Rights Commission at 800-457-4416 or Iowa Department of Transportation's affirmative action officer. If you need accommodations because of a disability to access the Iowa Department of Transportation's services, contact the agency's affirmative action officer at 800-262-0003.

The preparation of this report was financed in part through funds provided by the Iowa Department of Transportation through its "Second Revised Agreement for the Management of Research Conducted by Iowa State University for the Iowa Department of Transportation" and its amendments.

The opinions, findings, and conclusions expressed in this publication are those of the authors and not necessarily those of the Iowa Department of Transportation or the U.S. Department of Transportation Federal Highway Administration.

Technical Report Documentation Page

1. Report No. InTrans Project 13-458		2. Government Accession No.		3. Recipient's Catalog No.	
4. Title and Subtitle Evaluation of a Folded Plate Girder Bridge System				5. Report Date June 2017	
				6. Performing Organization Code	
7. Author(s) Brent Phares (orcid.org/0000-0001-5894-4774), Yaohua (Jimmy) Deng (orcid.org/0000-0003-0779-6112), and Owen Steffens (orcid.org/0000-0001-9130-8489)				8. Performing Organization Report No. InTrans Project 13-458	
9. Performing Organization Name and Address Bridge Engineering Center Iowa State University 2711 South Loop Drive, Suite 4700 Ames, IA 50010-8664				10. Work Unit No. (TRAVIS)	
				11. Contract or Grant No.	
12. Sponsoring Organization Name and Address Iowa Department of Transportation 800 Lincoln Way Ames, IA 50010				13. Type of Report and Period Covered Final Report	
12. Sponsoring Organization Name and Address FHWA Innovative Bridge Research and Deployment (IBRD) Program 1200 New Jersey Avenue, SE Washington, DC 20590					
15. Supplementary Notes Visit www.intrans.iastate.edu for color pdfs of this and other research reports.					
16. Abstract <p>With the assistance of the Iowa Department of Transportation (DOT) and the Institute for Transportation (InTrans) at Iowa State University, Buchanan County, Iowa was awarded a Federal Highway Administration (FHWA) Innovative Bridge Research and Deployment (IBRD) Program grant to help construct and evaluate an innovative short-span bridge (i.e., the Amish Sawmill Bridge). The bridge was designed and constructed using folded plate tub girders.</p> <p>This bridge utilizes a folded plate girder superstructure supported on geosynthetic-reinforced soil (GRS) abutments. To evaluate the structural behavior of the bridge, the researchers conducted laboratory and field testing with the goal of validating the adequacy of the folded plate girder for short-span bridge construction.</p> <p>The research team conducted three laboratory tests on a folded plate girder specimen similar to the girders that were used on the completed bridge to study the girder's construction-stage behavior, flexural behavior, and shear behavior. The researchers conducted live load field tests immediately after completion of the bridge with the girders and one year after bridge construction to evaluate the behavior of the bridge and its components. Full-scale finite element models of the bridge were established to interpret the test results. The researchers drew the following conclusions from experimental and numerical evaluation results:</p> <ul style="list-style-type: none"> • No noticeable, unwanted deformations or strain levels were found during laboratory tests, and the strains and displacements were well predicted by the design calculations. • The girder has two webs with large associated shear capacity; thus, the shear strength of the folded plate girder when placed is not a point of concern for design considerations. • Due to the shear lag effects, the strain near the bottom corners of the bottom flanges is larger; due to the biaxial bending effects, strains in the bottom flanges vary from one side to the other. • The GRS-integrated bridge system (GRS-IBS) and abutments provide significant restraint to the girder ends. And, the end supports have restraint characteristics of an intermediate support condition, between the pinned and fixed support conditions. • American Association of State Highway and Transportation Officials (AASHTO) equations were reasonably accurate at estimating the load distribution factors (LDFs) for interior and exterior girders of the investigated folded plate girder bridge. • The folded plate girder is an effective alternative for construction of short-span bridges. 					
17. Key Words Amish Sawmill Bridge—folded plate girders—GRS-IBS and abutments—IBRD—short-span bridge superstructures				18. Distribution Statement No restrictions.	
19. Security Classification (of this report) Unclassified.		20. Security Classification (of this page) Unclassified.		21. No. of Pages 106	22. Price NA

EVALUATION OF A FOLDED PLATE GIRDER BRIDGE SYSTEM

**Final Report
June 2017**

Principal Investigator
Brent Phares, Director
Bridge Engineering Center, Iowa State University

Authors
Brent Phares, Yaohua (Jimmy) Deng, and Owen Steffens

Sponsored by
Federal Highway Administration
Innovative Bridge Research and Deployment Program and
Iowa Department of Transportation
(InTrans Project 13-458)

Preparation of this report was financed in part
through funds provided by the Iowa Department of Transportation
through its Research Management Agreement with the
Institute for Transportation

A report from
**Bridge Engineering Center and
Institute for Transportation**
Iowa State University
2711 South Loop Drive, Suite 4700
Ames, IA 50010-8664
Phone: 515-294-8103 / Fax: 515-294-0467
www.intrans.iastate.edu

TABLE OF CONTENTS

ACKNOWLEDGMENTS	xi
EXECUTIVE SUMMARY	xiii
CHAPTER 1 INTRODUCTION	1
1.1 Background.....	1
1.2 Research Objectives and Scope	1
1.3 Research Description and Report Organization.....	1
CHAPTER 2 LITERATURE REVIEW	3
2.1 Introduction.....	3
2.2 Fabrication Process	3
2.3 Previous Design Efforts for Cold-Bent Steel Bridge Girders	5
2.3.1 Prefabricated Press-Formed Steel T-Box Girder Bridge System (Taly and Gangarao 1979).....	5
2.3.2 Behavior of Composite Girders with Cold Formed Steel U Section (Nakamura 2002)	7
2.3.3 Prefabricated Composite Steel Box Girder System (Burgueño and Pavlich 2008)	8
2.3.4 Constructability Testing of Folded Plate Girders (Glaser 2010)	10
2.3.5 Folded Plate Girders and Slab Joints Used in Modular Construction (Burner 2010)	11
2.3.6 Shallow Press Brake-Formed Steel Tub Girders for Short-Span Bridges (Barth et al. 2013)	12
CHAPTER 3 LABORATORY TESTING.....	13
3.1 Introduction.....	13
3.2 Beam Properties	13
3.2.1 Assumptions.....	13
3.2.2 Section Properties: Beam Only.....	13
3.2.3 Section Properties: Beam and Deck (Composite Action).....	15
3.3 Test A – Constructability	16
3.3.1 Test Setup.....	16
3.3.2 Predicted Results.....	19
3.4 Test B – Flexure.....	20
3.4.1 Test Setup.....	20

3.4.2	Predicted Results.....	23
3.5	Test C – Shear.....	26
3.5.1	Test Setup.....	26
3.5.2	Predicted Results.....	29
3.6	Summary of Section Properties and Loading	34
CHAPTER 4	LABORATORY TEST RESULTS	36
4.1	Test A – Constructability	36
4.2	Test B – Flexure.....	40
4.3	Test C – Shear.....	46
4.3.1	Flexural Data.....	46
4.3.2	Shear Data.....	53
4.4	Laboratory Test Summary and Conclusions.....	59
CHAPTER 5	FIELD TESTING AND FINITE ELEMENT MODELING OF A FOLDED PLATE GIRDER BRIDGE	61
5.1	Bridge Description.....	62
5.2	Details of Field Tests	64
5.2.1	Instrumentation and Loading Plan.....	64
5.2.2	Preliminary Analysis of Field Test Data.....	67
5.3	Details of FE Modeling.....	69
5.4	Comparisons and Discussions of Results	72
5.4.1	Comparisons of Measured and Predicted Strain Results	72
5.4.2	Strain Distribution in Bottom Flanges	80
5.4.3	Live Load Distribution Factor	83
5.5	Field Test and Finite Element Modeling Summary and Conclusions	88
CHAPTER 6	SUMMARY AND CONCLUSIONS	89
REFERENCES	91

LIST OF FIGURES

Figure 2.1. Bending of flanges by press brake.....	3
Figure 2.2. Press brake.....	4
Figure 2.3. Plate bending process	4
Figure 2.4. Folded plate girder modules cast together with longitudinal joints	5
Figure 2.5. Press-formed steel girder with 8 ft wide steel deck for 65-ft span.....	6
Figure 2.6. Press-formed steel girder with concrete deck for 45 ft span	7
Figure 2.7. Continuous U-girder bridge system test specimens	8
Figure 2.8. Scaled Con-Struct system test girder cross-section.....	9
Figure 2.9. University of Nebraska’s folded plate girder	10
Figure 2.10. University of Nebraska’s folded plate girder with deck.....	11
Figure 2.11. Press brake-formed steel tub girder with deck	12
Figure 3.1. Press-brake tub girder without deck	14
Figure 3.2. Adapted geometry for press-brake tub girder without deck.....	14
Figure 3.3. Press-brake tub girder with deck	15
Figure 3.4. Adapted geometry for press-brake tub girder with deck	15
Figure 3.5. Test A – Constructability setup	17
Figure 3.6. Test A – Constructability load and gauge locations.....	18
Figure 3.7. Test A – Constructability predicted displacements	19
Figure 3.8. Test A – Constructability predicted strain distributions.....	20
Figure 3.9. Test B – Flexure setup.....	21
Figure 3.10. Test B – Flexure load and gauge locations.....	22
Figure 3.11. Test B – Flexure predicted elastic deflections.....	23
Figure 3.12. Test B – Flexure predicted elastic strain distributions	24
Figure 3.13. Test B – Flexure predicted HL-93 loading displacements	25
Figure 3.14. Test B – Flexure predicted HL-93 loading strain distributions.....	25
Figure 3.15. Test B – Flexure actual loading predicted displacements	26
Figure 3.16. Test B – Flexure actual loading predicted strain distributions	26
Figure 3.17. Test C – Shear setup.....	27
Figure 3.18. Test C – Shear load and gauge locations.....	28
Figure 3.19. Test C – Shear plastic stress distribution.....	29
Figure 3.20. Test C – Shear predicted elastic strain distributions	30
Figure 3.21. Test C – Shear predicted elastic deflections.....	31
Figure 3.22. Test C – Shear predicted HL-93 loading displacements	31
Figure 3.23. Test C – Shear predicted HL-93 loading strain distributions.....	32
Figure 4.1. Test A – Constructability predicted vs. measured strain distributions, dead load	36
Figure 4.2. Test A – Constructability predicted vs. measured strain distributions, two times dead load	37
Figure 4.3. Test A – Constructability location S1 load vs. displacement.....	38
Figure 4.4. Test A – Constructability location S2 load vs. displacement.....	39
Figure 4.5. Test A – Constructability location S3 load vs. displacement.....	39
Figure 4.6. Test B – Flexure predicted vs. measured strain distributions, HS-20 truck load	41
Figure 4.7. Test B – Flexure predicted vs. measured strain distributions, HS-20 truck + lane load	42
Figure 4.8. Test B – Flexure predicted vs. measured strain distributions, load = 94 kips.....	43

Figure 4.9. Test B – Flexure load vs. displacement, location S1.....	44
Figure 4.10. Test B – Flexure load vs. displacement, location S2.....	45
Figure 4.11. Test B – Flexure load vs. displacement, location S3.....	45
Figure 4.12. Test C – Shear predicted vs. measured strain distributions, HS-20 truck load	47
Figure 4.13. Test C – Shear predicted vs. measured strain distributions, HS-20 truck + lane load.....	48
Figure 4.14. Test C – Shear predicted vs. measured strain distributions, load = 98.46 kips	49
Figure 4.15. Test C – Shear predicted vs. measured strain distributions, load = 196.91 kips	50
Figure 4.16. Test C – Shear load vs. displacement, Section S1.....	51
Figure 4.17. Test C – Shear load vs. displacement, Section S2.....	52
Figure 4.18. Test C – Shear load vs. displacement, Section S3.....	52
Figure 4.19. Test C – Shear load vs. support displacement.....	53
Figure 4.20. Test C – Shear load vs. shear strain, Section C1 top.....	54
Figure 4.21. Test C – Shear load vs. shear strain, Section C2 top.....	55
Figure 4.22. Test C – Shear load vs. shear strain, Section C3 top.....	55
Figure 4.23. Test C – Shear load vs. shear strain, Section C1 bottom.....	56
Figure 4.24. Test C – Shear load vs. shear strain, Section C2 bottom.....	57
Figure 4.25. Test C – Shear load vs. shear strain, Section C3 bottom.....	57
Figure 4.26. Calculated principal stresses from strain rosettes on the north side of Section C3.....	58
Figure 4.27. Deck failure	59
Figure 5.1. Location of Amish Sawmill Bridge on Dillon Avenue south of 135th Street in Buchanan County, Iowa.....	61
Figure 5.2. Cross-section view of Buchanan County folded plate girder bridge.....	62
Figure 5.3. Details of GRS-IBS and abutment	63
Figure 5.4. Strain gauges installed on the bridge – Test I.....	64
Figure 5.5. Strain gauges installed on the bridge – Test II	65
Figure 5.6. Load paths on the bridge	66
Figure 5.7. Dump truck configurations.....	66
Figure 5.8. Strain response in girder bottom flanges for Load Path 1	67
Figure 5.9. Strain response in girder top flanges for Load Path 1	68
Figure 5.10. Peak strains in girder bottom flanges from all gauges at mid-span for three load paths – Test I.....	69
Figure 5.11. Full model of the bridge	70
Figure 5.12. Comparisons of strain response in girder bottom flanges at mid-span for Load Path 1 of Test I - simply supported condition.....	73
Figure 5.13. Comparisons of strain response in girder bottom flanges at mid-span for Load Path 1 of Test I – fixed support condition.....	74
Figure 5.14. Comparisons of strain response in girder bottom flanges at mid-span for Load Path 2 of Test I – fixed support condition.....	75
Figure 5.15. Comparisons of strain response in girder bottom flanges at mid-span for Load Path 3 of Test I – fixed support condition.....	76
Figure 5.16. Comparisons of peak strains in girder bottom flanges at mid-span for three load paths of Test I – fixed support condition	77
Figure 5.17. Measured strain response in girder bottom flanges at abutment for Load Path 2 of Test II.....	78

Figure 5.18. Comparisons of peak strains in girder bottom flanges at mid-span for three load paths of Test II	79
Figure 5.19. Comparisons of peak strains in girder bottom flanges at abutment for three load paths of Test II	80
Figure 5.20. Comparisons of strain response in girder bottom flanges of Test I for Load Paths 1 and 2	81
Figure 5.21. Comparisons of moment LDFs based on test and FE results – Test I.....	85
Figure 5.22. Comparisons of moment LDFs based on test and FE strain results – Test II	86
Figure 5.23. Comparisons of calculated moment LDFs with those per AASHTO equations – Test I	87
Figure 5.24. Comparisons of calculated moment LDFs with those per AASHTO equations – Test II	87

LIST OF TABLES

Table 2.1. Selection criteria and importance factors.....	9
Table 3.1. Test C – Shear predicted elastic shear values for locations C1, C2, and C3	33
Table 3.2. Test C – Shear loading (HL-93) predicted shear values for locations C1, C2, and C3	34
Table 3.3. Section properties	34
Table 3.4. Summary of loading.....	35
Table 4.1. Test A – Constructability predicted and measured strain distribution values, dead load, folded plate girder.....	37
Table 4.2. Test A – Constructability predicted and measured strain distribution values, two times dead load, folded plate girder.....	38
Table 4.3. Test B – Flexure predicted and measured strain distribution values, HS-20 truck load.....	41
Table 4.4. Test B – Flexure predicted and measured strain distribution values, HS-20 truck + lane load.....	42
Table 4.5. Test B – Flexure predicted and measured strain distribution values, load = 94 kips.....	43
Table 4.6. Test C – Shear predicted and measured strain distribution values, HS-20 truck load.....	47
Table 4.7. Test C – Shear predicted and measured strain distribution values, HS-20 truck + lane load.....	48
Table 4.8. Test C – Shear predicted and measured strain distribution values, load = 98.46 kips.....	49
Table 4.9. Test C – Shear predicted and measured strain distribution values, load = 196.91 kips.....	50
Table 5.1. Truck and axle weights	67
Table 5.2. Forces and moments in bridge and girders at mid-span – Load Path 1	82
Table 5.3. Forces and moments in girders at mid-span in Y and Z coordinate directions – Load Path 1	82
Table 5.4. Forces and moments in bridge and girders at mid-span – Load Path 2	83
Table 5.5. Transformed section properties of folded plate girders of the tested bridge	84

ACKNOWLEDGMENTS

The research team would like to acknowledge the Federal Highway Administration (FHWA) for partially funding this project through its Innovative Bridge Research and Deployment (IBRD) Program and the Iowa Department of Transportation (DOT) for sponsoring this project.

We would also like to thank Doug Wood for the use of the Iowa State University Structures Laboratory and Jim Buban, Jason Malecha, and Yang Yang for their assistance with fabrication and removal of the folded plate girder specimen.

EXECUTIVE SUMMARY

With the assistance of the Iowa Department of Transportation (DOT) and the Institute for Transportation (InTrans) at Iowa State University, Buchanan County, Iowa was awarded a grant to help construct and evaluate an innovative short-span bridge. This bridge utilizes a folded plate girder superstructure supported on geosynthetic-reinforced soil (GRS) abutments.

The fabrication of a composite folded plate girder module starts with a single steel plate of the desired thickness. The plate is then cold formed into a U shape with a press brake, with each bend occurring along the plate's longitudinal axis. After the bending process is complete, diaphragms are welded at the locations specified by the engineer, and shear studs are also welded along both sides of the girder's top flanges. The steel portions of the girders are either shipped to the field or to a precast plant to have a concrete deck cast on them.

To evaluate the structural behavior of the folded plate girder, the researchers conducted three laboratory tests on a folded plate girder specimen similar to the girders that were used on the completed bridge constructed in Buchanan County.

For the first test (Test A – Constructability), the research team tested a single folded plate girder under two-point bending to assess the behavior of the folded plate girder during construction prior to acting compositely with the deck. The girder was tested up to a moment that was equal to a moment that would be created by two times the girder's own self-weight.

For the second test (Test B – Flexure), a concrete deck was cast on the folded plate girder that was used to perform Test A. The researchers then tested the specimen under two-point bending to determine the composite flexural behavior of the folded plate girder system in the elastic region.

For the last test (Test C – Shear), the researchers tested the same folded plate girder with the cast-in-place composite deck from Test B by loading the girder with two line loads located close to one of the supports. This test was completed to study the shear behavior of the folded plate girder system and its ultimate capacity.

Laboratory testing results were as follows:

- For Test A, no noticeable, unwanted deformations or strain levels were found, and the strains and displacements were well predicted by the design calculations.
- For Test B, at the loads comparable to the design truck (HS-20) and the design truck (HS-20) plus lane load, no noticeable, unwanted deformations or strain levels were found, and strains and displacements were similar to the predictions from the design calculations.

- For Test C, the bent plate girder performed similarly to that of Test B in respect to predictions. In terms of the shear data, all the shear strain data were much lower than predicted for the yield load. Due to the boundary conditions (the load points were relatively farther away from the support), the beam ultimately failed in flexure with the deck concrete crushing, which was consistent with the results using hand calculations. Given this girder has two webs, and thus a large shear capacity, the shear strength of the folded plate girder when placed is not a point of concern for design considerations.

The researchers conducted live load field tests immediately after completion of the bridge and about one year after bridge construction to evaluate the behavior of the bridge and its components. Full bridge finite element (FE) models were established to interpret the test results and further study the behavior of the bridge under the tested loading conditions.

The researchers drew the following conclusions based on the field measured data and the predictions using the FE models:

- Due to the shear lag effects, the strain near the bottom corners of the bottom flanges is larger; due to biaxial bending effects, strains in the bottom flanges vary from one side to the other.
- The GRS-integrated bridge system (GRS-IBS) and abutments provide significant restraint to the girder ends. And, the end supports have restraint characteristics of an intermediate support condition, between the pinned and fixed support conditions.
- The strong-axis bending moment is the major contributor to the stress/strain in the girders. The weak-axis bending moment, which is small in the bridge but large in individual girders, causes a linear change in strains in the bottom flanges.
- Due to the biaxial bending moments in the folded plate girders, it is feasible to use the strain in the center of the bottom flanges to calculate live load distribution factors (LDFs).
- American Association of State Highway and Transportation Officials (AASHTO) equations were reasonably accurate at estimating the LDFs for interior and exterior girders of the folded plate girder bridge.

In summary, based on the laboratory and field test results and FE simulation results, the researchers concluded that the folded plate girder is an effective alternative for construction of short-span bridges that are designed based on the AASHTO LRFD specifications for bridges.

CHAPTER 1 INTRODUCTION

1.1 Background

Bridge owners and engineers focusing on bridge design, management, and maintenance continue to search for more efficient ways to design, construct, and maintain their bridge inventory. In the past, steel bridges, which are one of the most common types, have been comprised of superstructures consisting of either rolled steel beams or welded steel girders.

Recently, a relatively new concept has been promoted as a cost-effective alternative. This concept consists of what is known as a folded plate girder. The folded plate girder starts as a single sheet of plate steel that is strategically bent into a structural shape. These folded plate girders offer the potential to be cost-effective due to the relatively low cost of plate steel.

With the assistance of the Iowa Department of Transportation (DOT) and the Institute for Transportation (InTrans) at Iowa State University, Buchanan County, Iowa was awarded a grant to construct and evaluate an innovative short-span bridge. This bridge utilizes a folded plate girder superstructure supported on geosynthetic-reinforced soil (GRS) abutments. Partial funding for this project was obtained through the Innovative Bridge Research and Deployment (IBRD) Program sponsored by the Federal Highway Administration (FHWA). The work summarized in this report constitutes the evaluation of the bridge design.

1.2 Research Objectives and Scope

The objective of this research was to validate the adequacy of the folded plate girder system for short-span bridge construction. To help achieve this goal, a bridge was designed and constructed using folded plate tub girders on the secondary road system in Buchanan County.

The researchers conducted laboratory tests on a folded plate girder specimen to study its construction-stage behavior, flexural behavior, and shear behavior. They conducted live load field tests immediately after completion of the bridge and one year after bridge construction to evaluate the actual bridge behavior. Full-scale finite element (FE) models of the bridge were established to interpret the test results and further understand the bridge behavior under live loads.

1.3 Research Description and Report Organization

This final report consists of five additional chapters with a References list at the end of it.

Literature Review (Chapter 2)

This research included a literature search and review to investigate other work related to development, details, and performance evaluation of existing folded plated girder systems.

Laboratory Testing (Chapters 3 and 4)

The laboratory testing consisted of three separate tests performed on a single folded plate girder.

Test A – Constructability

To examine how the folded plate girder system behaves when being transported and erected and prior to attaining full composite action with the concrete deck, the researchers tested a single girder in the laboratory under two-point, flexural loading. To minimize the chances of damaging the girder, testing was limited to inducing moments in the girder not to exceed two times those produced by the beam's self-weight (to simulate impact-type loadings). The researchers installed instrumentation to monitor the global and local behaviors of the girder.

Test B – Flexural Capacity

To evaluate the flexural behavior and ultimate flexural capacity of the composite girder, the researchers tested the single girder, with a concrete deck placed on it, under two-point loading until the non-linear behavior was observed. This testing was useful in better understanding how the composite girder behaves up to the lower bounds of design limits.

Test C – Shear Capacity

For the shear behavior and ultimate shear capacity of the composite girder, the researchers tested the single girder plus concrete deck under a single-point load (load located near one beam end) until the ultimate capacity was reached. This testing was valuable in understanding how the composite girder behaves up to the upper bounds of design limits.

Field Testing (Chapter 5)

When bridge construction was completed, the researchers conducted a field live load test to evaluate the structural performance of the bridge. They conducted a similar follow-up load test about a year after construction.

Summary and Conclusions (Chapter 6)

The work completed during this project is summarized and concluded in Chapter 6.

CHAPTER 2 LITERATURE REVIEW

2.1 Introduction

The purpose of this chapter is to familiarize the reader with the fabrication process and previous design efforts for press-brake girders (also referred to as folded plate girders). The beginning of this chapter introduces the equipment used for fabrication and lead the reader through the fabrication process of a folded plate girder. The second part of this chapter will introduce the reader to some of the previous design efforts and testing done on folded plate girders.

2.2 Fabrication Process

The fabrication of a composite folded plate girder module starts with a single steel plate of the desired thickness. The plate is then cold formed with a press brake, with each bend occurring along the plate's longitudinal axis. A press brake generally consists of a large upper beam with a U-shaped tool attached to the bottom of it and a long steel table. The tool and beam are pushed with two hydraulic pistons into an opening in the long steel table (see Figure 2.1).



Courtesy of Dan Snyder, Steel Market Development Institute

Figure 2.1. Bending of flanges by press brake

This type of bending is called air bending, which is a process that uses three-point bending to achieve the desired bend angle. The angle of the bend is determined by how far the U-shaped tool is pushed into the opening in the table. The possible maximum length of the girder to be formed is dependent on the size of press brake available (see Figure 2.2).



Courtesy of Dan Snyder, Steel Market Development Institute

Figure 2.2. Press brake

The bending sequence of the folded plate girder that was tested for this project is shown in Figure 2.3.

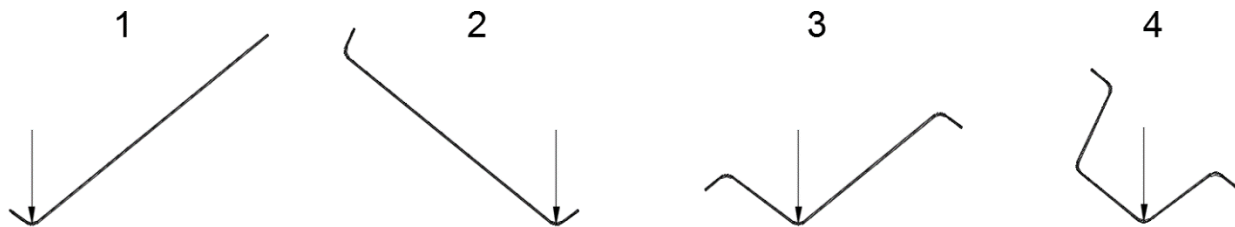
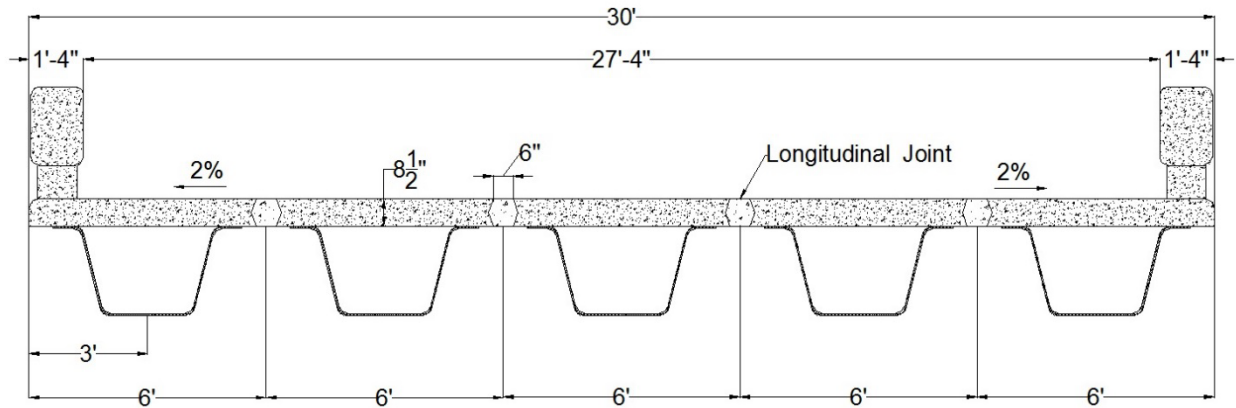


Figure 2.3. Plate bending process

After the bending process is complete, diaphragms are welded at the locations specified by the engineer, and shear studs are also welded along both sides of the girder's top flanges. The steel portions of the girders can now be either shipped to the field or to a precast plant to have a concrete deck cast on them. For an accelerated bridge construction system, these composite folded plate girder modules can be placed side by side and have the longitudinal joints between adjacent beams cast to allow for transverse load distribution between girders (see Figure 2.4).



Adapted from Buchanan County preliminary alternative plans

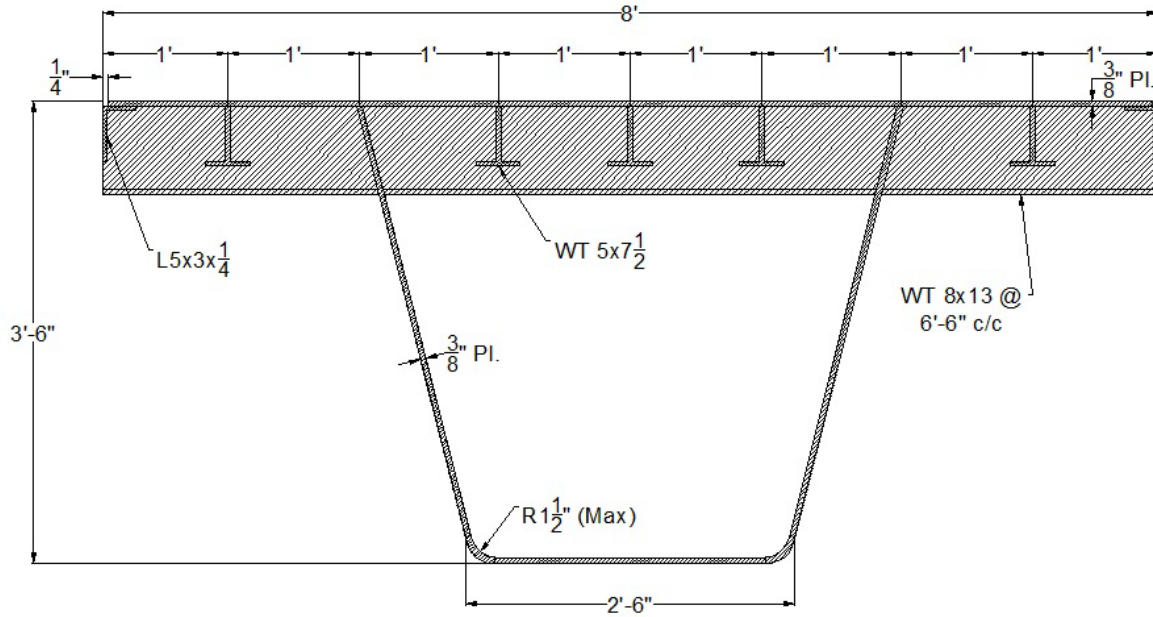
Figure 2.4. Folded plate girder modules cast together with longitudinal joints

2.3 Previous Design Efforts for Cold-Bent Steel Bridge Girders

From the early proposed design of a short-span bridge using press-formed U sections with a concrete deck from Taly and Gangarao in 1979 to the more recent efforts of Barth et al. 2013, it can be seen that press-formed girders may be becoming a viable alternative for short-span bridges. Summaries of previous design efforts follow.

2.3.1 Prefabricated Press-Formed Steel T-Box Girder Bridge System (Taly and Gangarao 1979)

In work by Taly and Gangarao (1979), two bridge systems were proposed for HS20-44 loading for spans up to 65 ft. These were only proposed designs, and no information on one being fabricated or tested was presented. The first design was composed of an entirely steel superstructure (see Figure 2.5).

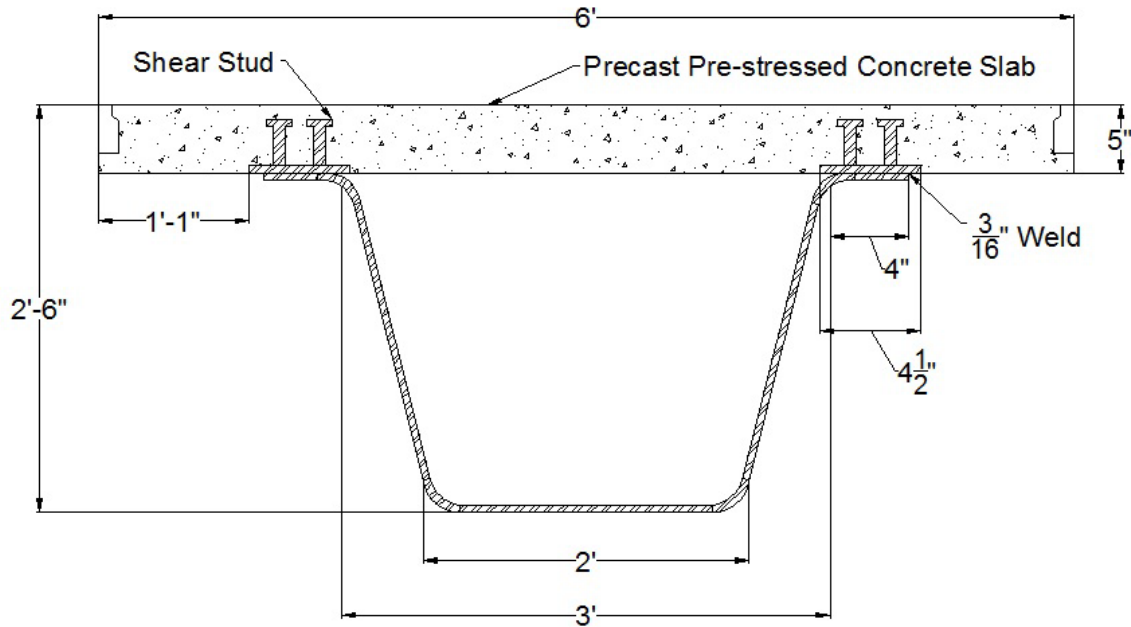


Adapted from Taly and Gangarao 1979

Figure 2.5. Press-formed steel girder with 8 ft wide steel deck for 65-ft span

The girder consisted of a trapezoidal U section press-formed from a 3/8 in. thick A36 steel plate and an entirely steel deck. The deck was comprised of a 3/8 in. steel plate and a system of WT sections welded parallel and perpendicular to the beam to increase the stiffness of the deck plate. Bearing stiffeners were provided in the U section and the ends of the girder were entirely enclosed by a steel plate diaphragm.

The alternative system that was proposed was to retain the press-formed U section, but use precast, pre-stressed panels instead of an entirely steel deck (see Figure 2.6).



Taly and Gangarao 1979

Figure 2.6. Press-formed steel girder with concrete deck for 45 ft span

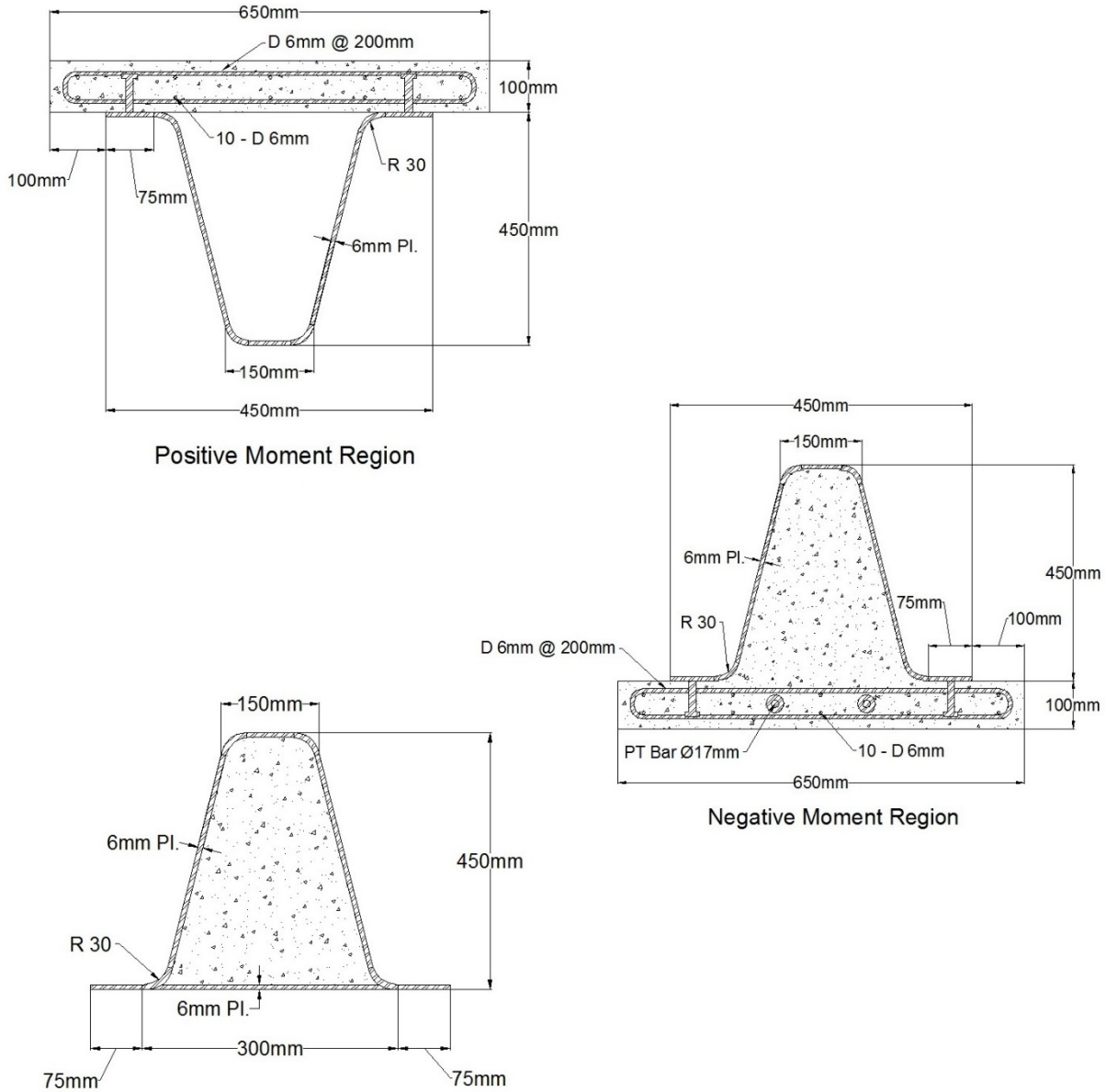
The precast, pre-stressed panels would be 5 in. thick and have a studded plate embedded in them that would be shop-welded to the steel U section. The welding of the embedded plates to the steel U section would allow the deck and U section to act compositely. It was also stated that, due to the higher torsional stiffness of a closed section, the lateral distribution of the live load is more favorable than with the traditional bridge system.

2.3.2 Behavior of Composite Girders with Cold Formed Steel U Section (Nakamura 2002)

Work by Nakamura (2002) proposed a bridge system composed of continuous U girders and a reinforced concrete slab. The top flange of the U section attached to the concrete slab with studs, which allowed the U section and deck to act compositely. The studs also restrained the top flange, which was in compression, from local buckling.

At intermediate supports, where there is a negative bending moment, the entire U section was filled with concrete to prevent the bottom flange from buckling due to the compressive forces in the flange. The deck of the girder was also post-tensioned in these locations to resist tensile forces and prevent cracking.

Testing was conducted on three different one-quarter-sized specimens to determine the bending behavior of the composite girder in both the positive and negative bending moment regions (see Figure 2.7).



Negative Moment Region Buckling Test

Adapted from Nakamura 2002

Figure 2.7. Continuous U-girder bridge system test specimens

The tests found that the girder and deck acted compositely in the positive moment regions, the girder behaved as a post-tensioned beam in the negative moment regions, and the filled concrete region restrained the local buckling of the bottom flange of the girder.

2.3.3 Prefabricated Composite Steel Box Girder System (Burgueño and Pavlich 2008)

Burgueño and Pavlich’s study (2008) focused on the idea of a prefabricated box girder bridge system post-tensioned together transversely. One part of the study was to identify the best configuration for a composite steel, box girder system.

The concrete deck, box girder, and longitudinal deck connection design were the three main components examined. Several designs for each component were ranked on selected criteria. These criteria had designated importance factors determined by the research team (see Table 2.1).

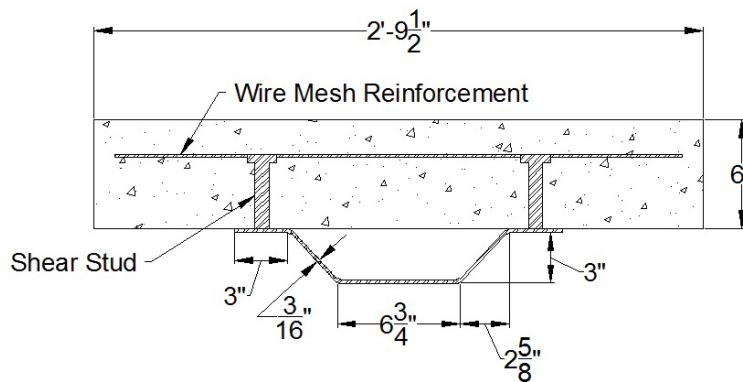
Table 2.1. Selection criteria and importance factors

Criteria ID	Description	Importance Factor
A	Cost efficiency	3
B	Structural efficiency	2
C	Design versatility	1
D	Design/analysis ease	1
E	Construction ease	3
F	Fatigue performance	3
G	Durability and corrosion resistance	3
H	Replacement/removal ease	2

Importance Factor: 1 = Low, 2 = Medium, 3 = High
 Adapted from Burgueño and Pavlich 2008

The study found that the best configuration for a box girder system would have either an unstressed or pre-stressed press-formed steel girder section with a concrete deck that was cast in place at the shop or yard. The best transverse deck connection type for the configuration was a grouted female-to-female shear key.

A three-point bending test was also done on a 12 ft long cold bend girder (see Figure 2.8).



Adapted from Burgueño and Pavlich 2008

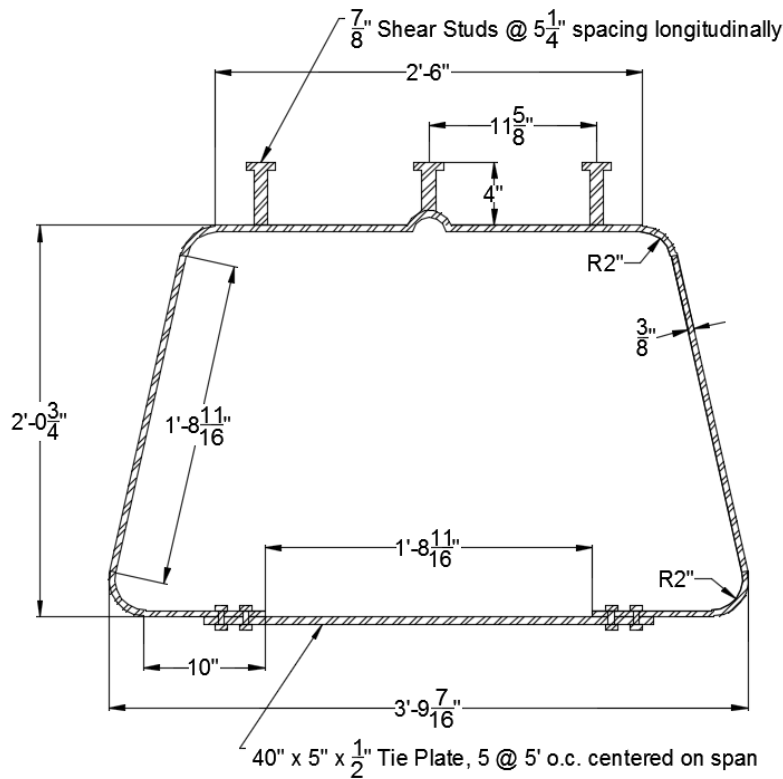
Figure 2.8. Scaled Con-Struct system test girder cross-section

This girder was a scaled down model of Nelson Engineering Services' Con-Struct composite box girder system. The data collected were then compared to an FE model. Most of the study focused on very detailed FE modeling of longitudinal joint connections and load distribution.

The researchers found that the simplified analysis method presented in the AASHTO LRFD specifications for bridges was generally applicable for the analysis of the prefabricated box girder bridges studied, although, when determining load distribution factors (LDFs), the method was found to be lacking due to the geometry of the girder. All in all, this study showed that prefabricated composite box girder units connected with longitudinal deck joints are a viable option for accelerated bridge construction.

2.3.4 Constructability Testing of Folded Plate Girders (Glaser 2010)

The folded plate girder used in Glaser's study (2010) was similar to the previous designs, but with a different shape (see Figure 2.9).



Adapted from Glaser 2010

Figure 2.9. University of Nebraska's folded plate girder

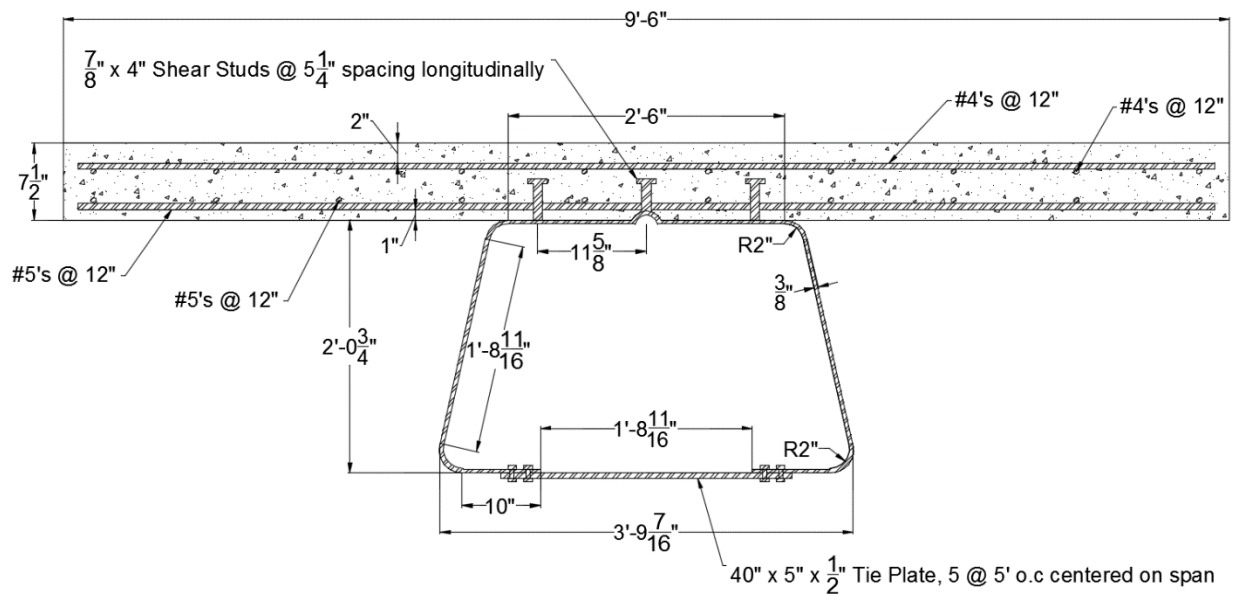
The open bottom of this design makes inspection much quicker and easier than that of traditional box girders. The girders have tie plates across the opening between their bottom flanges to prevent the flanges from separating. The girders were tested in two-point bending over a 41-ft simply supported span. The testing completed by Glaser was limited to constructability testing.

Under moments equivalent to those experienced during construction, no undesirable deformations were seen or measured.

The testing confirmed that the tie plates were required for preventing flange separation at construction load levels. It was also observed that the top flange experiences the highest stresses during construction. Buckling in the top flange was seen even at elastic load levels, although this was at a loading above that of constructability loads. Glaser went on to state that, if the beam and a deck were to be tested compositely together, the stresses in the top flange of the beam should be much lower in comparison to the beam acting alone. This is due to the neutral axis shifting closer to the top flange of the beam.

2.3.5 *Folded Plate Girders and Slab Joints Used in Modular Construction (Burner 2010)*

The basic girder evaluated by Glaser (2010) and shown in Figure 2.10 was tested under 219 million fatigue cycles to evaluate the Nebraska folded plate girder's ability to withstand 75 years of live loads by Burner (2010).



Adapted from Burner 2010

Figure 2.10. University of Nebraska's folded plate girder with deck

The number of cycles determined for a 75-year bridge life was 219 million. After completing the testing cycles, no damage was seen, and it was determined that the folded plate girder system can withstand the equivalent of a 75-year bridge life without a significant loss in stiffness.

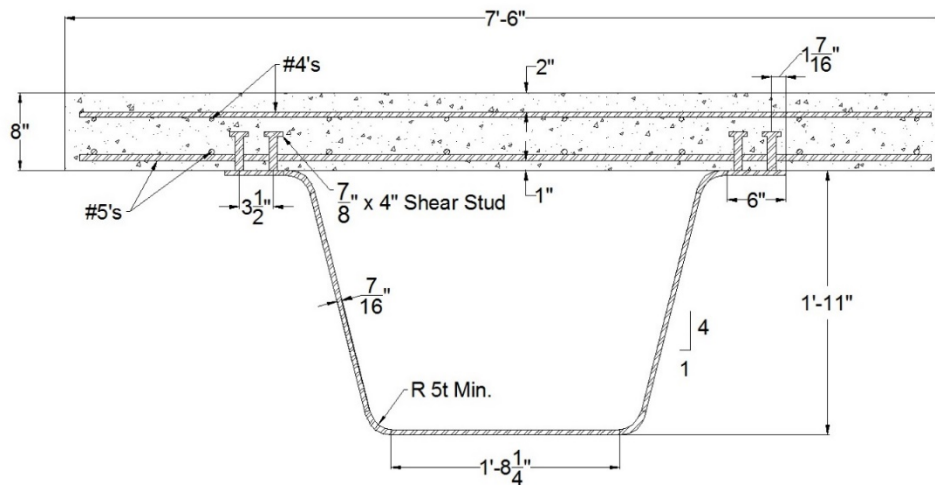
Proposed longitudinal joint connections between folded plate girders were also included in Burner's research. The original design for the longitudinal joints relied on headed reinforcing steel bars in the joint between girders. The proposed design uses a hooked reinforcing steel bar

detail that aims to increase clear cover and reduce the cost of fabrication and shipment of the reinforcing steel bar.

Six specimens were tested for both negative and positive bending to investigate behavior and failure modes. After testing, the study found that using the hooked reinforcing steel bar detail was a viable alternative to the more costly headed reinforcing steel bar detail.

2.3.6 Shallow Press Brake-Formed Steel Tub Girders for Short-Span Bridges (Barth et al. 2013)

Initially, in the Barth et al. study (2013), an optimal folded plate girder section needed to be determined. To determine the optimum girder configuration, a design study was performed and the optimum section was determined to be an 84 in. \times 7/16 in. plate with top flange widths of 6 in. and a girder depth a 23 in. (see Figure 2.11).



Adapted from Barth et al. 2013

Figure 2.11. Press brake-formed steel tub girder with deck

After this was determined, a specimen was fabricated and tested for one-point bending with a span of 34.5 ft. Two separate analytical tools were used to determine two sets of predicted results for the tub girder system. The test data collected were then compared to the two different sets of predicted results. The researchers found that both analytical tools agreed closely with the test results and that they could be used for further analysis of the folded girder system.

CHAPTER 3 LABORATORY TESTING

3.1 Introduction

This chapter summarizes the laboratory testing that was employed for the folded plate tub girder. Three basic laboratory tests were completed. The first was called Test A – Constructability, where a single girder was tested under two-point bending to determine how the folded plate girder would behave during construction, prior to acting compositely with the deck. The second was called Test B – Flexibility, where the same girder from Test A with a concrete deck acting compositely were tested under two-point bending to determine the composite flexural behavior of the folded plate girder system in the elastic behavior region. The third was called Test C – Shear, where the same folded plate girder with the deck from Test B was tested to failure to determine the shear behavior of the folded plate girder system and its ultimate shear capacity. Where applicable, predicted responses were compared to measured responses.

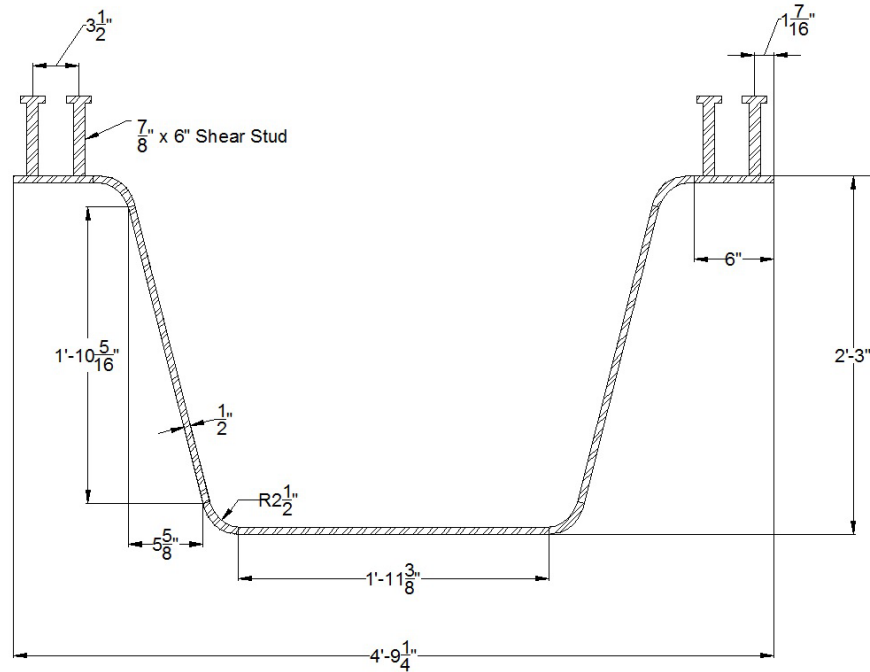
3.2 Beam Properties

3.2.1 Assumptions

Several assumptions were made throughout this research, such as there being no residual strains in the girder prior to testing, aside from those due to the girder's own self-weight. The girder was also expected to be straight and have a constant cross-section along its length. In addition, it was assumed that there were no torsional or axial loads present and that the beam was only under longitudinal bending. The assumption that plane sections remain plane during elastic loading was also maintained.

3.2.2 Section Properties: Beam Only

To estimate the moment of inertia and the centroid location, the original beam geometry (see Figure 3.1) was altered slightly for ease of calculation.



Adapted from Buchanan County plans

Figure 3.1. Press-brake tub girder without deck

For calculating the section properties of the beam, the bend radii in the original beam geometry were changed to corners (see Figure 3.2).

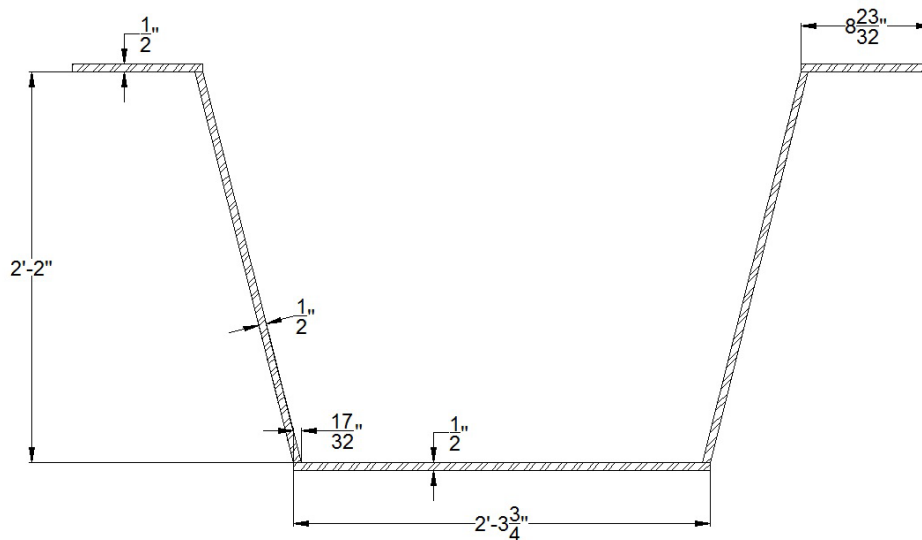


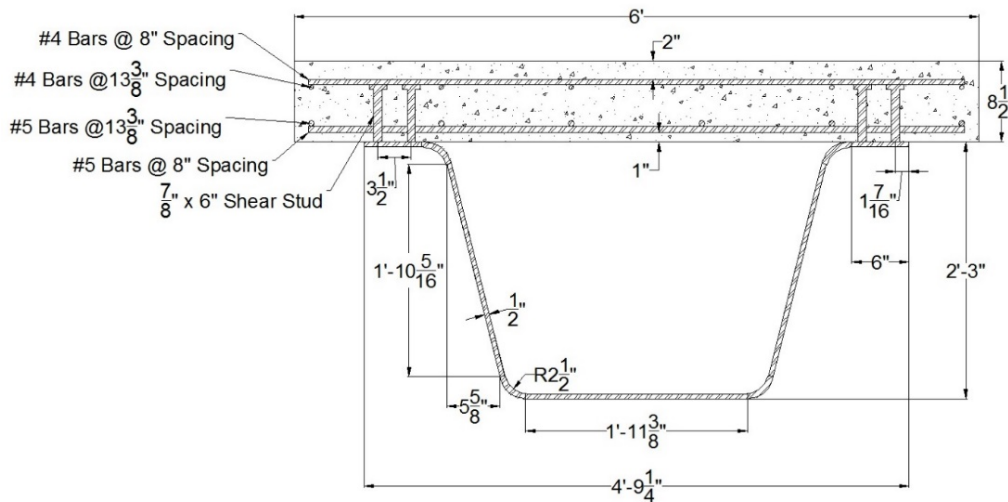
Figure 3.2. Adapted geometry for press-brake tub girder without deck

Doing this changes the section properties slightly from the original geometry, but should only have a small influence on predicting and analyzing the response. The value calculated for the

centroid's distance (for the beam only) from the bottom of the beam (Y) was found to be 12.14 in., and the moment of inertia (I) calculated for the beam was 5,430 in.⁴.

3.2.3 Section Properties: Beam and Deck (Composite Action)

The moment of inertia (I) and the centroidal distance from the bottom of the specimen (Y) were also needed for predicting and analyzing the elastic flexural response of the composite tub girder. The original beam geometry is shown in Figure 3.3, with the adapted geometry used for calculating section properties shown in Figure 3.4.



Adapted from Buchanan County

Figure 3.3. Press-brake tub girder with deck

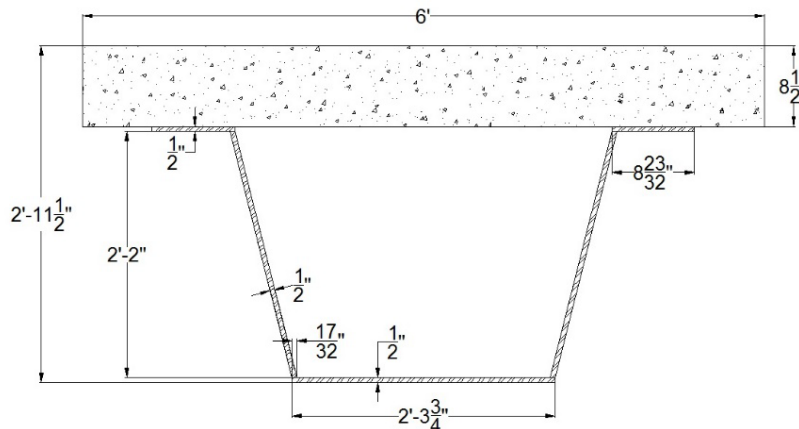


Figure 3.4. Adapted geometry for press-brake tub girder with deck

Transformed section properties were used in which the concrete deck was transformed into an equivalent steel area by reducing its width (with this reduction not shown in Figure 3.4) by the ratio of the modulus of elasticity for the steel to the modulus of elasticity for the concrete. The

modulus of elasticity used for the steel was 29,000 ksi and the modulus of elasticity used for the concrete was 4,463 ksi.

The modulus of elasticity for the concrete was calculated using Equation 3.1 (AASHTO 2012) with a 28-day strength of 6,000 psi, which was determined from compressive tests on cylinders.

$$Ec = 33,000 \times 0.145^{1.5} \times \sqrt{f'_c} \quad (3.1)$$

where, f'_c is the 28-day compressive strength of concrete in ksi.

Again, the original beam geometry (see Figure 3.3) was altered slightly for ease of calculation. For calculating the section properties of the beam, the bend radii in the original beam geometry were changed to corners and the reinforcing steel in the deck was neglected (see Figure 3.4). Doing this changes the section properties slightly from the original geometry, but should only have a small influence on predicting and analyzing the response. The value calculated for the centroid's distance (for the beam and deck) from the bottom of the specimen (Y) was found to be 24.6 in., and the moment of inertia (I) calculated for the beam was 17,959 in.⁴

The first moment (Q), the thickness of the beam (t), and the moment of inertia (I) were the three section properties needed to predict and analyze the elastic shear response of the composite tub girder. The first moment (Q) and the thickness of the beam (t) were needed at two predetermined locations, where strain rosettes were attached to the beam. One set of these strain rosettes was located 3 in. up from the bottom of the girder, where the girder had a thickness (t) of 1.06 in. (twice the plate thickness given there are two webs at an angle) and a first moment (Q) of 368.20 in.³. The other set of strain rosettes was located close to the neutral axis of the composite tub girder, where the shear stress would be the highest. This location of the strain rosettes was 23.75 in. from the bottom of the beam, which is not quite at the neutral axis of the composite section, so the predicted and measured shear values will be slightly lower than the maximum shear values that the beam actually experienced. The first moment (Q) and the thickness of the beam (t) at this set of strain gauges were 646.15 in.³ and 1.06 in., respectively. The moment of inertia (I) that used for the shear response was the same as previously used in the flexural response for composite action.

3.3 Test A – Constructability

3.3.1 Test Setup

A single girder was tested under two-point bending to determine how the folded plate girder would behave during construction prior to acting compositely with the deck. The girder was tested up to a load of 6.36 kips at each load location, which induced a moment in the beam of 117.74 kip-ft at mid-span. This moment is equal to a moment that would be created by two times the girder's own self-weight (348.32 lb/ft).

Uniaxial strain gauges were attached to the beam in several locations to determine how the folded plate girder was behaving in flexure. Instrumentation to measure displacements was also attached at several locations to determine the girder's overall behavior. The instrumentation and loading setup are shown in Figure 3.5 and Figure 3.6.



Figure 3.5. Test A – Constructability setup

Gauge location S4 (shown in Figure 3.6) was added after preliminary testing showed that strain concentrations due to the center diaphragm caused strain measurements at location S2 to misrepresent the beam's global flexural behavior.

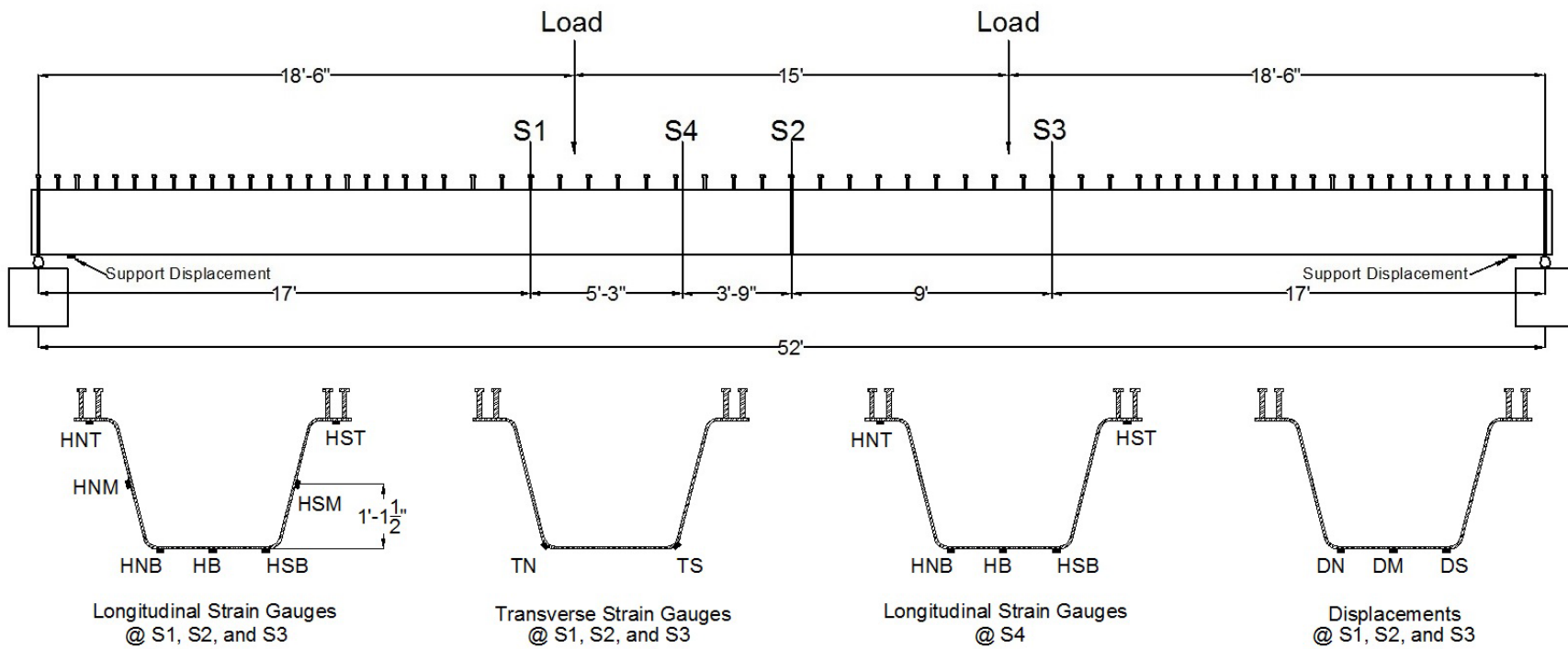


Figure 3.6. Test A – Constructability load and gauge locations

3.3.2 Predicted Results

Knowing the support and loading conditions, the magnitude of moments at gauge locations S1, S2, S3, and S4 can be predicted. The previously calculated section properties of the beam were used to determine what the deflections, stresses, and strains at these locations could be.

Equations 3.2 and 3.3 (AISC 2005) were used to determine the girder's deflections at locations S1, S2, and S3 (see Figure 3.7).

$$\Delta S2 = \frac{P \times 222}{24EI} \times 970992 \quad (3.2)$$

where, $\Delta S2$ is the deflection at location S2, P is the load at each of the two load locations, E is the modulus of elasticity, and I is the moment of inertia.

$$\Delta S1, \Delta S3 = \frac{P \times 204}{6EI} \times 226116 \quad (3.3)$$

where, $\Delta S1, \Delta S3$ is the deflection at locations S1 and S3, P is the load at each of the two load locations, E is the modulus of elasticity, and I is the moment of inertia.

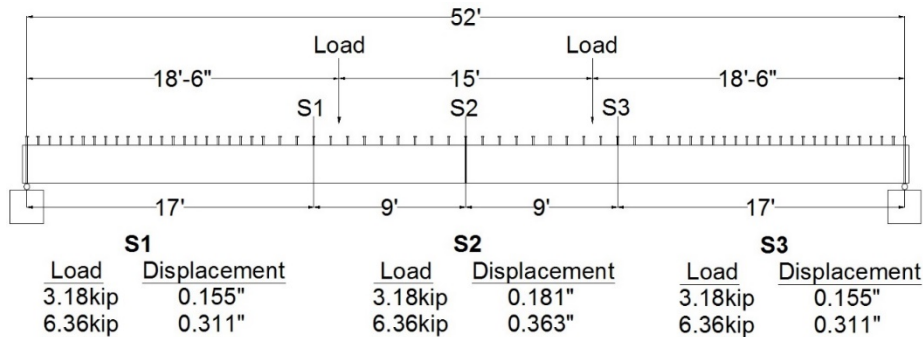


Figure 3.7. Test A – Constructability predicted displacements

The elastic flexural formula in Equation 3.4 (Riley 2007) can be used to determine stress values at a distance (c) from the neutral axis, as long as strains remain linear elastic.

$$\sigma = \frac{Mc}{I} \quad (3.4)$$

where, σ is the stress, M is the moment, c is the distance from the neutral axis, and I is the moment of inertia.

Hooke's law in Equation 3.5 (Riley 2007) can then be used to convert the stress values to strain values, which will then be compared to measured strain values.

$$\varepsilon = \frac{\sigma}{E} \quad (3.5)$$

where, ϵ is the strain, σ is the stress, and E is the modulus of elasticity (assumed as 29,000 ksi).

Predicted strain distributions for loading are shown in Figure 3.8.

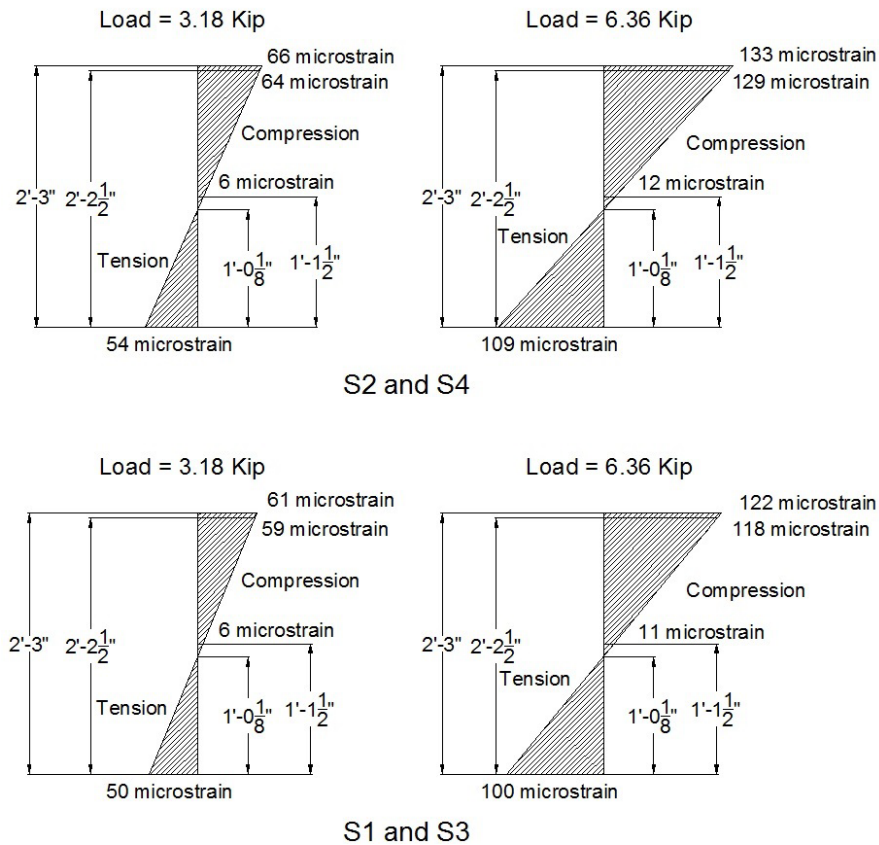


Figure 3.8. Test A – Constructability predicted strain distributions

3.4 Test B – Flexure

3.4.1 Test Setup

A concrete deck was cast on the folded plate girder used to perform Test A. The specimen was then tested under two-point bending to determine the composite flexural behavior of the folded plate girder system in the elastic region. The girder was tested up to, but not beyond, a load that created non-linear behavior. The calculated load per actuator required to create non-linear behavior with the support and loading conditions was 149.59 kips and created a moment in the composite tub girder of 2,767.49 kip-ft.

Uniaxial strain gauges were attached to the beam in several locations to determine how the folded plate girder was behaving in flexure. Instrumentation to measure displacements was also attached in several locations to determine the girder's overall behavior. The instrumentation and loading setup are shown in Figure 3.9 and Figure 3.10.

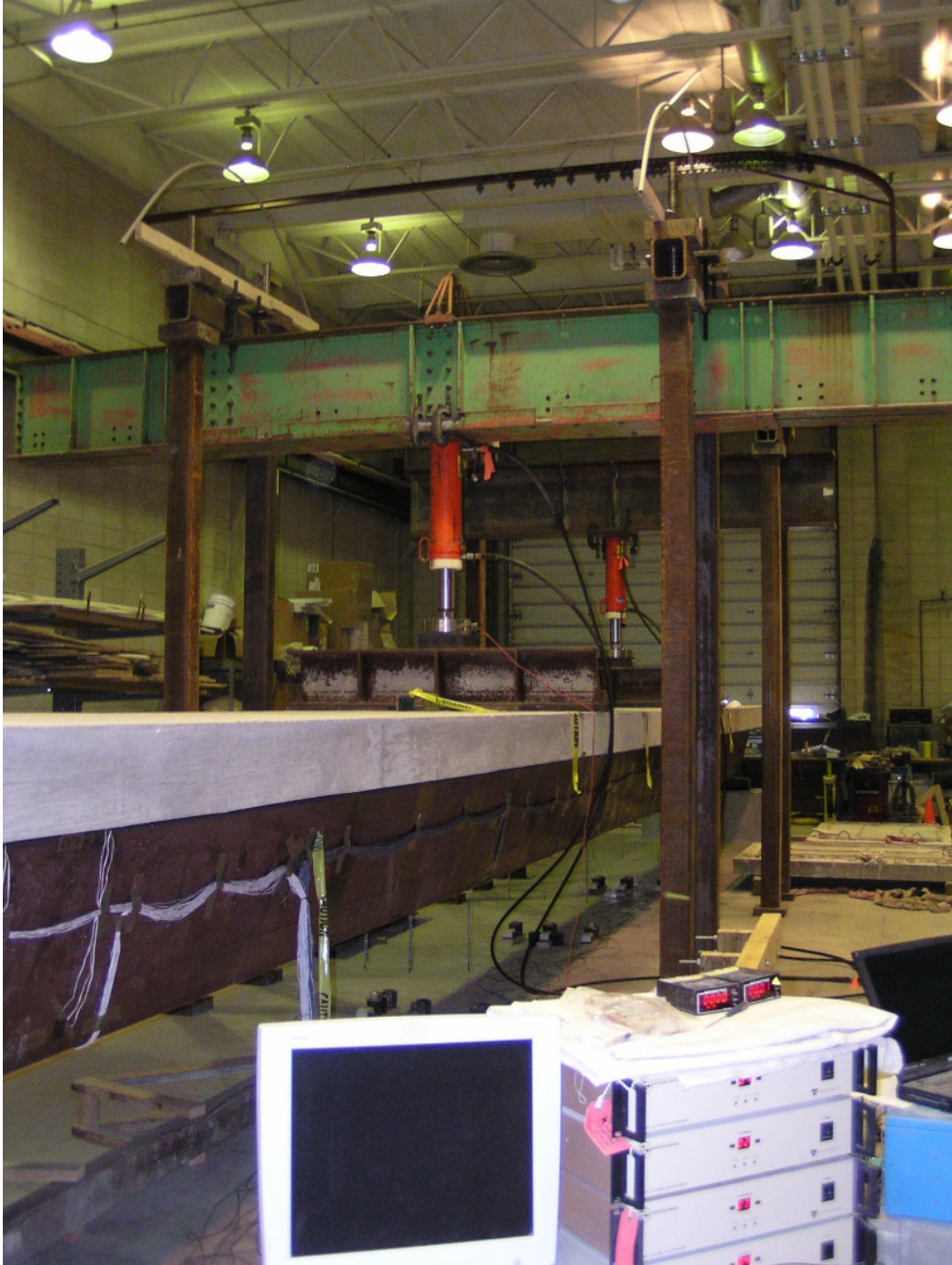


Figure 3.9. Test B – Flexure setup

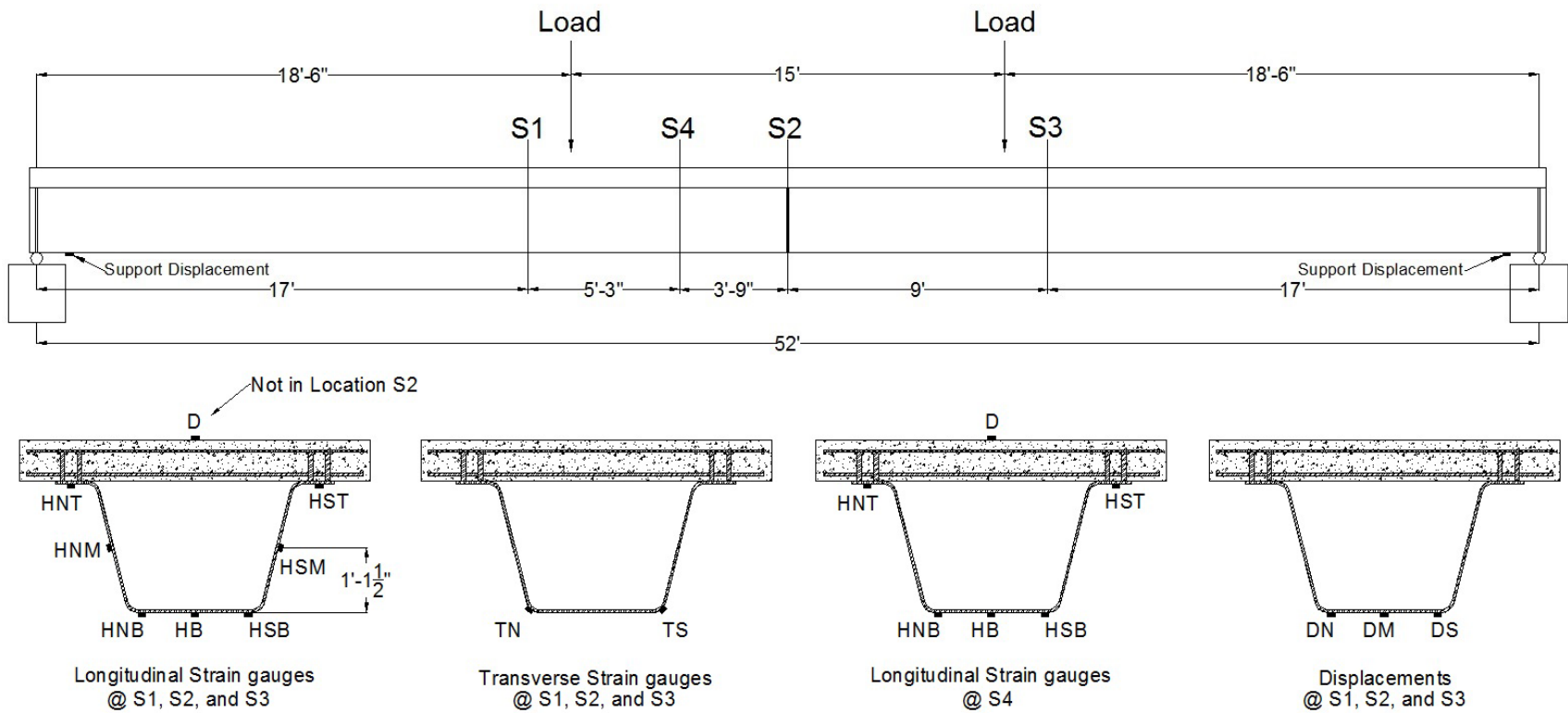


Figure 3.10. Test B – Flexure load and gauge locations

3.4.2 Predicted Results

When determining the additional moment required to cause inelastic behavior in the girder, the amount of moment being imposed on the girder by its own self-weight and support conditions must first be calculated. The self-weight of the girder was calculated as 812 lb/ft and induced a moment of 274 kip-ft at the mid-span of the girder. Using the moment induced by the self-weight of the girder in Equation 3.6, the additional moment that is required to cause inelastic girder behavior was calculated as 2,768 kip-ft.

$$F_y = \frac{M_y \times y}{I} + \frac{M_\omega \times y}{I} \quad (3.6)$$

where, F_y is the yield stress of the steel, M_y is the additional moment required to cause inelastic behavior at mid-span, M_ω is the moment induced by the beam's own self-weight at mid-span, y is the distance from the centroid to the extreme tension fiber in the beam, and I is the moment of inertia.

Next, using the support and loading conditions, the load per loading location that would cause this moment in the girder was calculated as 150 kips. The magnitude of moments at gauge locations S1, S2, S3, and S4 can then be predicted based on these load values. The previously calculated section properties of the beam were used to predict what the deflections, stresses, and strains at these locations could be. The previous Equations 3.2 and 3.3 (AISC 2005) were used to determine the girder's deflections at locations S1, S2, and S3 (see Figure 3.11).

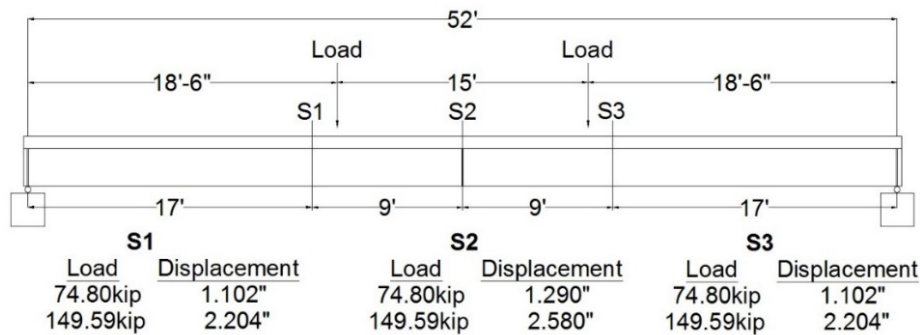


Figure 3.11. Test B – Flexure predicted elastic deflections

The elastic flexural formula in the previous Equation 3.4 (Riley 2007) can be used to determine stress values at a distance (c) from the neutral axis, as long as strains remain linear elastic. Hooke's law in the previous Equation 3.5 (Riley 2007) can then be used to convert the stress values to strain values, which will then be compared to measured strain values. Predicted strain distributions for loading are shown in Figure 3.12, but they do not include the initial strains in the girder from its own self-weight.

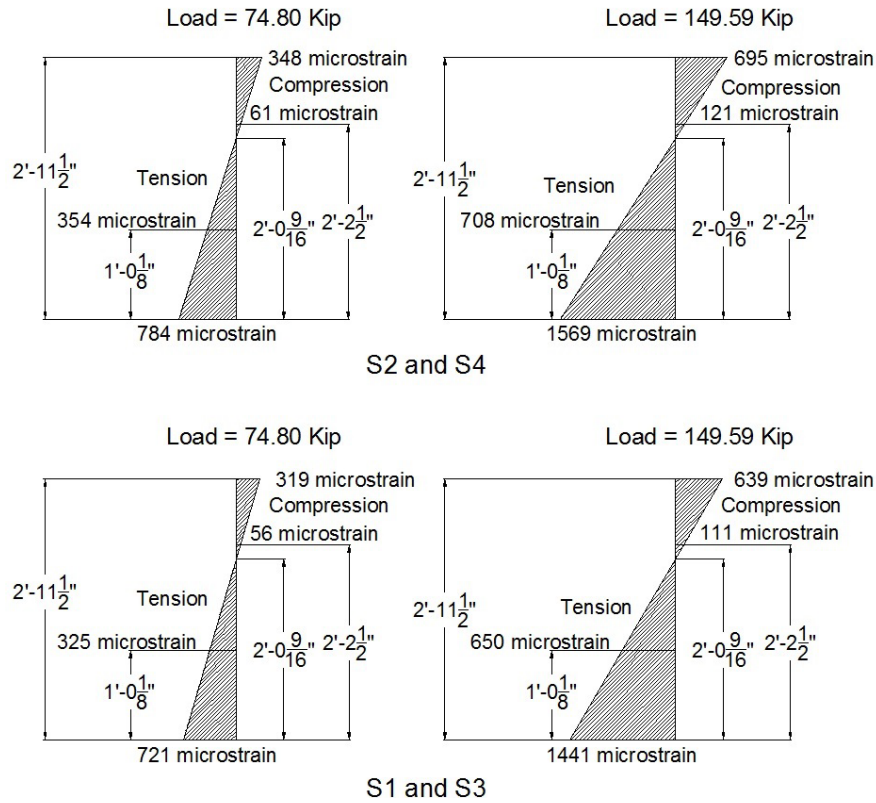


Figure 3.12. Test B – Flexure predicted elastic strain distributions

For comparison purposes, the displacements and strain distributions were also determined for the LRFD live load (HL-93) using the design truck (HS-20) with and without a lane load. To generate the maximum moment, the design truck (HS-20) with a 14-ft center axle wheel spacing was located 2.33 ft past mid-span of the beam.

The maximum moment created by the design truck (HS-20) on the beam using no distribution factor was determined to be 664 kip-ft. To reach this moment with the beam's loading and support conditions, it would require a force of 35.87 kips per load location.

The maximum moment imposed by the design truck (HS-20) including a distributed lane load of 0.64 kip/ft without using any distribution factors was determined to be 878 kip-ft. To reach this moment with the beam's loading and support conditions, it would require a force of 47.5 kips per load location.

The predicted displacements and strain distributions for the loading case (HL-93) are shown in Figure 3.13 and Figure 3.14, respectively.

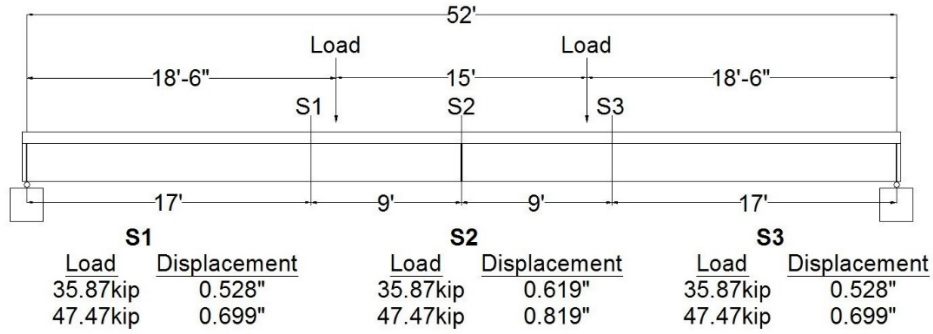


Figure 3.13. Test B – Flexure predicted HL-93 loading displacements

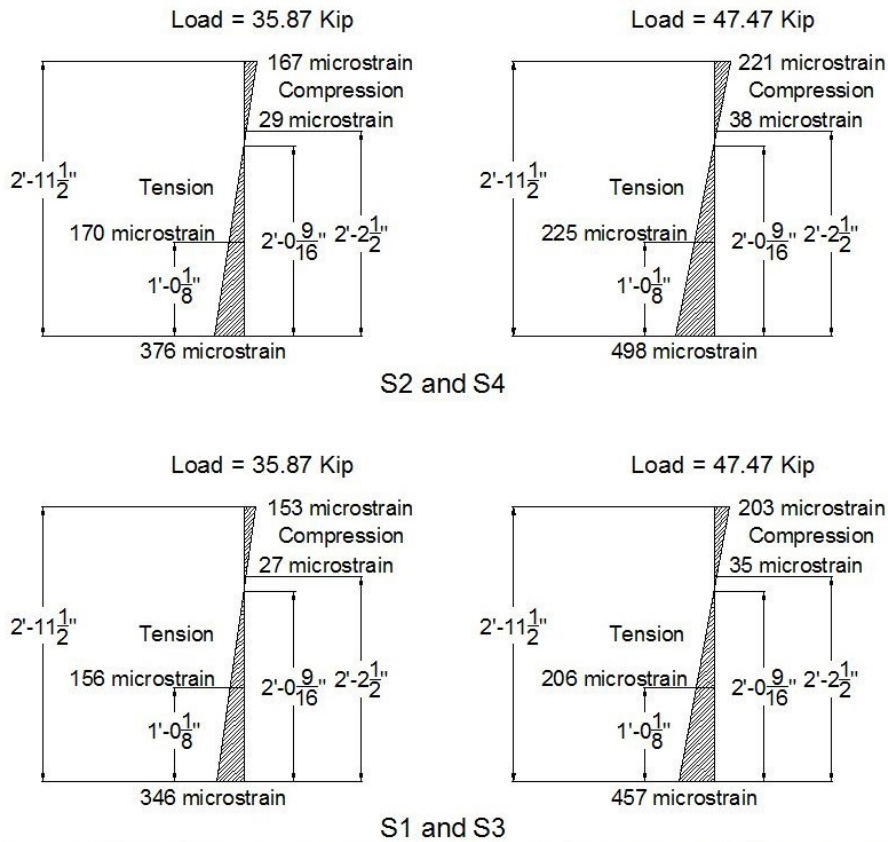


Figure 3.14. Test B – Flexure predicted HL-93 loading strain distributions

Loading was stopped at a load of 94 kips per actuator during testing due to measured strains that were larger than the predicted strain values. This load would create a moment of 1,739 kip-ft at the mid-span of the girder with the given loading and support conditions. These predicted displacements and strain distributions are shown in Figure 3.15 and Figure 3.16, respectively.

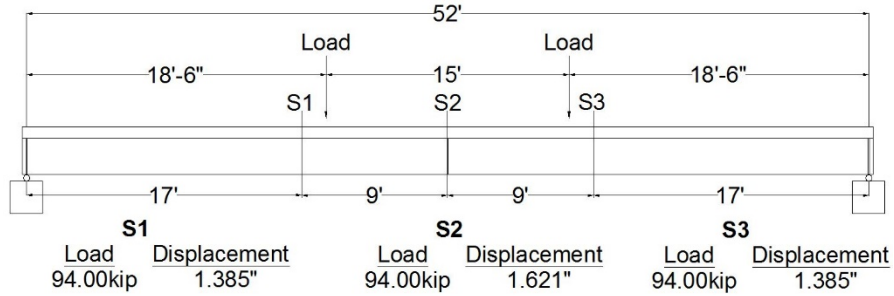


Figure 3.15. Test B – Flexure actual loading predicted displacements

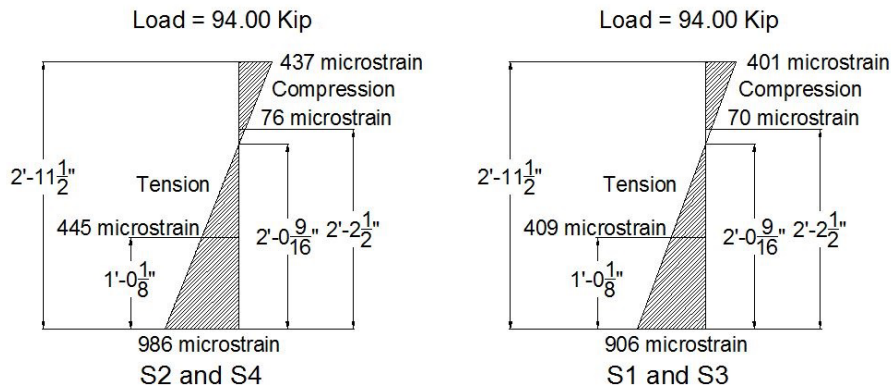


Figure 3.16. Test B – Flexure actual loading predicted strain distributions

3.5 Test C – Shear

3.5.1 Test Setup

The same folded plate girder with the cast-in-place composite deck from Test B was tested by loading the girder with a two-line load located close to one of the supports. This test was completed to study the shear behavior of the folded plate girder system and its ultimate capacity.

To determine how the folded plate girder was behaving in shear, strain gauge rosettes were attached to the girder near the loading locations. Instrumentation to measure displacements was also attached in several locations to determine the girder's overall behavior. Uniaxial strain gauges from the previous tests remained attached to monitor the girder's flexural behavior. Tilt sensors were also attached to each end of the beam to monitor the support rotation. The instrumentation and loading setup are shown in Figure 3.17 and Figure 3.18, respectively.



Figure 3.17. Test C – Shear setup

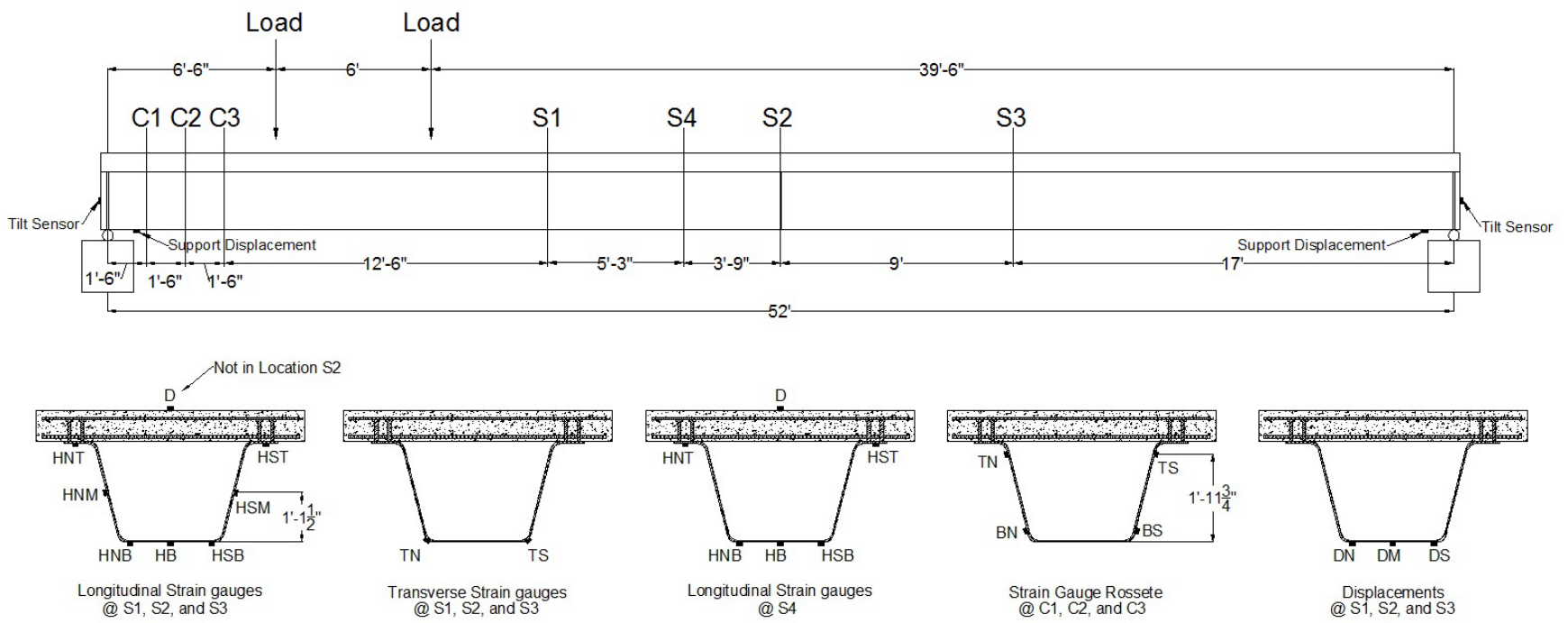


Figure 3.18. Test C – Shear load and gauge locations

3.5.2 Predicted Results

Initially, the shear capacity of the composite tub girder was determined according to AASHTO 6.10.9.2 – nominal resistance of unstiffened webs. The web thickness used when determining the girder’s shear capacity was the sum of the horizontal thicknesses of the two webs. By doing this, the nominal shear capacity of the girder was found to be 801 kips. With the support and loading conditions being used, it would require a load of 492 kips at each load location to reach the nominal shear capacity of the girder.

Next, the plastic moment capacity of the composite tub girder was determined. First, it was required to find the plastic neutral axis of the section. This was done by using Equation 3.7 (Riley 2007) and determining where the sum of the tensile and compressive stresses is equal to zero.

$$\sum F_x = \int_{Area} \sigma_x dA = 0 \quad (3.7)$$

where, F_x is the force in the x direction and σ_x is the stress in the x direction.

The stress distribution used for determining the plastic centroid is shown in Figure 3.19.

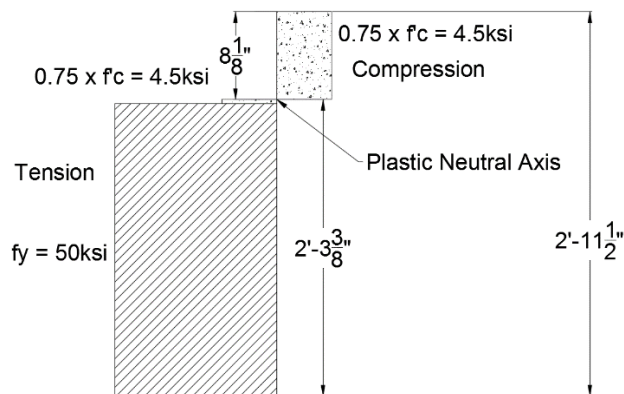


Figure 3.19. Test C – Shear plastic stress distribution

The plastic neutral axis was found to be 27.375 in. from the bottom of the girder. The plastic moment capacity was then determined to be 4,003 kip-ft by summing up the moments created by the tensile and compressive forces about the plastic neutral axis. With the support and loading conditions being used, it would require a load of 277 kips at each load location to reach the plastic moment capacity of the girder.

After determining that the composite tub girder would ultimately fail in flexure before it would fail in shear, the elastic response was determined for both flexure and shear. The elastic flexural response of the girder was determined similarly to Test B. The self-weight of the girder was calculated as 812 lb/ft and induced a moment of 200 kip-ft at the line load located 12.5 ft from the support. Using the moment induced by the self-weight of the girder in the previous Equation

3.6, the additional moment that is required to cause inelastic behavior in the girder was calculated as 2,841 kip-ft.

Next, using the support and loading conditions, the load per loading location that would cause this moment in the girder was calculated as 197 kips. The magnitude of the moments at gauge locations S1, S2, S3, and S4 can then be predicted. The previously calculated section properties of the beam were used to determine what the deflections, stresses, and strains at these locations could be. The elastic flexural formula in the previous Equation 3.4 (Riley et al. 2007) can be used to determine stress values at a distance (c) from the neutral axis, as long as strains remain linear elastic. Hooke's law in the previous Equation 3.5 (Riley et al. 2007) can then be used to convert the stress values to strain values, which will then be compared to measured strain values. Predicted strain distributions for the loading considered are shown in Figure 3.20, but they do not include the initial strains in the girder from its own self-weight.

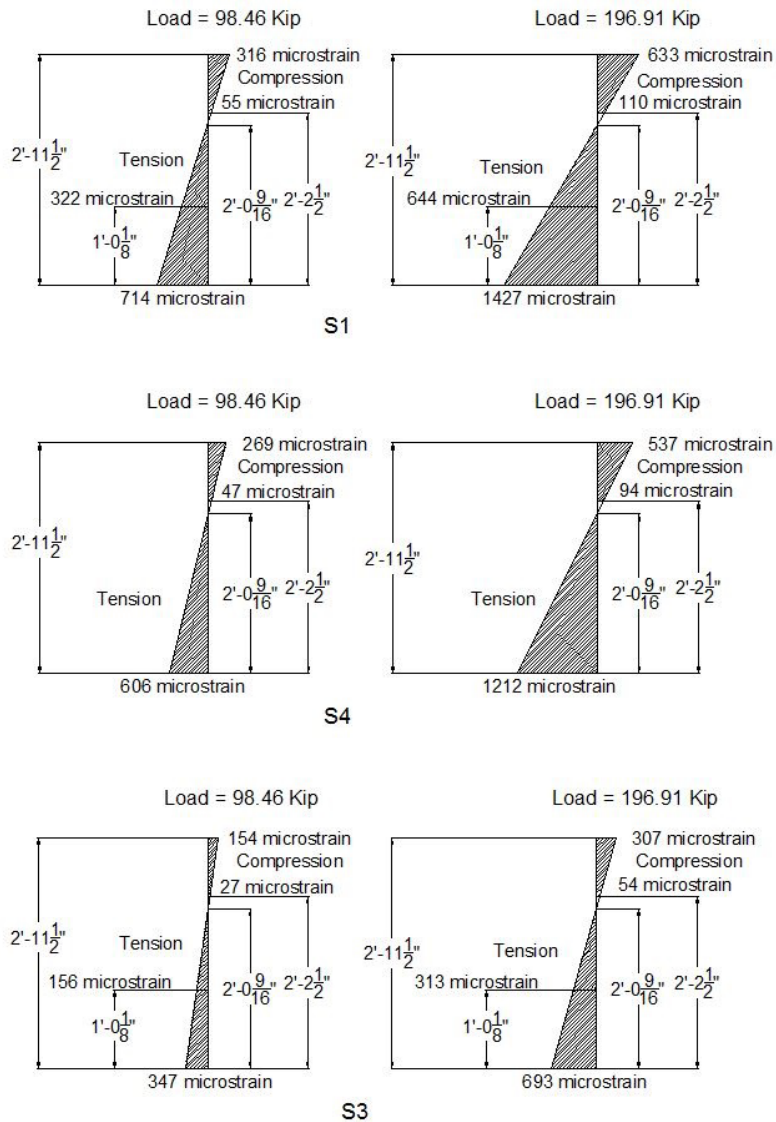


Figure 3.20. Test C – Shear predicted elastic strain distributions

The moment-area theorems were used to determine the girder's deflections at locations S1, S2, and S3 (see Figure 3.21).

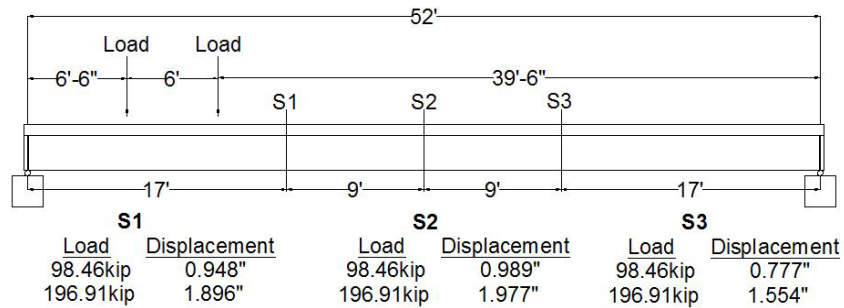


Figure 3.21. Test C – Shear predicted elastic deflections

For comparison purposes, the displacements and strain distributions were also determined for the LRFD live load (HL-93) using the design truck (HS-20) with and without a lane load. To generate the maximum moment, the design truck (HS-20) with 14-ft center axle wheel spacing was located 2.33 ft past mid-span of the beam.

The maximum moment imposed by the design truck (HS-20) on the beam using no distribution factors was determined to be 664 kip-ft. To reach this moment with the beam's loading and support condition, it would require a force of 46.0 kips per load location.

The maximum moment imposed by the design truck (HS-20) including a distributed lane load of 0.64 kip/ft without using any distribution factors was determined to be 878 kip-ft. To reach this moment with the beam's loading and support condition, it would require a force of 60.9 kips per load location.

The predicted displacements and strain distributions are shown in Figure 3.22 and Figure 3.23, respectively.

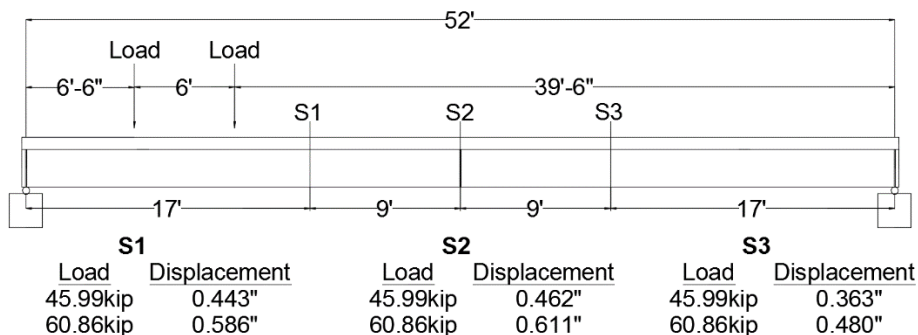


Figure 3.22. Test C – Shear predicted HL-93 loading displacements

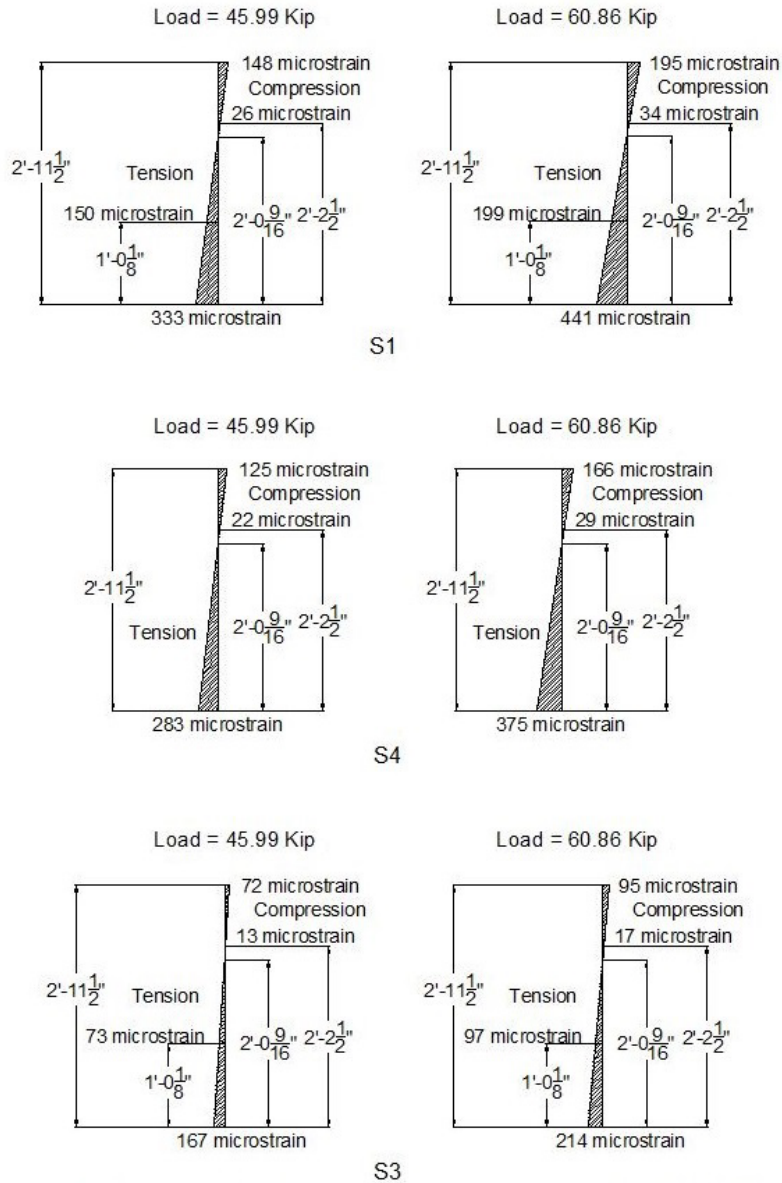


Figure 3.23. Test C – Shear predicted HL-93 loading strain distributions

The predicted shear response was then found using the same loading as the elastic flexural response. The shear formula is subject to the same assumptions as the flexural formula and is only applicable as long as strains remain linear elastic. By knowing the largest elastic load that will be applied to the girder, the accompanying shear force at locations C1, C2, and C3 was determined to be 321 kips. This shear force and the previously calculated section properties were then used in Equation 3.8 (Riley et al. 2007) to determine the vertical and horizontal shearing stresses in the girder at the strain rosette locations.

$$\tau = \frac{VQ}{It} \quad (3.8)$$

where, τ is the vertical and horizontal shear stress, V is the shear force, Q is the first moment, I is the moment of inertia, and t is the thickness (used as $2 \times t$ to account for both webs).

Predicted values for shear stresses and strains are shown in Table 3.1.

Table 3.1. Test C – Shear predicted elastic shear values for locations C1, C2, and C3

Load (kips)	Shear (kips)	Stress (ksi)	Strain (micro radians)
23.75 in. from Bottom of Beam			
98.46	160.48	8.86	805
196.91	320.96	17.72	1,611
3 in. from Bottom of Beam			
98.46	160.48	5.05	459
196.91	320.96	10.10	918

Using the shear modulus of steel in Equation 3.9 (Riley et al. 2007), shear stresses can then be converted to shear strains and compared to measured strain values.

$$\gamma = \frac{\tau}{G} \tag{3.9}$$

where, γ is the shear strain, τ is the vertical and horizontal shear stress, and G is the shear modulus (assumed as 11,000 ksi).

For comparison purposes, the shear stress and strain values were also determined for the LRFD live load (HL-93) using the design truck (HS-20) with and without a lane load. The back tire of the design truck (HS-20) with a 14-ft center axle wheel spacing was located 3 ft (roughly the height of the beam) away from the support.

With this loading condition, the maximum shear force imposed by the design truck (HS-20) on the beam using no distribution factors was determined to be 54.9 kips. To reach this shear load with the beams loading and support condition, it would require a force of 33.7 kips per load location.

The maximum shear imposed by the design truck (HS-20) including a distributed lane load of 0.64 kip/ft without using any distribution factors was determined to be 71.6 kips. To reach this shear load with the beam’s loading and support condition, it would require a force of 43.9 kips per load location.

Predicted values for shear stresses and strains are shown in Table 3.2.

Table 3.2. Test C – Shear loading (HL-93) predicted shear values for locations C1, C2, and C3

Load (kips)	Shear (kips)	Stress (ksi)	Strain (micro radians)
23.75 in. from Bottom of Beam			
33.69	54.91	3.03	276
43.90	71.56	3.95	359
3 in. from Bottom of Beam			
33.69	54.91	1.73	157
43.90	71.56	2.25	205

3.6 Summary of Section Properties and Loading

A summary of the section properties of both the folded plate girder alone and with the composite deck are shown in Table 3.3.

Table 3.3. Section properties

Section Properties	Beam	Beam with Deck
Elastic Centroid, Y (in.) from bottom	12.14	24.60
Plastic Centroid, Y_p (in.) from bottom		27.375
Moment of Inertia, I (in. ⁴)	5,430.00	17,959.00
First Moment, Q (in. ³) @ 3 in. from the bottom		368.20
First Moment, Q (in. ³) @ 23.75 in. from the bottom		646.15
Self Weight, w (lb/ft)	174.16	811.66
Modulus of Elasticity of Steel, E_s (ksi)	29,000.00	29,000.00
Yield Stress of Steel, F_y (ksi)	50.00	50.00
Modulus of Elasticity of Concrete, E_c (psi)		4,463.00
Compressive Strength of Concrete, f'_c (psi)		6,000.00

The summary of the loading conditions that correlate to the predicted displacements and strain values seen in previous figures for Tests A, B, and C are listed in Table 3.4.

Table 3.4. Summary of loading

Test	Beam	Beam with Deck
Test A – Constructability		
One Times Dead Load, Moment @ midspan (kip-ft)	58.87	
One Times Dead Load, Load (kip)	3.18	
Two Times Dead Load, Moment @ midspan (kip-ft)	117.74	
Two Times Dead Load, Load (kip)	6.36	
Test B – Flexibility		
Dead Load, Moment @ midspan (kip-ft)		274.34
Predicted Yield Moment @ midspan (kip-ft)		2,767.49
Predicted Yield Line Load (kip)		149.59
Actual Moment Loaded to @ midspan (kip-ft)		1,739.00
Actual Line Load (kip)		94.00
HS-20 Truck, Max Moment (kip-ft)		663.67
HS-20 Truck, Line Load (kip)		35.87
HS-20 Truck + Lane Load, Max Moment (kip-ft)		878.25
HS-20 Truck + Lane Load, Line Load (kip)		47.47
Test C – Shear		
Dead Load, Moment @ 12.5 ft from support (kip-ft)		200.38
Half of Predicted Yield Moment @ 12.5 ft from support (kip-ft)		1,420.73
Half of Predicted Yield Line Load (kip)		98.46
Predicted Yield Moment @ 12.5 ft from support (kip-ft)		2,841.46
Predicted Yield Line Load (kip)		196.91
Predicted Ultimate Moment @ 12.5 ft from support (kip-ft)		4,002.56
Predicted Ultimate Line Load (kip)		277.38
Actual Ultimate Moment @ about 13 ft from support (kip-ft)		4,611.68
Actual Ultimate Line Load (kip)		319.59
Nominal Shear Capacity, V_n (kip)		801.00
Nominal Shear Capacity, Line Load (kip)		491.50
HS-20 Truck, Max Moment (kip-ft)		663.67
HS-20 Truck, Line Load (kip)		45.99
HS-20 Truck + Lane Load, Max Moment (kip-ft)		878.25
HS-20 Truck + Lane Load, Line Load (kip)		60.86
HS-20 Truck, Max Shear (kip)		54.92
HS-20 Truck, Line Load (kip)		33.69
HS-20 Truck + Lane Load, Max Shear (kip)		71.56
HS-20 Truck + Lane Load, Line Load (kip)		43.90

CHAPTER 4 LABORATORY TEST RESULTS

4.1 Test A – Constructability

As previously stated in the constructability predicted results section of the last chapter, a single girder was tested under two-point bending to determine how the folded plate girder would behave during construction prior to acting compositely with the deck.

The girder was tested up to a load of 6.36 kips at each load location, which induced a moment in the beam of 118 kip-ft at mid-span. This moment is approximately equal to the moment that would be created by two times the girder's own self-weight (348 lb/ft).

Uniaxial strain gauges were attached to the beam in several locations to determine how the folded plate girder was behaving in flexure. Instrumentation to measure displacements was also attached in several locations to determine the girder's overall behavior. The instrumentation setup was shown previously in Figure 3.6.

The measured strain values for a load comparable to the beam's dead load are shown in comparison to the predicted strain distribution in Figure 4.1.

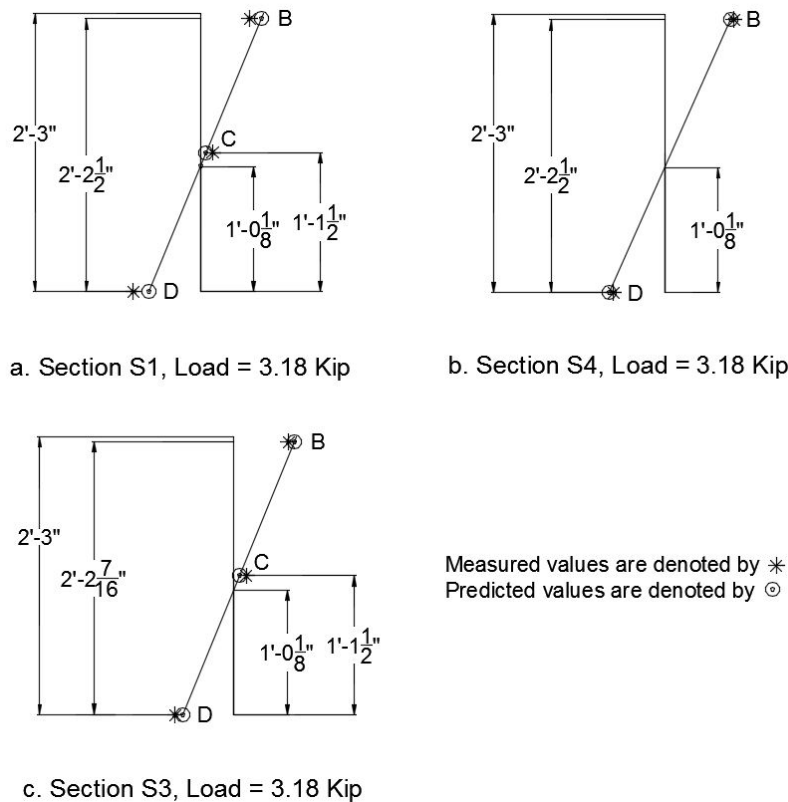


Figure 4.1. Test A – Constructability predicted vs. measured strain distributions, dead load

The predicted and measured strain values that go along with Figure 4.1 are shown in Table 4.1.

Table 4.1. Test A – Constructability predicted and measured strain distribution values, dead load, folded plate girder

	Predicted Values			Measured Values		
	micro-strain			micro-strain (Avg, Std Dev)		
	S1	S4	S3	S1	S4	S3
Top (B)	-59	-64	-59	(-48,0)	(-67,3)	(-53,12)
Middle (C)	-6	X	-6	(-12,5)	X	(-12,1)
Bottom (D)	50	54	50	(65,6)	(50,2)	(57,6)

Measured versus predicted strain values appear to be similar, other than some slight variations in strain values in the B and D locations of Section S1.

The measured strain values for a load comparable to two times the beam’s dead load are shown in comparison to the predicted strain distribution in Figure 4.2.

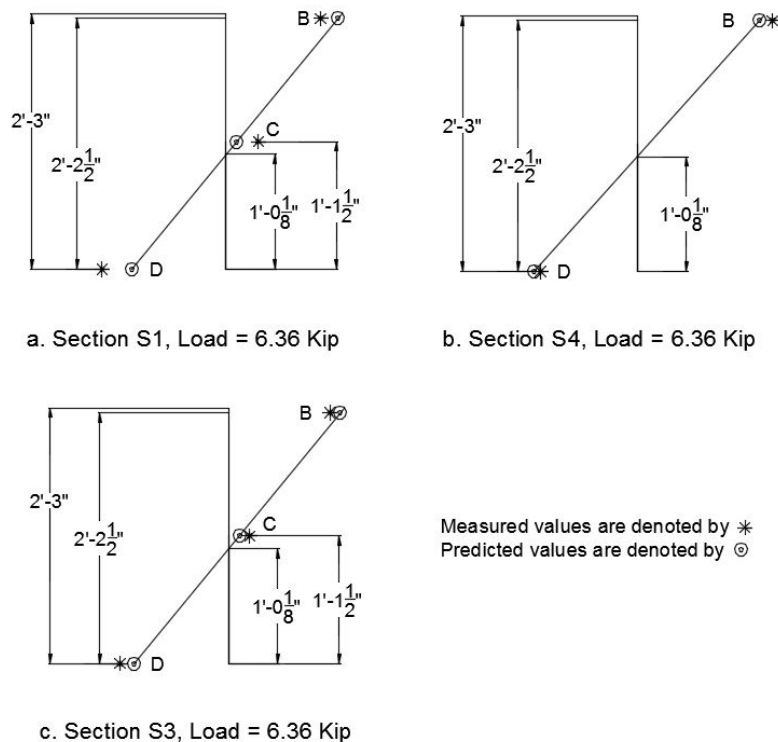


Figure 4.2. Test A – Constructability predicted vs. measured strain distributions, two times dead load

The predicted and measured strain values that go along with Figure 4.2 are shown in Table 4.2.

Table 4.2. Test A – Constructability predicted and measured strain distribution values, two times dead load, folded plate girder

	Predicted Values micro-strain			Measured Values micro-strain (Avg, Std Dev)		
	S1	S4	S3	S1	S4	S3
Top (B)	-118	-129	-118	(-100,0)	(-143,6)	(-107,2)
Middle (C)	-11	X	-11	(-34,12)	X	(-22,2)
Bottom (D)	100	109	100	(131,14)	(102,3)	(115,11)

Measured versus predicted strain values appear to be similar, other than some slight variations in strain values in all locations of Section S1. The D location of Section S1 had a more significant difference than the other locations with a measurement of 31 micro-strain above the predicted value.

The measured and predicted loads versus displacements for Test A of Sections S1, S2, and S3 are shown in Figure 4.3, Figure 4.4, and Figure 4.5, respectively.

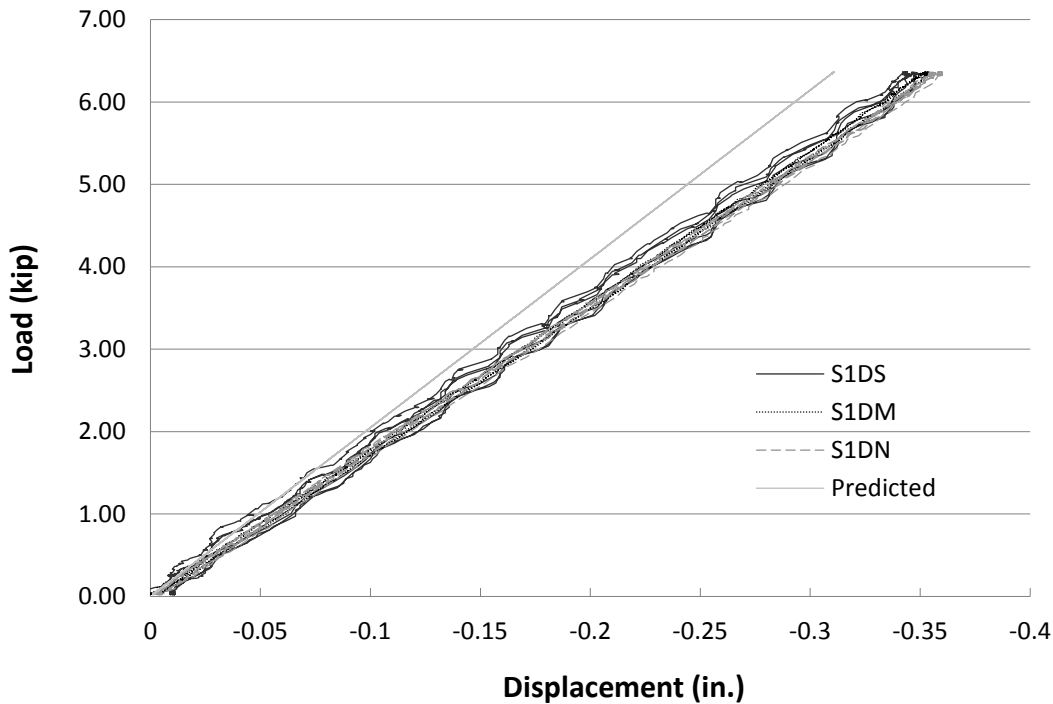


Figure 4.3. Test A – Constructability location S1 load vs. displacement

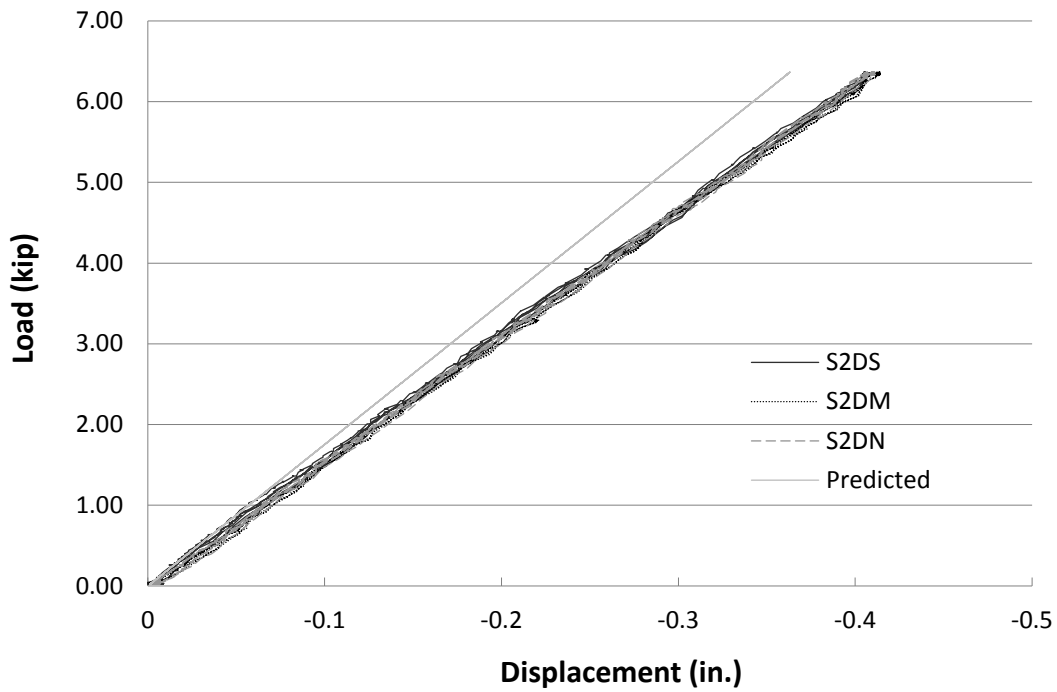


Figure 4.4. Test A – Constructability location S2 load vs. displacement

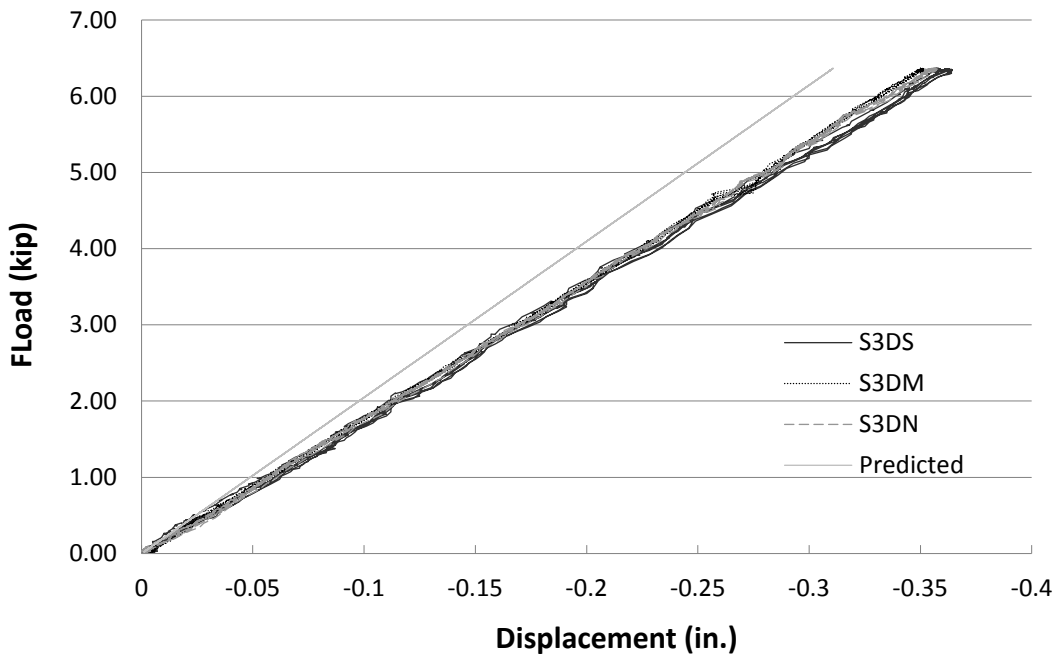


Figure 4.5. Test A – Constructability location S3 load vs. displacement

Displacements measured for all three sections were consistently larger than predicted displacements. Displacements at mid-span were 0.023 in. larger than the predicted 0.181 in. for a

load comparable to the beam's dead load and 0.047 in. larger than the predicted 0.363 in. for a load comparable to two times the beam's dead load.

4.2 Test B – Flexure

As stated in the previous chapter, a concrete deck was cast onto the same folded plate girder from Test A for Test B. The specimen was then tested under two-point bending to determine the composite flexural behavior of the folded plate girder system and its elastic flexural capacity.

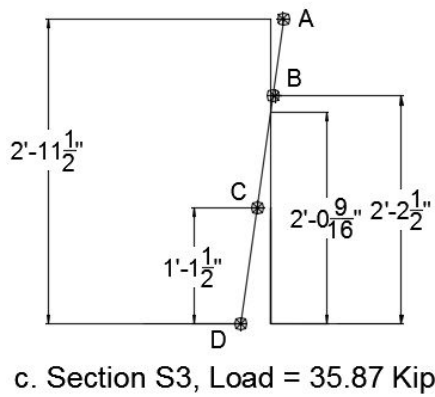
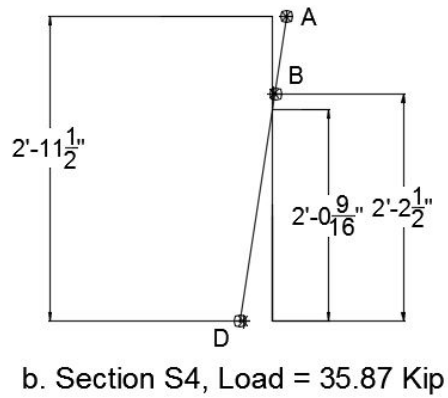
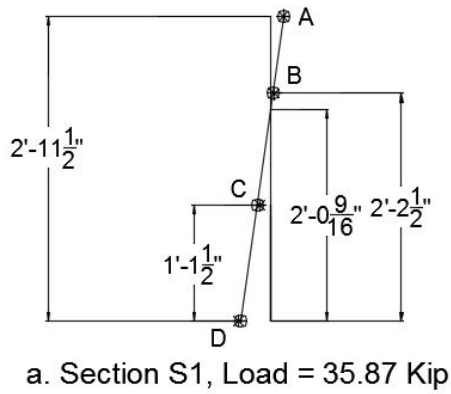
The girder was tested up to, but not beyond, a load that created non-linear behavior. Loading was stopped at a load of 94 kips, short of the predicted 150 kips per load location during testing due to larger than predicted strain values. This load would create a moment of 1,739 kip-ft, short of the predicted 2,767 kip-ft, at the mid-span of the girder with the given loading and support conditions.

For comparison purposes, the displacements and strain distributions were also determined, without using any distribution factors, for the LRFD live load (HL-93) using the design truck (HS-20) with and without a lane load.

Uniaxial strain gauges were attached to the beam in several locations to determine how the folded plate girder was behaving in flexure. Instrumentation to measure displacements was also attached at several locations to determine the girder's overall behavior.

Deck gauges that measured data for locations S3 and S4 were swapped for all of Test B. It was believed that these gauges may have been wired into the wrong channel when being hooked up to the data acquisition system. The instrumentation setup was shown in the previous Figure 3.10.

The measured strain values for a load comparable to the design truck (HS-20) are shown in comparison to the predicted strain distribution in Figure 4.6.



Measured values are denoted by *
 Predicted values are denoted by ◻

Figure 4.6. Test B – Flexure predicted vs. measured strain distributions, HS-20 truck load

The predicted and measured strain values that go along with Figure 4.6 are shown in Table 4.3.

Table 4.3. Test B – Flexure predicted and measured strain distribution values, HS-20 truck load

	Predicted Values micro-strain			Measured Values micro-strain (Avg, Std Dev)		
	S1	S4	S3	S1	S4	S3
Top of Concrete Deck (A)	◻ -153	◻ -167	◻ -153	* (-141,0)	* (-157,0)	* (-137,0)
Girder Top (B)	◻ -27	◻ -29	◻ -27	* (-40,2)	* (-14,1)	* (-46,5)
Girder Middle (C)	◻ 156	X	◻ 156	* (131,17)	X	* (156,1)
Girder Bottom (D)	◻ 346	◻ 376	◻ 346	* (377,23)	* (346,6)	* (356,14)

Measured versus predicted strain values appear to be similar in all locations of all sections.

The measured strain values for a load comparable to the design truck (HS-20) with a lane load are shown in comparison to the predicted strain distribution in Figure 4.7.

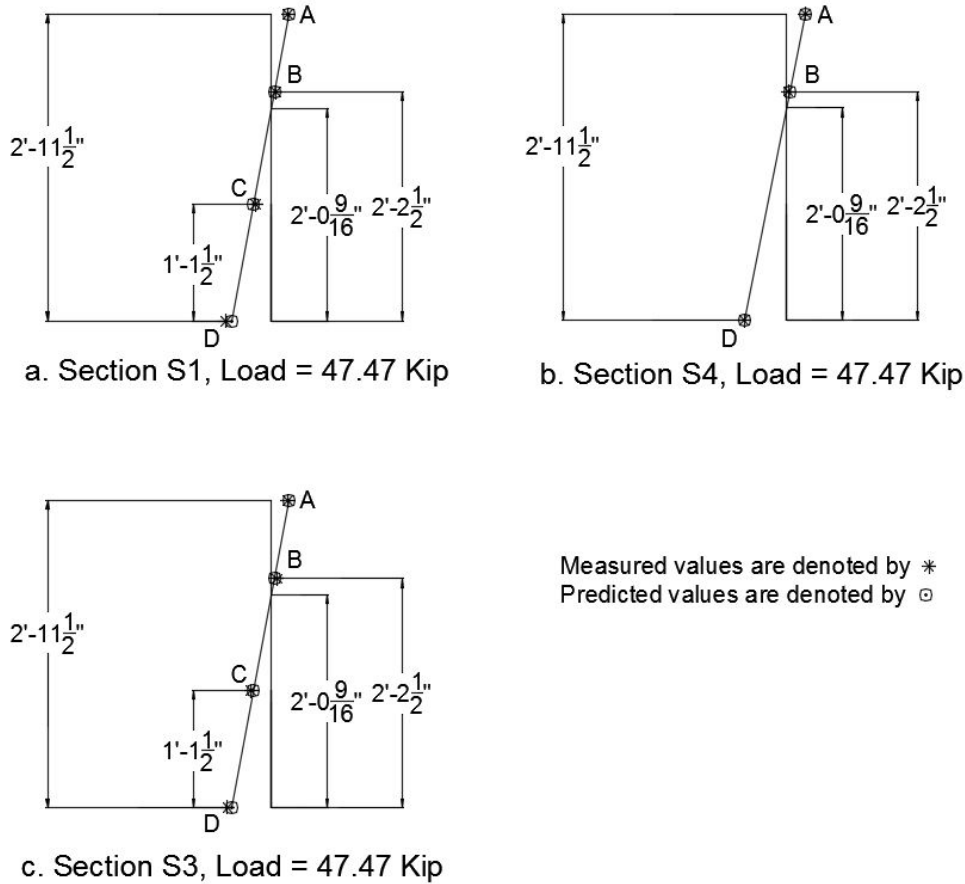


Figure 4.7. Test B – Flexure predicted vs. measured strain distributions, HS-20 truck + lane load

The predicted and measured strain values that go along with Figure 4.7 are shown in Table 4.4.

Table 4.4. Test B – Flexure predicted and measured strain distribution values, HS-20 truck + lane load

	Predicted Values			Measured Values		
	micro-strain			micro-strain (Avg, Std Dev)		
	S1	S4	S3	S1	S4	S3
Top of Concrete Deck (A)	-203	-221	-203	(-192,0)	(-216,0)	(-188,0)
Girder Top(B)	-35	-38	-35	(-53,2)	(-17,0)	(-62,6)
Girder Middle (C)	206	X	206	(182,19)	X	(235,2)
Girder Bottom (D)	457	498	457	(533,30)	(497,10)	(510,20)

Measured versus predicted strain values appear to be similar, other than some slight variations in strain values in the D locations of Sections S1 and S3.

The measured strain values for a load equal to 94 kips per load location are shown in comparison to the predicted strain distribution in Figure 4.8.

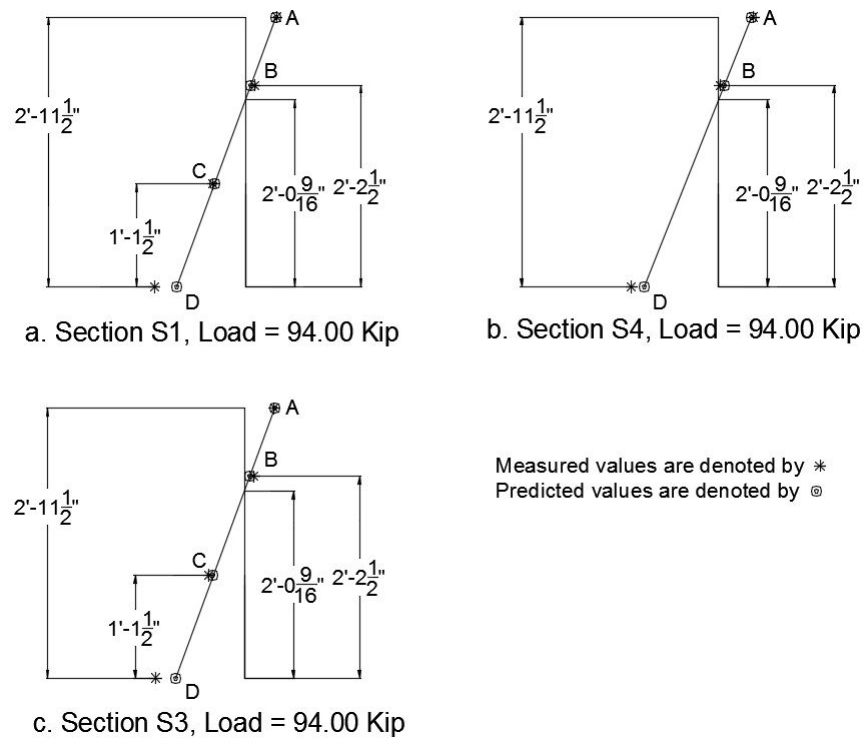


Figure 4.8. Test B – Flexure predicted vs. measured strain distributions, load = 94 kips

The predicted and measured strain values that go along with Figure 4.8 are shown in Table 4.5.

Table 4.5. Test B – Flexure predicted and measured strain distribution values, load = 94 kips

	Predicted Values			Measured Values		
	micro-strain			micro-strain (Avg, Std Dev)		
	S1	S4	S3	S1	S4	S3
Top of Concrete Deck (A)	-401	-437	-401	(-408,0)	(-454,0)	(-395,0)
Girder Top (B)	-70	-76	-70	(-117,18)	(-22,0)	(-124,16)
Girder Middle (C)	409	X	409	(430,0)	X	(463,31)
Bottom (D)	906	986	906	(1199,45)	(1152,27)	(1167,27)

Measured versus predicted strain values appear to be similar, other than significant variations in strain values in the D locations of all sections. Section S1 had a measured value of 293 micro-strain higher than the predicted value, Section S2 had a measured value of 166 micro-strain higher than the predicted value, and Section S3 had a measured value of 261 micro-strain higher than the predicted value.

The measured and predicted load versus displacement for Test B of Sections S1, S2, and S3 are shown in Figure 4.9, Figure 4.10, and Figure 4.11, respectively.

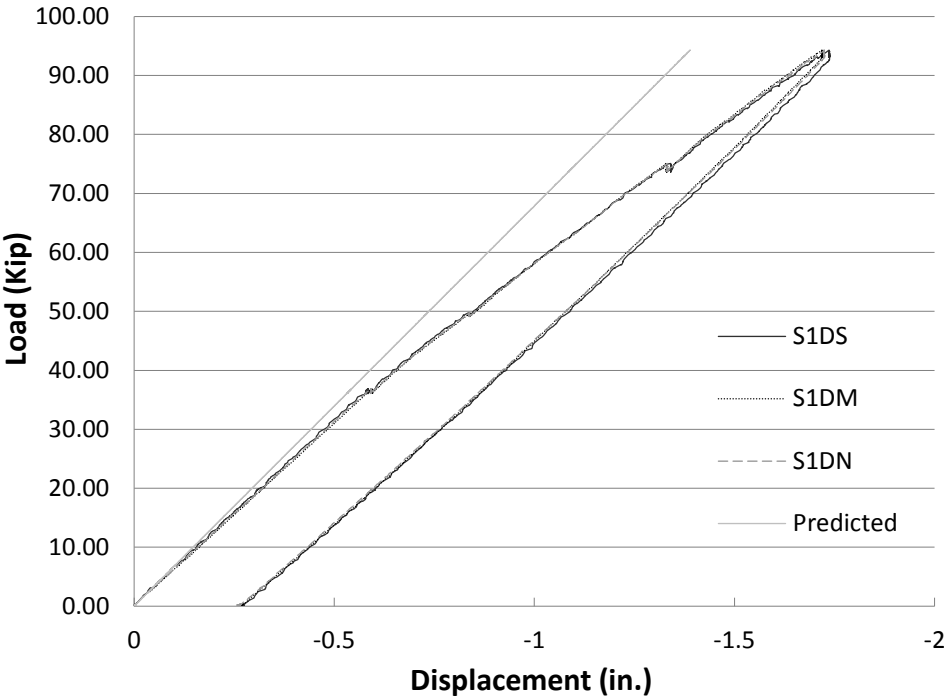


Figure 4.9. Test B – Flexure load vs. displacement, location S1

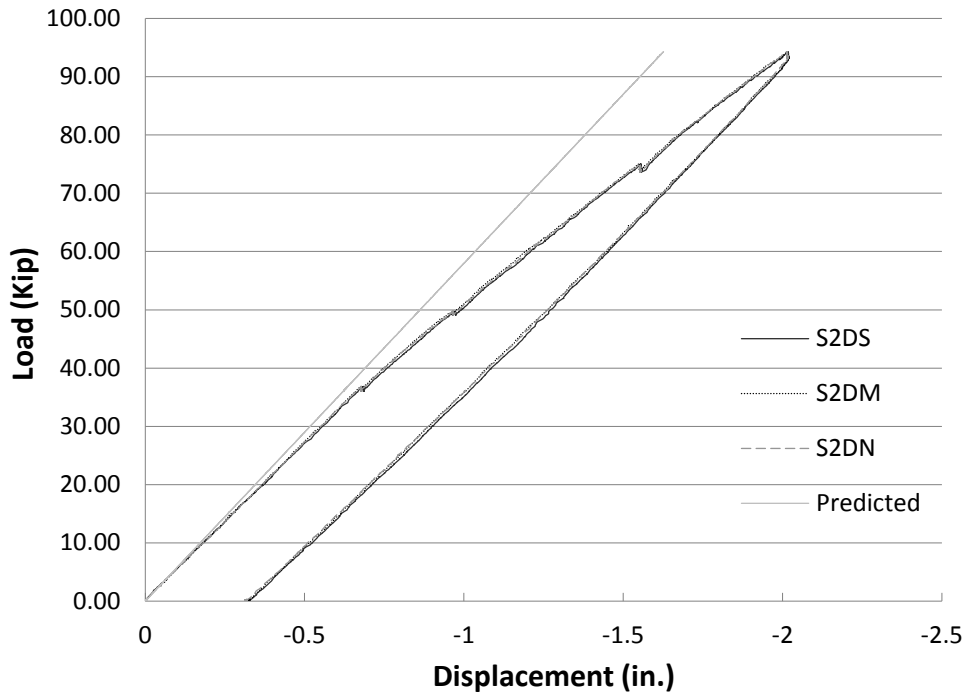


Figure 4.10. Test B – Flexure load vs. displacement, location S2

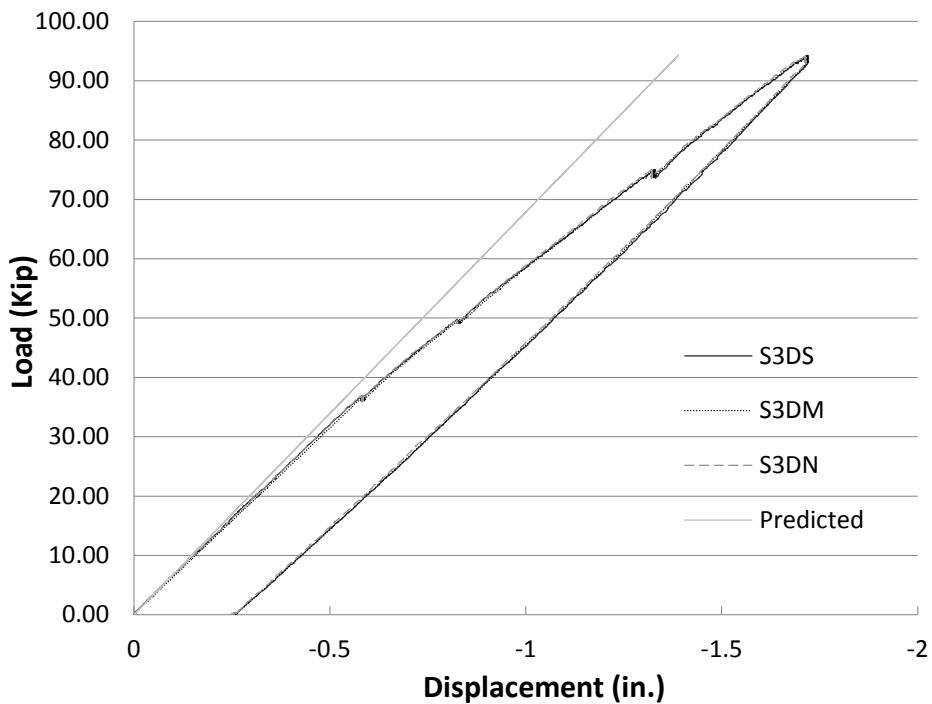


Figure 4.11. Test B – Flexure load vs. displacement, location S3

Displacements measured for all three sections were consistently larger than predicted values. Displacements at mid-span were 0.044 in. larger than the predicted 0.619 in. for a load

comparable to the design truck (HS-20), 0.094 in. larger than the predicted 0.819 in. for a load comparable to the design truck (HS-20) with lane load, and 0.389 in. larger than the predicted 1.621 in. for a load of 94 kips per load location.

4.3 Test C – Shear

4.3.1 Flexural Data

As previously stated in the Test C predicted results section of the last chapter, the same folded plate girder with a deck from Test B was tested by loading the girder with a two-line load located close to one of the supports. This test was done to determine the shear behavior of the folded plate girder system and its ultimate capacity.

The folded plate girder was tested up to failure. A moment of 2,841 kip-ft would cause inelastic behavior in the girder and would require a load of 197 kips per line load. The plastic moment capacity of the girder was determined to be 4,640 kip-ft and would require a load of 322 kips per line load to be reached.

For comparison purposes, the displacements and strain distributions were also determined, without using any distribution factors, for the LRFD live load (HL-93) using the design truck (HS-20) with and without a lane load. To determine how the folded plate girder was behaving in shear, strain gauge rosettes were attached to the girder near the loading location. Instrumentation to measure displacements was also attached in several locations to determine the girder's overall behavior.

Uniaxial strain gauges from the previous tests remained attached to monitor the girder's flexural behavior. Tilt sensors were also attached to each end of the girder to monitor the support rotation. The instrumentation setup was shown in the previous Figure 3.18.

The measured strain values for a load comparable to the design truck (HS-20) are shown in comparison to the predicted strain distribution in Figure 4.12.

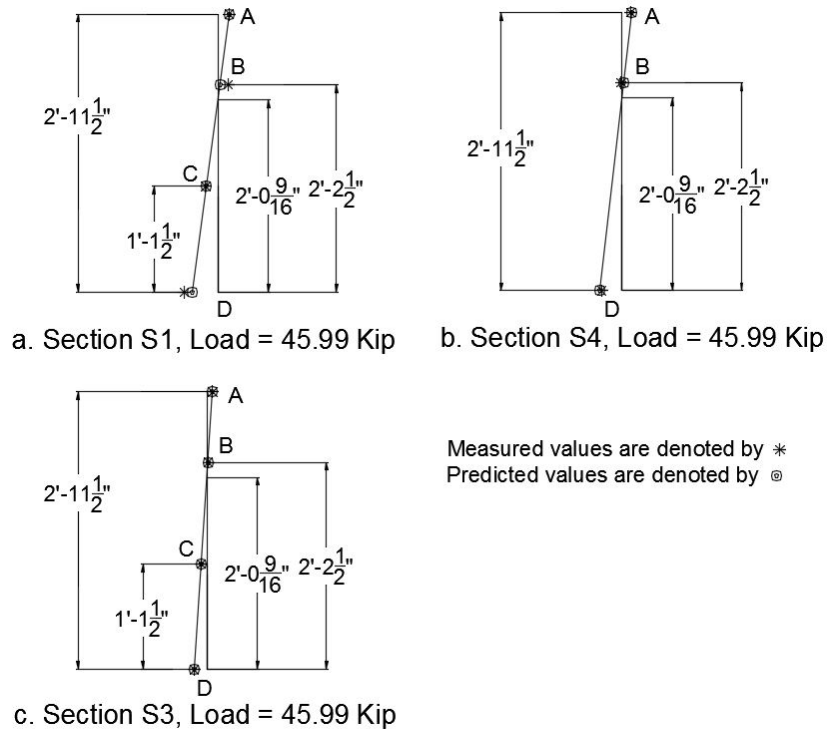


Figure 4.12. Test C – Shear predicted vs. measured strain distributions, HS-20 truck load

The predicted and measured strain values that go along with Figure 4.12 are shown in Table 4.6.

Table 4.6. Test C – Shear predicted and measured strain distribution values, HS-20 truck load

	Predicted Values			Measured Values		
	micro-strain			micro-strain (Avg, Std Dev)		
	S1	S4	S3	S1	S4	S3
Top of Concrete Deck (A)	-148	-125	-72	(-141,0)	(-107,0)	(-73,0)
Girder Top (B)	-26	-22	-13	(-132,10)	(12,4)	(-22,1)
Girder Middle (C)	150	X	73	(161,20)	X	(76,1)
Girder Bottom (D)	333	283	162	(436,28)	(261,7)	(162,4)

Measured versus predicted strain values appear to be similar, other than significant variations in strain values in the B and D locations of Section S1. Location B had a measured value of 106 micro-strain higher than the predicted value, and location D had a measured value of 103 micro-strain higher than the predicted value. After examining the data further, it was seen that the difference between the predicted and measured strain values at these two locations were due to an offset in the data from a prior loading step and should be ignored.

The measured strain values for a load comparable to the design truck (HS-20) with a lane load are shown in comparison to the predicted strain distribution in Figure 4.13.

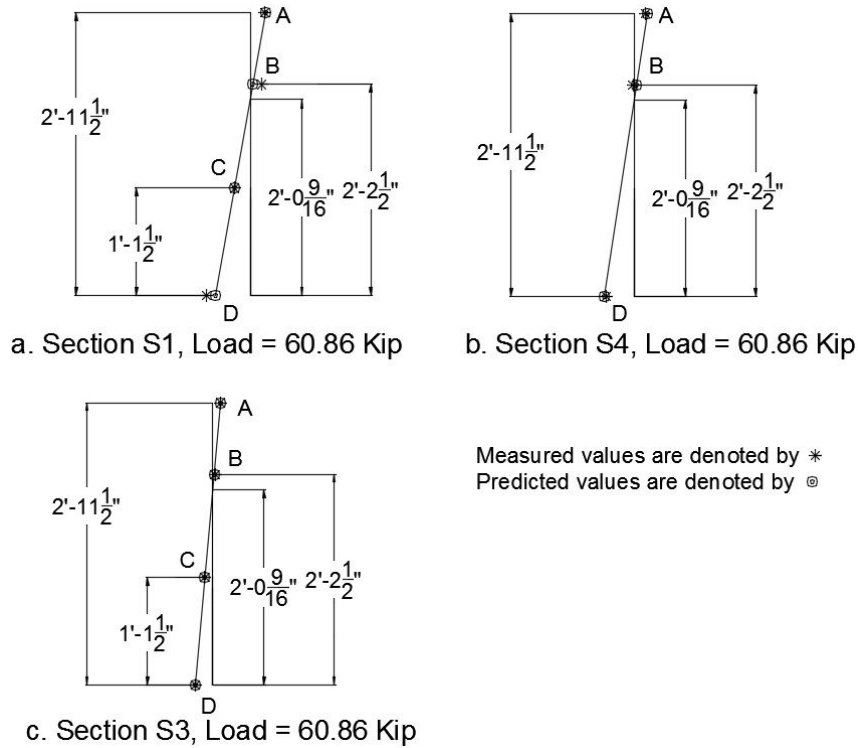


Figure 4.13. Test C – Shear predicted vs. measured strain distributions, HS-20 truck + lane load

The predicted and measured strain values that go along with Figure 4.13 are shown in Table 4.7.

Table 4.7. Test C – Shear predicted and measured strain distribution values, HS-20 truck + lane load

	Predicted Values			Measured Values		
	micro-strain			micro-strain (Avg, Std Dev)		
	S1	S4	S3	S1	S4	S3
Top of Concrete Deck (A)	-195	-166	-95	(-185,0)	(-143,0)	(-97,0)
Girder Top (B)	-34	-29	-17	(-142,8)	(12,3)	(-32,1)
Girder Middle (C)	199	X	97	(202,8)	X	(101,2)
Girder Bottom (D)	441	375	214	(551,30)	(349,10)	(218,5)

Measured versus predicted strain values appear to be similar, other than significant variations in strain values in the B and D locations of Section S1. Location B had a measured value of 108 micro-strain higher than the predicted value, and location D had a measured value of 110 micro-strain higher than the predicted value. After examining the data further, it was seen that the difference between the predicted and measured strain values at these two locations were due to an offset in the data from a prior loading step and should be ignored.

The measured strain values for a load equal to half of the predicted yield load, or 98.5 kips per line load, are shown in comparison to the predicted strain distribution in Figure 4.14.

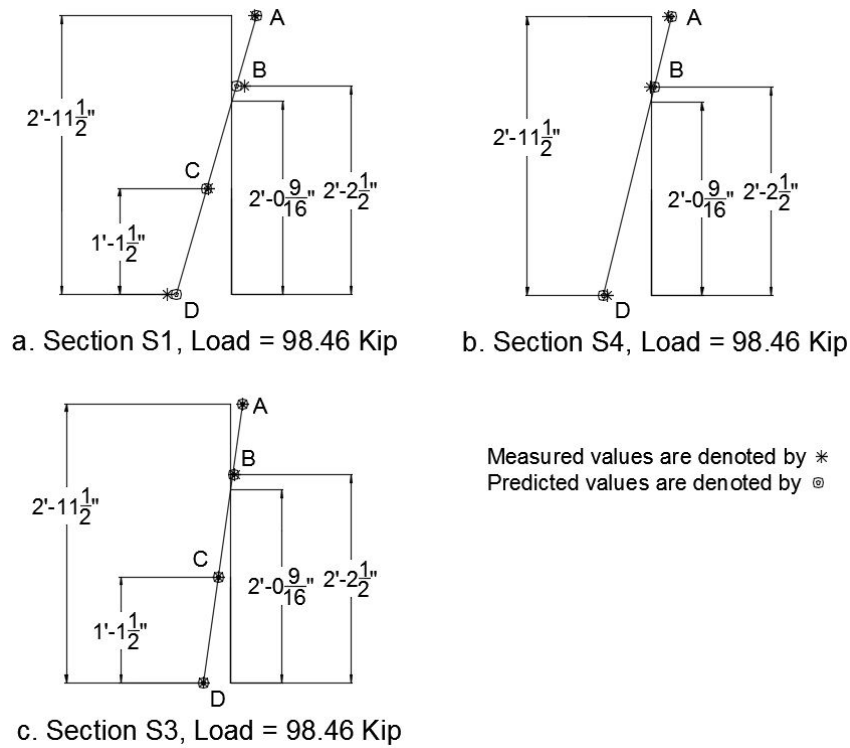


Figure 4.14. Test C – Shear predicted vs. measured strain distributions, load = 98.46 kips

The predicted and measured strain values that go along with Figure 4.14 are shown in Table 4.8.

Table 4.8. Test C – Shear predicted and measured strain distribution values, load = 98.46 kips

	Predicted Values			Measured Values		
	micro-strain			micro-strain (Avg, Std Dev)		
	S1	S4	S3	S1	S4	S3
Top of Concrete Deck (A)	-316	-269	-154	(-285,0)	(-227,0)	(-153,0)
Girder Top (B)	-55	-47	-27	(-165,2)	(11,2)	(-53,1)
Girder Middle (C)	322	X	156	(302,41)	X	(159,1)
Girder Bottom (D)	714	606	347	(824,33)	(559,16)	(347,7)

Measured versus predicted strain values appear to be similar, other than significant variations in strain values in the B and D locations of Section S1. Location B had a measured value of 110 micro-strain higher than the predicted value, and location D had a measured value of 110 micro-strain higher than the predicted value. After examining the data further, it was seen that the

difference between the predicted and measured strain values at these two locations were due to an offset in the data from a prior loading step and should be ignored.

The measured strain values for a load equal to the predicted yield load, or 197 kips per line load, are shown in comparison to the predicted strain distribution in Figure 4.15.

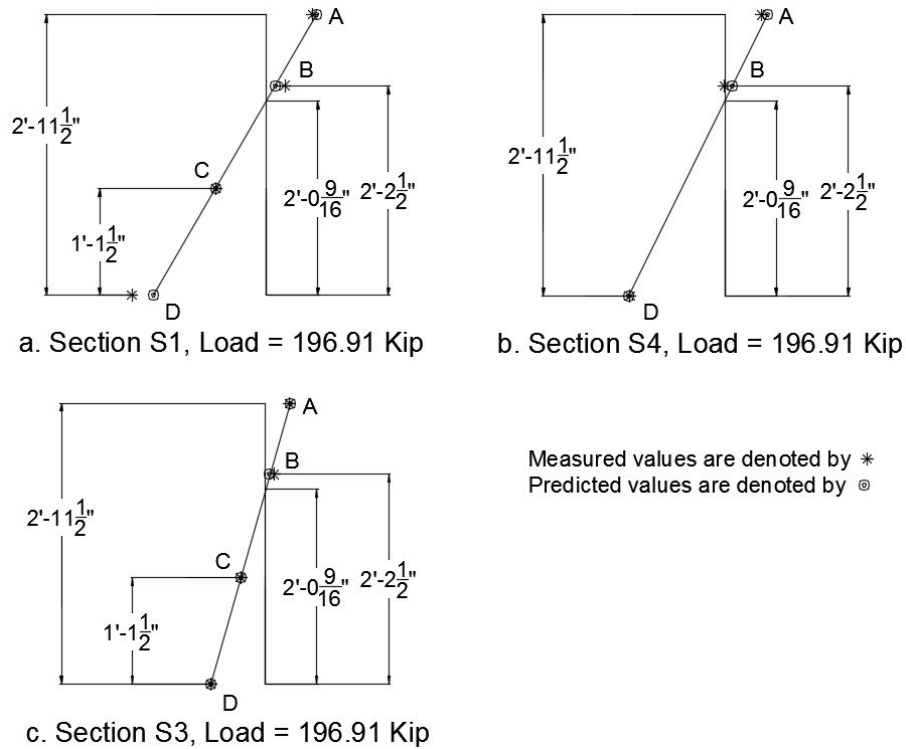


Figure 4.15. Test C – Shear predicted vs. measured strain distributions, load = 196.91 kips

The predicted and measured strain values that go along with Figure 4.15 are shown in Table 4.9.

Table 4.9. Test C – Shear predicted and measured strain distribution values, load = 196.91 kips

	Predicted Values			Measured Values		
	micro-strain			micro-strain (Avg, Std Dev)		
	S1	S4	S3	S1	S4	S3
Top of Concrete Deck (A)	-633	-537	-307	(-580,0)	(-463,0)	(-301,0)
Girder Top (B)	-110	-94	-54	(-233,6)	(9,3)	(-109,0)
Girder Middle (C)	644	X	313	(635,77)	X	(314,1)
Girder Bottom (D)	1427	1212	693	(1695,72)	(1197,29)	(693,12)

Measured versus predicted strain values appear to be similar, other than significant variations in strain values in the B and D locations of Section S1 and the B location of Section S4.

In Section S1, location B had a measured value of 123 micro-strain higher than the predicted value, and location D had a measured value of 268 micro-strain higher than the predicted value. After examining the data further, it was seen that the difference between the predicted and measured strain values at these two locations were due to an offset in the data from a prior loading step and should be ignored for location B only. The offset was only 126 micro-strain in location D, which still leaves a significant difference of 142 micro-strain above the predicted value.

In Section S4, location B had a measured value of 103 micro-strain lower than the predicted value. After further inspection of the data, it was found that the strain gauge in this location may not have been working properly during Test C and should be ignored.

The measured and predicted loads versus displacements for Test C of Sections S1, S2, and S3 are shown in Figure 4.16, Figure 4.17, and Figure 4.18, respectively.

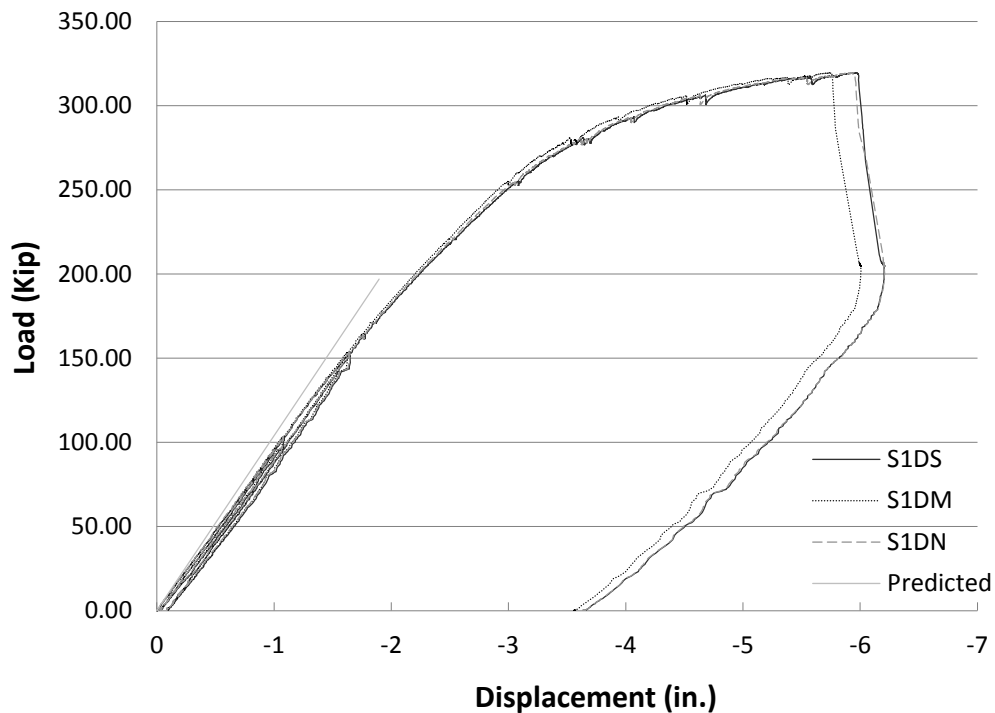


Figure 4.16. Test C – Shear load vs. displacement, Section S1

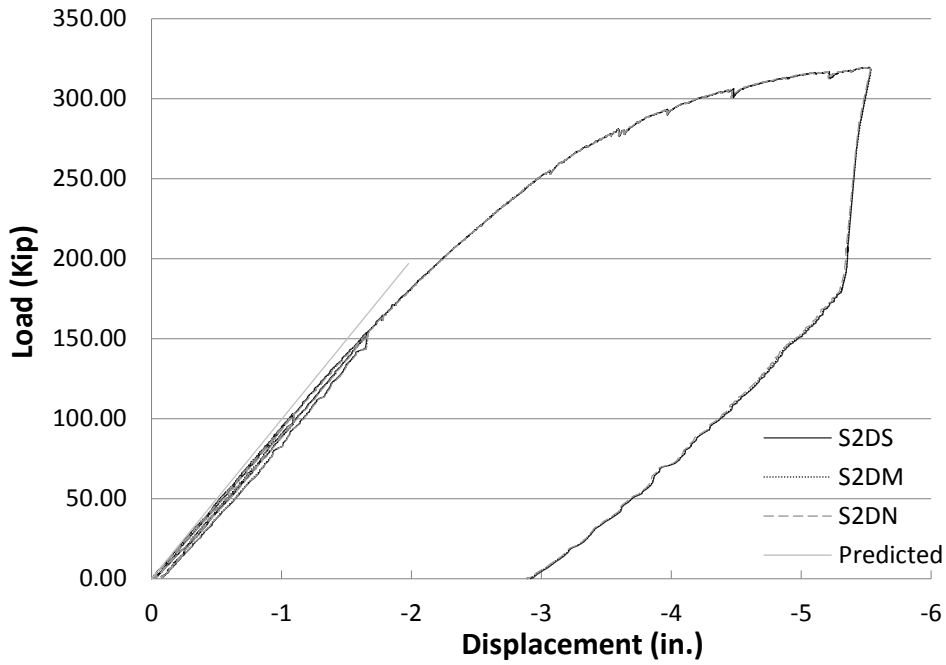


Figure 4.17. Test C – Shear load vs. displacement, Section S2

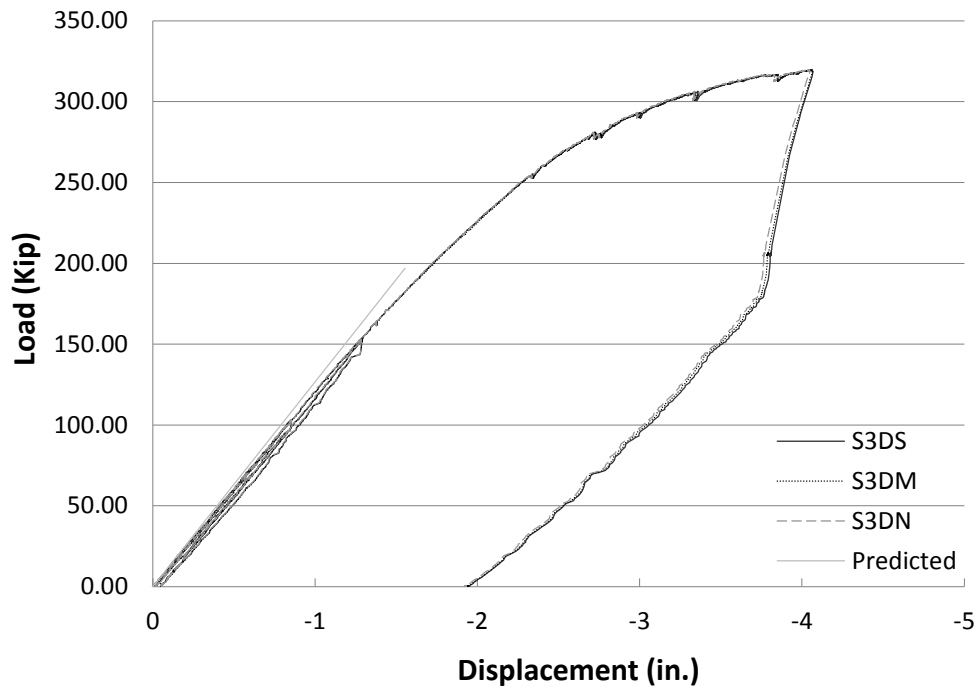


Figure 4.18. Test C – Shear load vs. displacement, Section S3

Displacements measured for all three sections were consistently larger than predicted values. Displacements of Section S1 were 0.088 in. larger than the predicted 0.462 in. for a load

comparable to the design truck (HS-20) and 0.105 in. larger than the predicted 0.611 in. for a load comparable to the design truck (HS-20) with lane load. Displacements of Section S1 were 0.112 in. larger than the predicted 0.989 in. for half of the yield load or 98.5 kips per line load and 0.221 in. larger than the predicted 1.977 in. for the yield load or 197 kips per line load.

After further examination of the data, it was seen that there was an additional offset of 0.079 in. due to a prior loading step, which these displacements should be reduced by. Including this reduction makes both of the HL-93 loading displacements similar to their predicted values.

An additional amount of displacement took place due to an unexpected support displacement on the west end, which was measured to be a total of 0.25 in. after failure had taken place.

The support displacements are shown in Figure 4.19, but due to the measured displacements not being exactly under the support, it is unknown how the additional support displacement would have gradually affected the other displacement values.

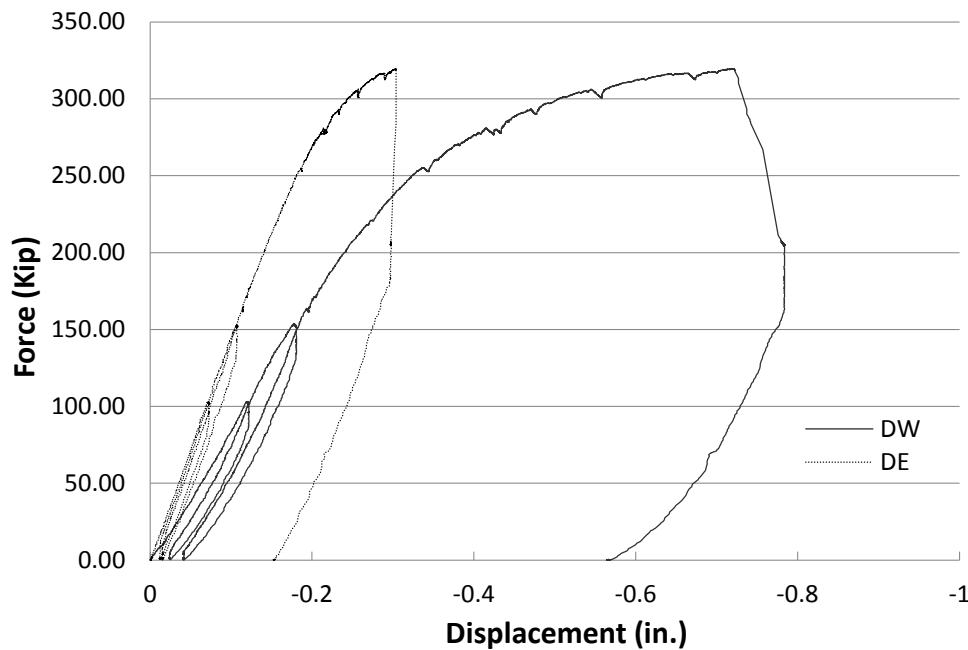


Figure 4.19. Test C – Shear load vs. support displacement

4.3.2 Shear Data

Before the strain rosette data were useful, the shear strain values had to be calculated from the raw data. The strain rosettes measure three normal strains acting in different directions. These three normal strain values can be used to compute the shear strain at the intersection of the three directions using the strain transformation Equation 4.1 (Riley et al. 2007).

$$\varepsilon_n = \varepsilon_x \times \cos^2(\theta_n) + \varepsilon_y \times \sin^2(\theta_n) + \gamma_{xy} \times \sin(\theta_n) \times \cos(\theta_n) \quad (4.1)$$

where, ϵ_n is the measured strain, ϵ_x is the strain in the x direction, ϵ_y is the strain in the y direction, γ_{xy} is the shear strain, and θ_n is the angle from the reference x axis to the axis of the measured strain value ϵ_n .

Creating three equations from the three normal strains and their respective angles from the x axis and solving them simultaneously generates the values for ϵ_x , ϵ_y , and γ_{xy} . The measured shear strain values can now be compared to their predicted values.

The measured and predicted loads versus shear strains for Test C of Sections C1, C2, and C3 for the top location are shown in Figure 4.20, Figure 4.21, and Figure 4.22, respectively.

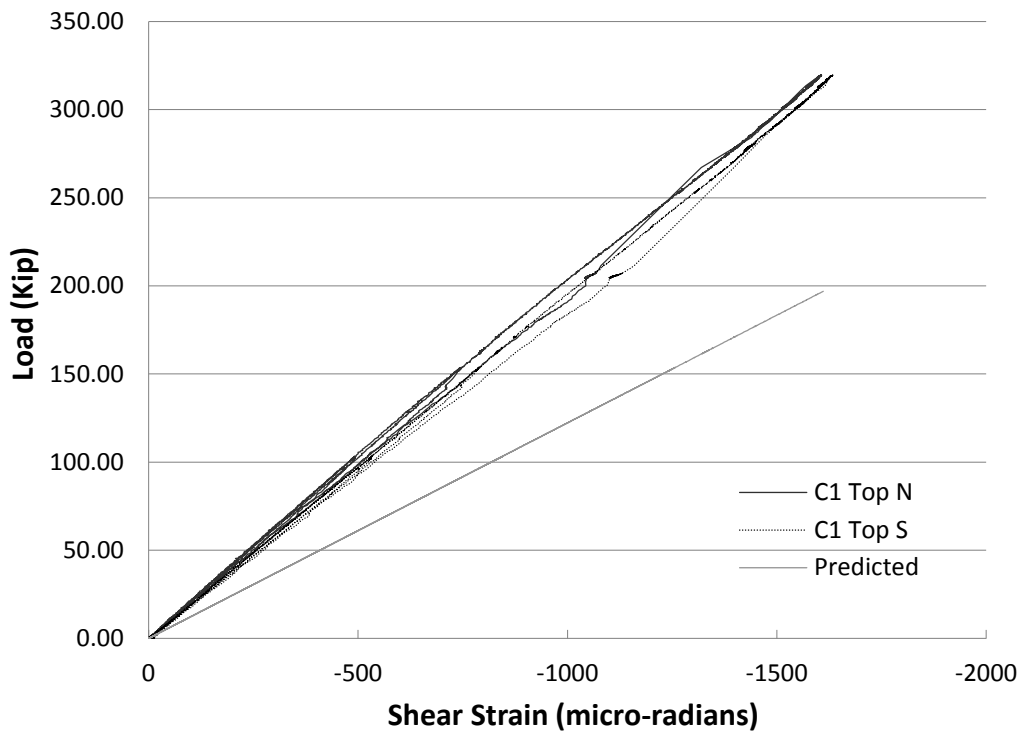


Figure 4.20. Test C – Shear load vs. shear strain, Section C1 top

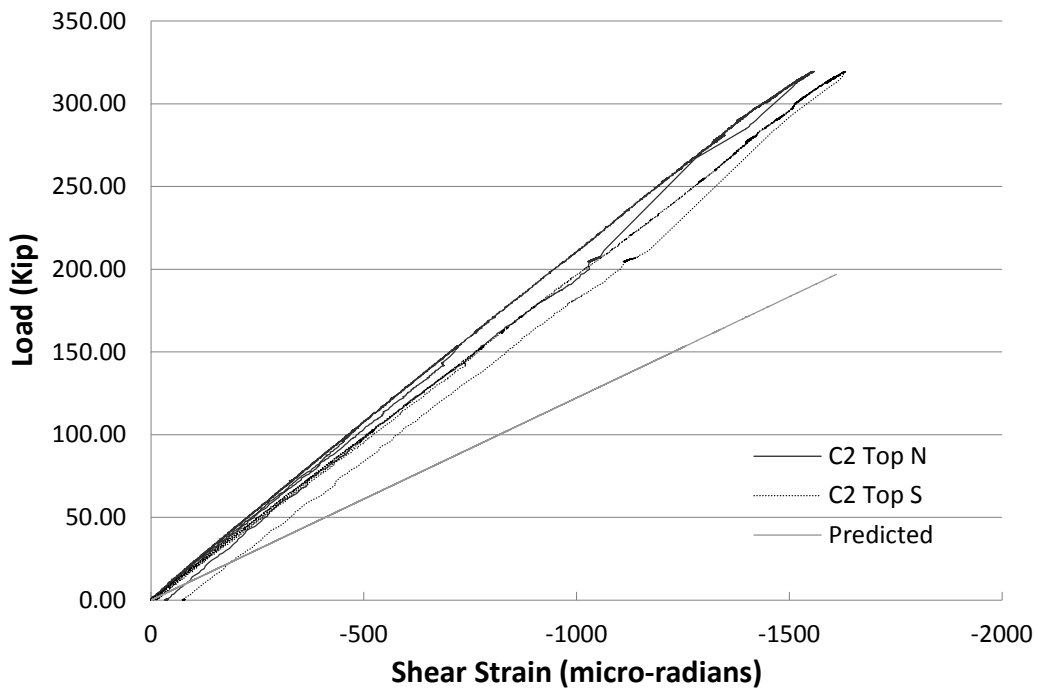


Figure 4.21. Test C – Shear load vs. shear strain, Section C2 top

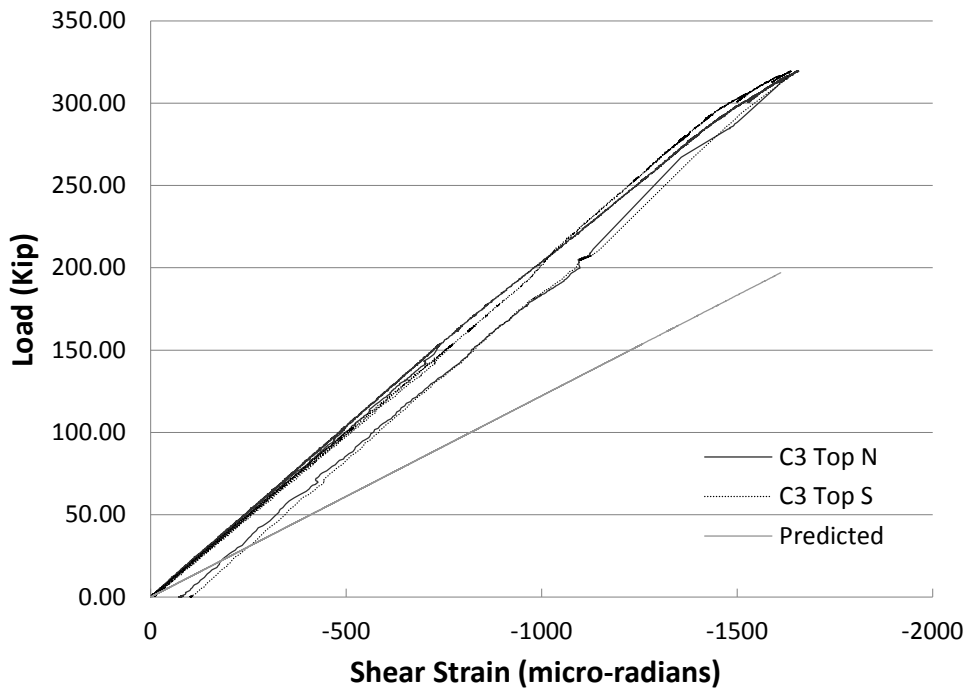


Figure 4.22. Test C – Shear load vs. shear strain, Section C3 top

Shear stains measured for all three sections were consistently smaller than predicted values. At the predicted yield load in all locations, the measured values were all about 600 micro-radians lower than predicted.

The measured and predicted load versus shear strain for Test C of Sections C1, C2, and C3 for the bottom location are shown in Figure 4.23, Figure 4.24, and Figure 4.25, respectively.

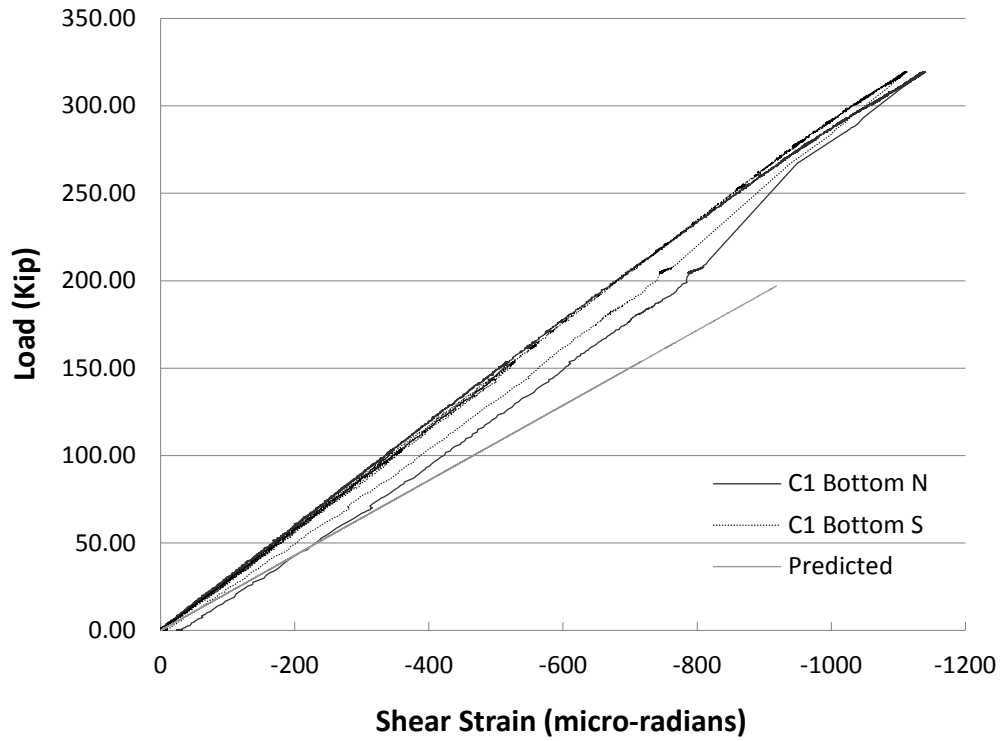


Figure 4.23. Test C – Shear load vs. shear strain, Section C1 bottom

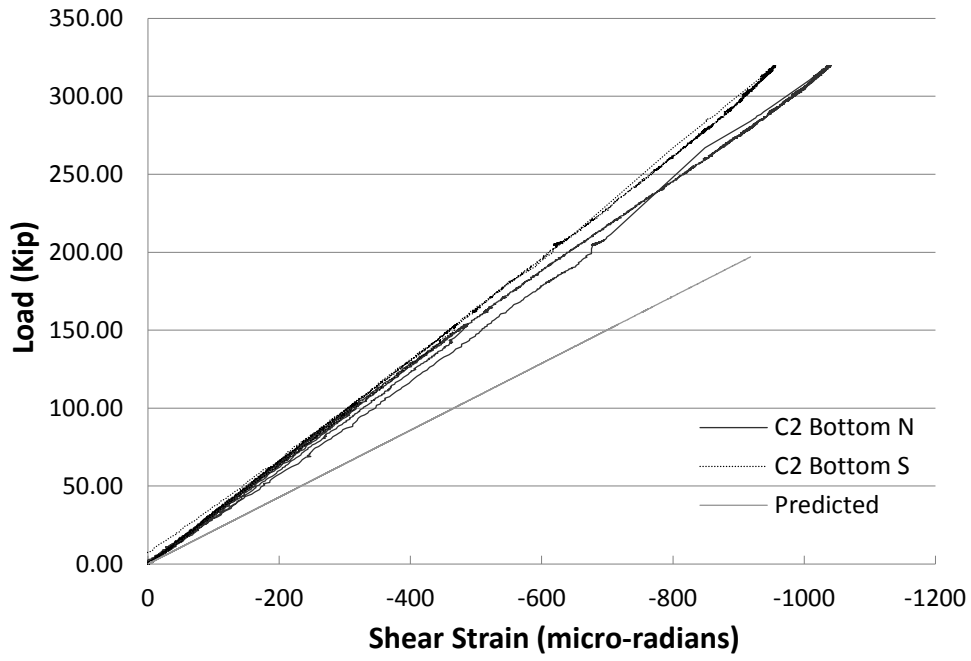


Figure 4.24. Test C – Shear load vs. shear strain, Section C2 bottom

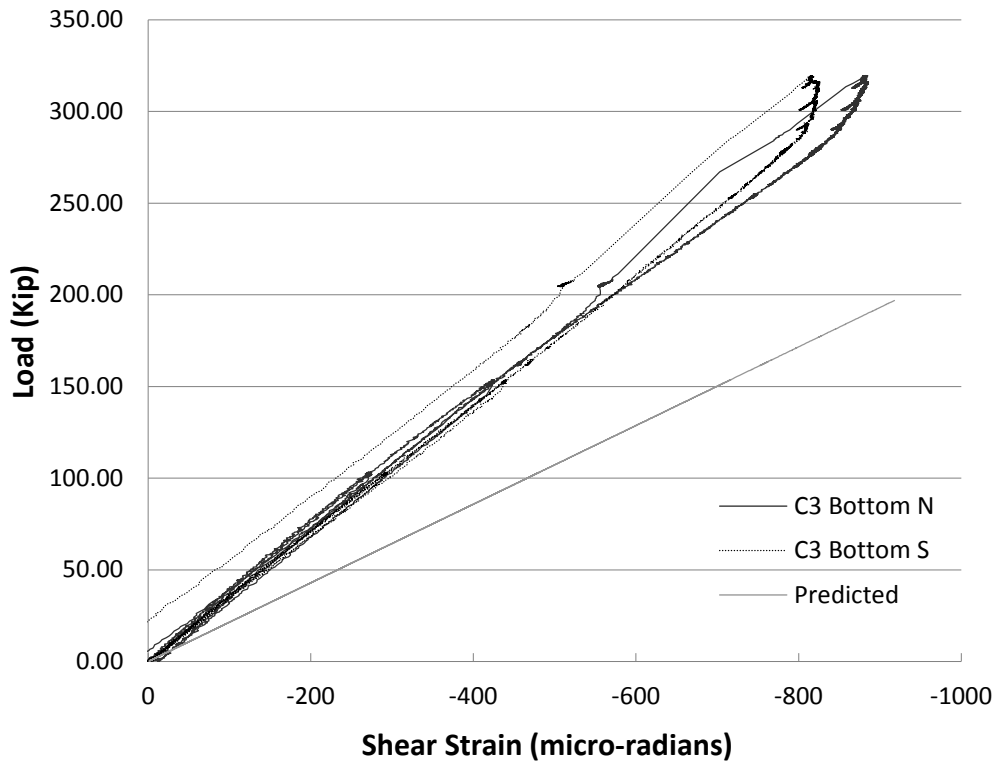


Figure 4.25. Test C – Shear load vs. shear strain, Section C3 bottom

Shear stains measured for all three sections were consistently smaller than predicted values. At the predicted yield load in all locations, the measured values were all about 300 micro-radians lower than predicted.

The largest principal stresses measured for both the top and bottom strain rosette locations were found to be on the north side of the beam in Section C3. These principal strains were measured at a load of 320 kips per line load right before beam failure. The principal stresses and the maximum shear stresses were found using Mohr's circle for plane stresses (Riley et al. 2007) and are shown in Figure 4.26.

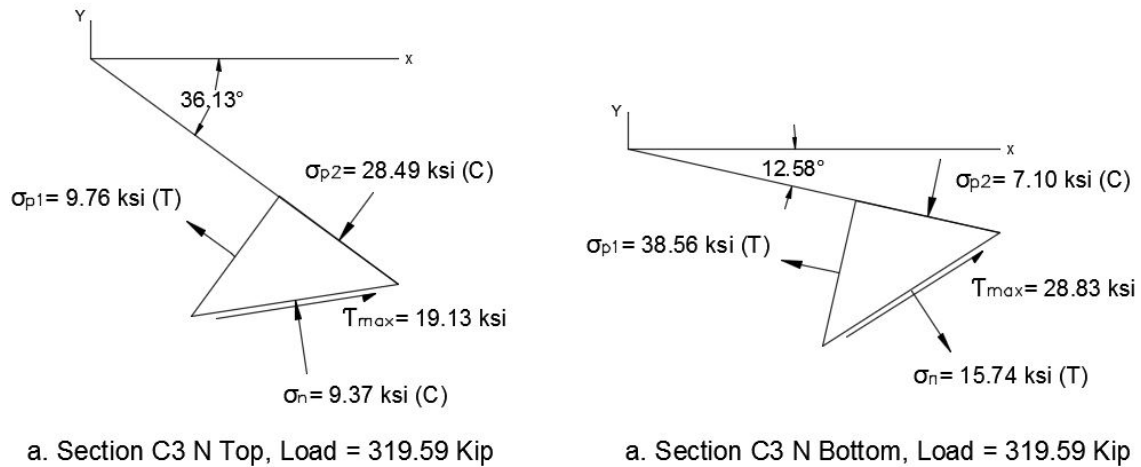


Figure 4.26. Calculated principal stresses from strain rosettes on the north side of Section C3

The bottom location had a maximum shear stress of 28.8 ksi and its largest principal stress was σ_{p1} with a tensile stress of 38.6 ksi. The top location had a maximum shear stress of 19.13 ksi and its largest principal stress was σ_{p2} with a compressive stress of 28.5 ksi. The beam ultimately failed in flexure due to the deck failing at 320 kips per line load, or a moment of 4,612 kip-ft, which is not too far from the predicted plastic moment capacity of 277 kips per line load, or a moment of 4,003 kip-ft. The deck failure is shown in Figure 4.27.



Figure 4.27. Deck failure

4.4 Laboratory Test Summary and Conclusions

For the first test (Test A – Constructability), there were slight differences in measured microstrains and slightly larger than predicted displacements.

For the second test (Test B – Flexure), at a load comparable to the design truck (HS-20), or a moment of 664 ft-kip, strain values were similar to those predicted and the mid-span displacement was 0.663 in., which was 0.044 in. larger than predicted. A displacement of 0.663 in. equates to a displacement of L over 941 without any lateral LDFs considered.

For a load comparable to the design truck (HS-20) plus lane load, or a moment of 878 kip-ft, there were slightly higher strains on the bottom flange than predicted and the mid-span displacement was 0.913 in., which was 0.094 in. larger than predicted. A displacement of 0.913 in. equates to a displacement of L over 684.

Strain values started to become much larger than those that were predicted at a moment of 1,739 kip-ft, so loading was stopped. This was well below the predicted yield moment of 2,767 kip-ft.

The micro-strains along the bottom flange in all three locations read about 1,170 micro-strain, which is a few hundred micro strain above predicted values.

The total displacement at mid-span was 2.01 in., which was 0.389 in. higher than the predicted displacement. A displacement of 2.01 in. equates to a displacement of L over 310.

For the last test (Test C – Shear), the bent plate girder performed similarly to that of Test B in respect to predictions, but resembled the predicted yield load much more closely than in Test B. There were some issues with an unexpected support displacement that could slightly skew some of the load-displacement data at higher loads.

In terms of the shear data, all of the shear strains that were measured for both the top and bottom gauge locations were much lower than predicted for the yield load: 600 micro-radians lower for the top and 300 micro-radians lower for the bottom.

The beam ultimately failed in flexure due to deck concrete failing in compression at a moment of 4,612 kip-ft which is not, all things considered, too different from the predicted plastic moment capacity of 4,003 kip-ft. From this, it can be seen that shear capacity should not be an issue with the bent plate girder design.

CHAPTER 5 FIELD TESTING AND FINITE ELEMENT MODELING OF A FOLDED PLATE GIRDER BRIDGE

Field testing was conducted on the Amish Sawmill Bridge, which was designed using folded plate girders on the secondary road system in Buchanan County, Iowa (see Figure 5.1).

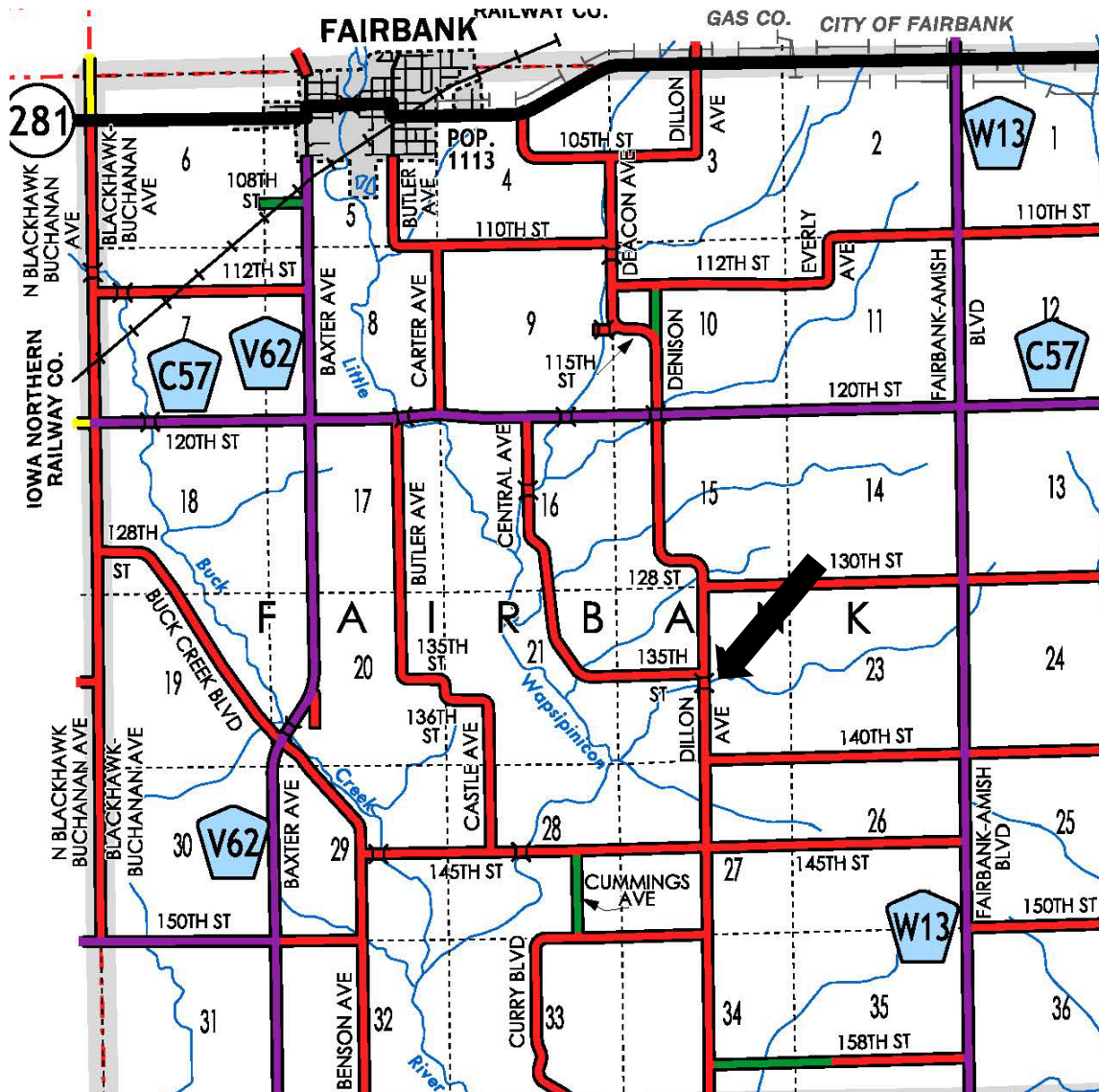


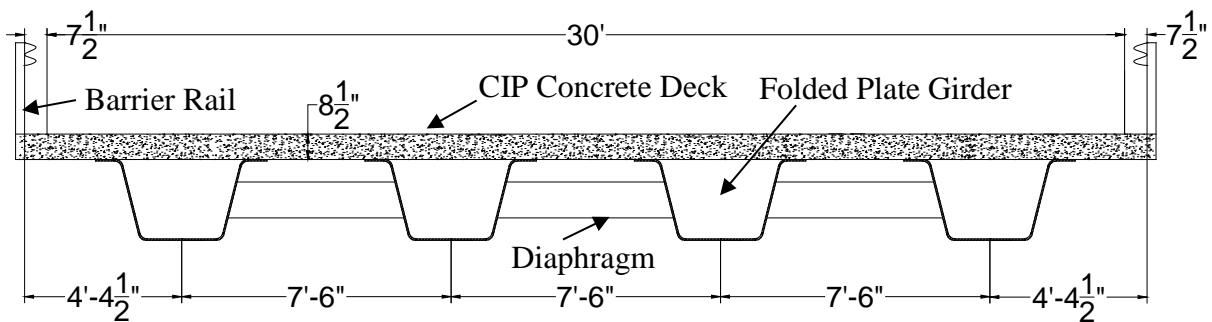
Figure 5.1. Location of Amish Sawmill Bridge on Dillon Avenue south of 135th Street in Buchanan County, Iowa

Shortly after completion of bridge construction, the researchers conducted a live load field test (Test I) to evaluate the structural behavior of the bridge. About a year after construction, they conducted a similar follow-up load test (Test II) to further track the bridge behavior over time. FE models were established to further study the bridge behavior and interpret the test results.

5.1 Bridge Description

The Amish Sawmill Bridge is a single-span folded plate girder bridge with a span length of 52 ft and a roadway width of 30 ft. The bridge has four folded plate girders, each of which has the same material and geometric details as those of the girder specimen that was used for the laboratory testing.

Two bid alternatives were deemed feasible to construct the bridge. One alternative (shown previously in Figure 2.4) was to use precast deck modules connected using ultra-high performance concrete (UHPC) closure pours, and the other was to use a cast-in-place (CIP) concrete deck. The Amish Sawmill Bridge was constructed using the CIP concrete deck, as shown in Figure 5.2.

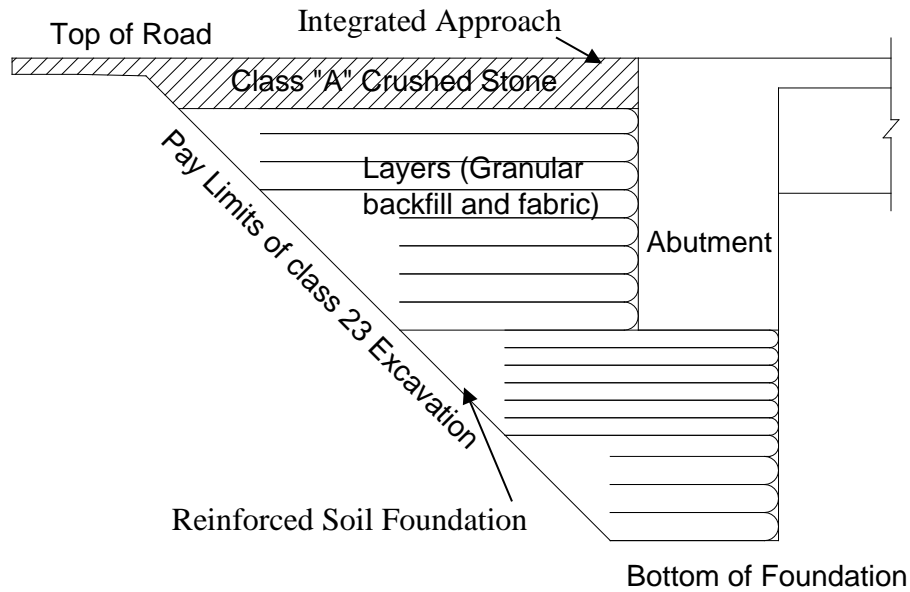


Adapted from Buchanan County plans

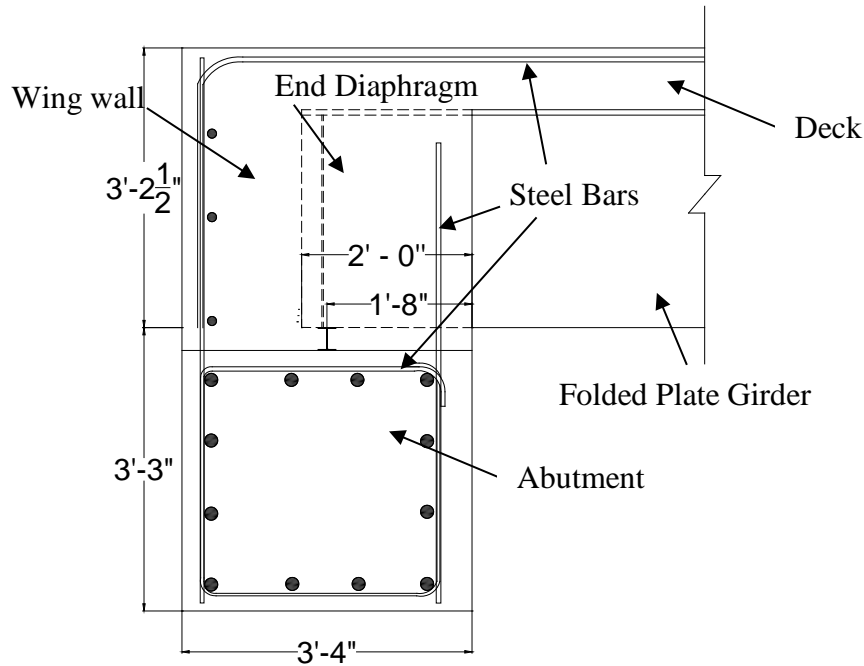
Figure 5.2. Cross-section view of Buchanan County folded plate girder bridge

The girder length is 52 ft 6 in., the girder spacing is 7 ft 6 in., and the deck depth is 8.5 in. Six diaphragms were placed between the girders at the one-third and two-third points of the girder length, and all diaphragms have a cross-section of MC12x31.

A GRS-IBS was utilized due to the merits of this innovative technology, including reduction of bridge construction time and cost, as well as elimination of settlement issues associated with the joint between the approach slab and the bridge deck, which can create bumps in the approach (FHWA 2016). The GRS-IBS consists of three elements—reinforced soil foundation, integrated approach, and abutment—as shown in Figure 5.3(a).



(a) GRS-IBS



(b) Abutment

Figure 5.3. Details of GRS-IBS and abutment

The reinforced soil foundation includes alternating layers of compacted granular soil and geosynthetic fabric and provides support to the abutment. The integrated approach eliminates the need for joints, creates a smooth transition between the bridge end and the approach roadway, and alleviates the bump at the bridge end due to differential settlement.

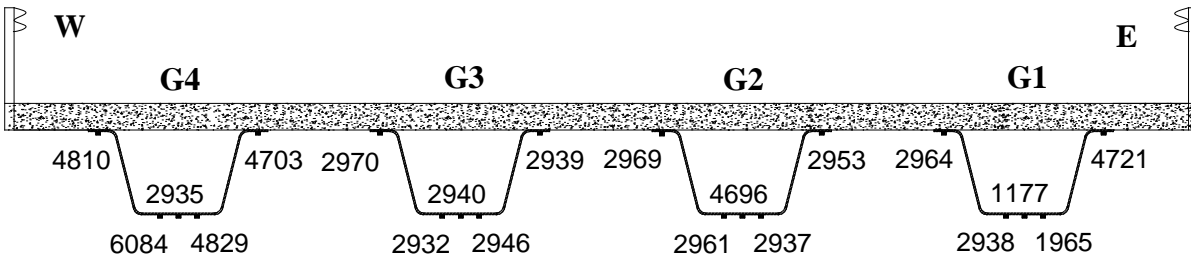
The details of the abutments are shown in Figure 5.3(b). The wing walls are monolithically constructed along with the deck and is integrated with the integral abutment by the steel bars.

The girder ends are embedded into the end abutment supports, which have direct interaction with the foundation and provide significant end restraint to the girders.

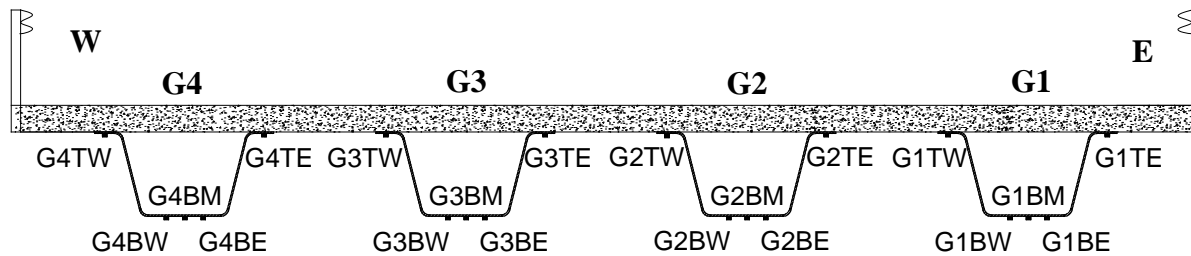
5.2 Details of Field Tests

5.2.1 Instrumentation and Loading Plan

The researchers conducted two field tests to measure the bridge behavior under live loading. For Test I, 20 strain gauges were installed on the four girders at mid-span, as shown in Figure 5.4.



(a) Original Test I gauge identifiers at mid-span



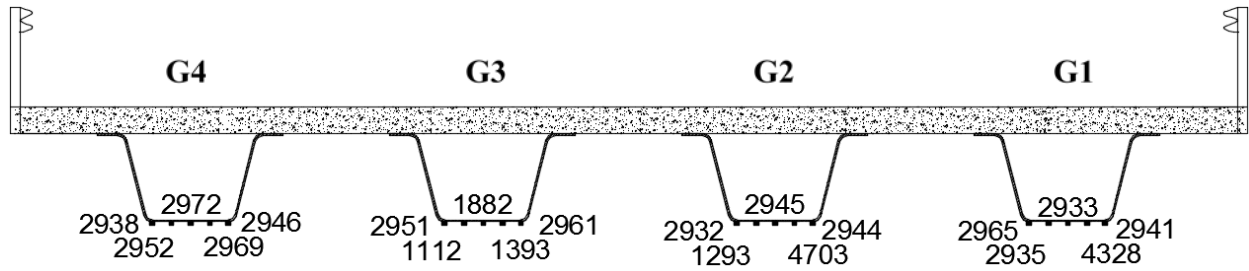
(b) Revised Test I gauge identifiers at mid-span

Figure 5.4. Strain gauges installed on the bridge – Test I

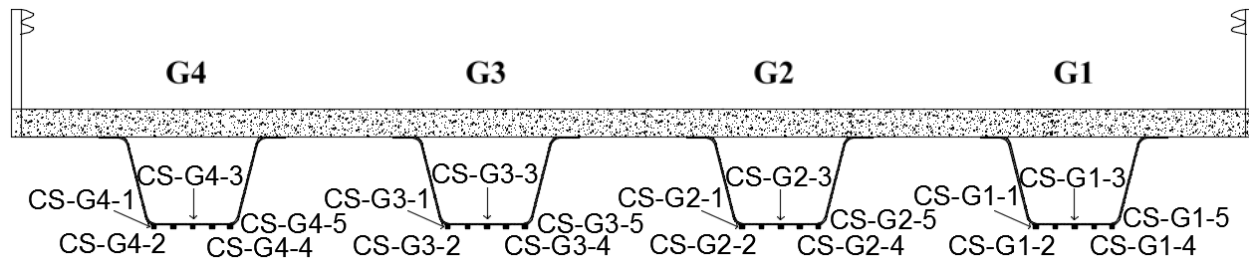
The gauge identifiers originally used during Test I field testing are shown in Figure 5.4(a), and the revised identifiers given to the gauges to more clearly indicate their locations on the bridge girders (for presentation in this final report) are shown in Figure 5.4(b). Specifically, G, the numbers, and B, T, W, and E represent girder, girder number from east to west, and bottom, top, west, and east, respectively.

As shown, five strain gauges were installed on each girder as follows: one on the bottom of each side of the top flange, one on each one-fourth point, and one on the mid-point of the bottom of the bottom flange.

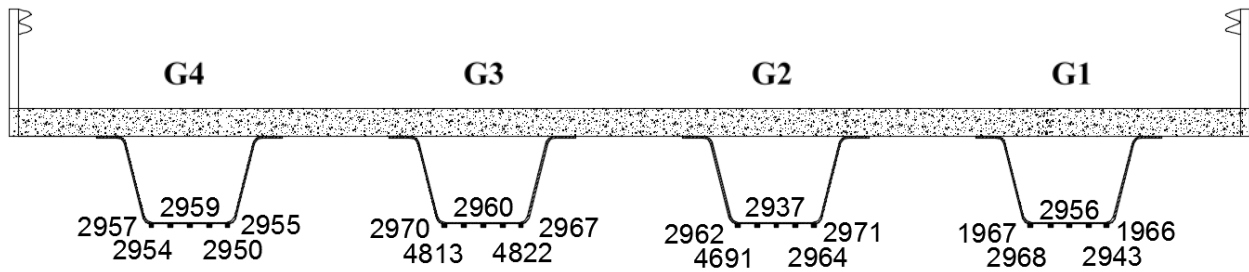
As shown in Figure 5.5, for Test II, 20 strain gauges were installed on the four girders (at the mid-span and abutment) as follows: one on each end, one on each one-fourth point, and one on the mid-point of the bottom of the bottom flange.



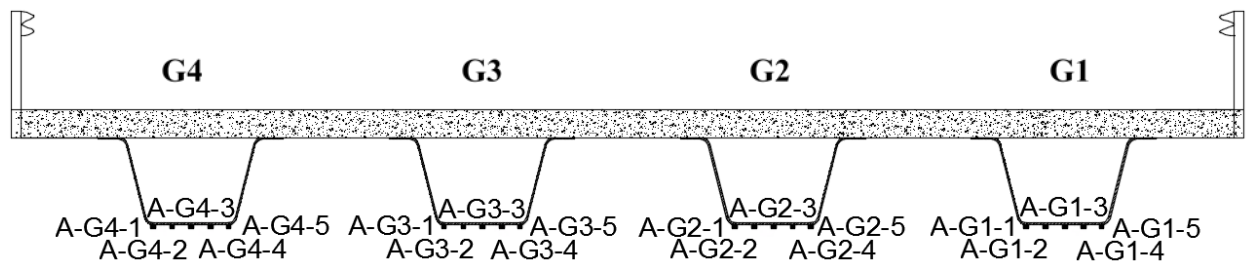
(a) Original Test II gauge identifiers at mid-span



(b) Revised Test II gauge identifiers at mid-span



(c) Original Test II gauge identifiers at abutment



(d) Revised Test II gauge identifiers at abutment

Figure 5.5. Strain gauges installed on the bridge – Test II

For Test II, the gauge identifiers originally used during the field testing are shown in Figure 5.5(a) and Figure 5.5(c), and the revised identifiers given to the gauges to more clearly indicate their locations on the bridge girders at mid-span and the abutment (for presentation in this final report) are shown in Figure 5.5(b) and Figure 5.5(d). CS and A represent center span and abutment, respectively, in Figure 5.5(b) and Figure 5.5(d), respectively.

The live loads were applied to the bridge using a dump truck traveling across the bridge at a crawl speed from the south to north. Three load paths were utilized to simulate different load scenarios, as shown in Figure 5.6.

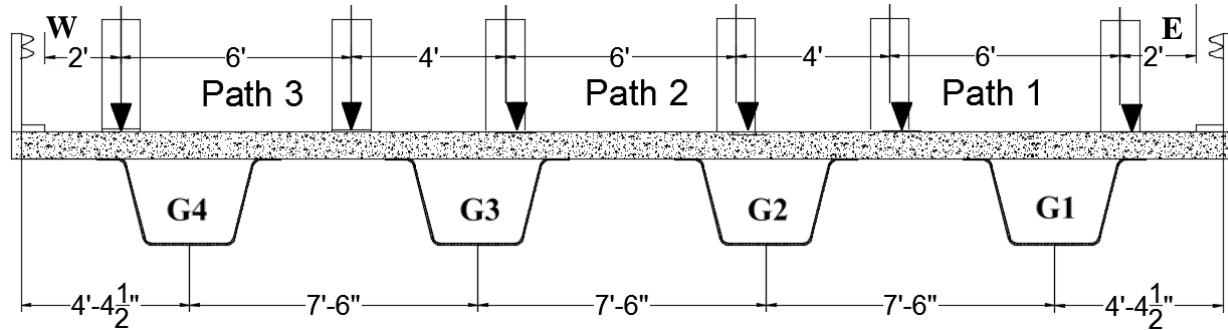


Figure 5.6. Load paths on the bridge

Load Path 1 or 3 represents the loading scenario with the exterior wheel line center located 2 ft away from the inside of the barrier rail. Load Path 1 plus 2 and Load Path 3 plus 2 represent the loading scenarios with two side-by-side trucks spaced at 4 ft. The axle and wheel spacing configurations of the dump trucks for Test I and Test II are shown in Figure 5.7(a) and (b), respectively.

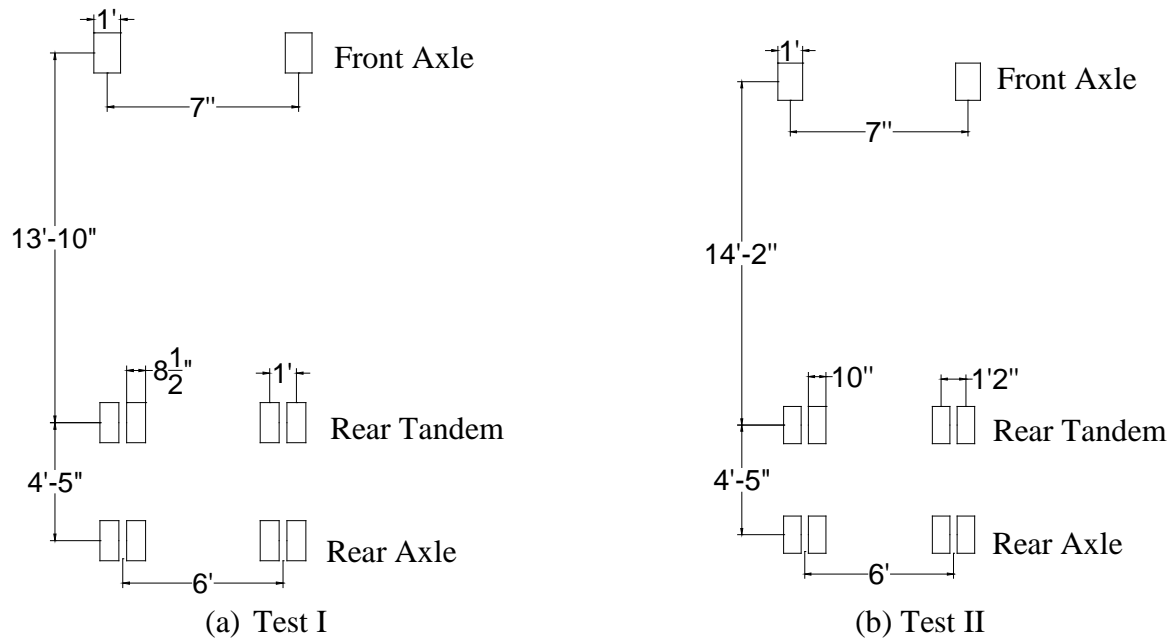


Figure 5.7. Dump truck configurations

As shown, each dump truck had three axles (front, rear tandem, and rear). The gross weight and each axle weight for the two tests are summarized in Table 5.1.

Table 5.1. Truck and axle weights

	Gross Weight (lbs)	Front Axle (lbs)	Rear Tandem (lbs)	Rear Axle (lbs)
Test I	55,580	17,340	19,300	18,940
Test II	55,880	25,700	12,780	17400

5.2.2 Preliminary Analysis of Field Test Data

To preliminarily understand the behavior of the bridge, the measured strain response due to the three load paths from Test I was selected. The strain from Load Path 1 was utilized as an example to present the influence lines due to the truck crossing the bridge. The strain response in the girder bottom flanges for Load Path 1 was plotted against the travel position and is shown in Figure 5.8.

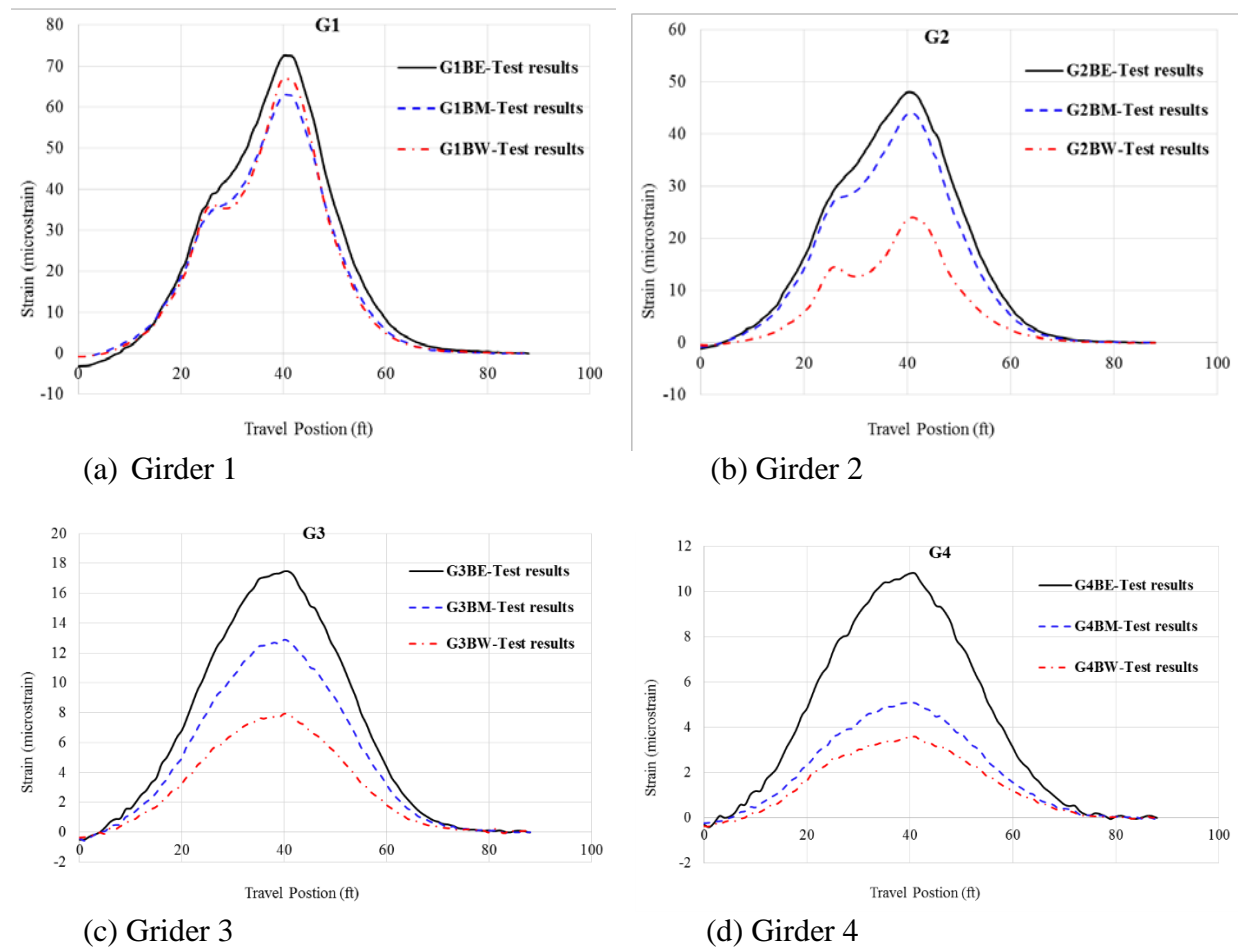
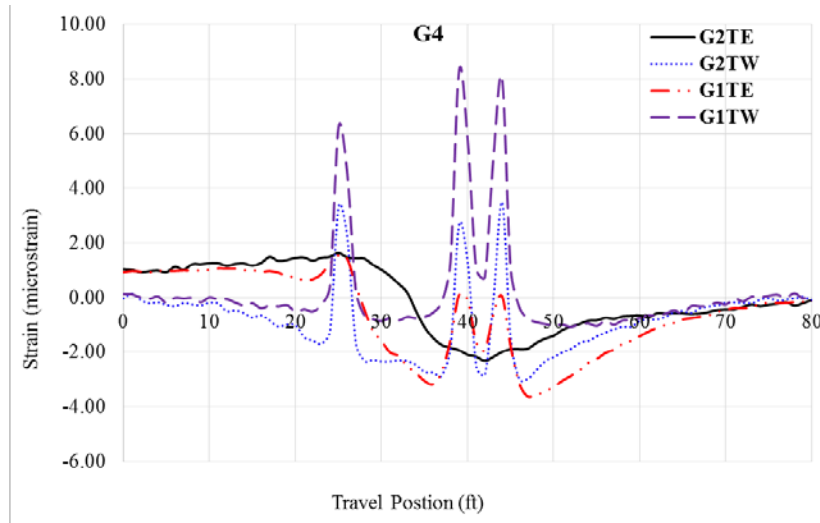


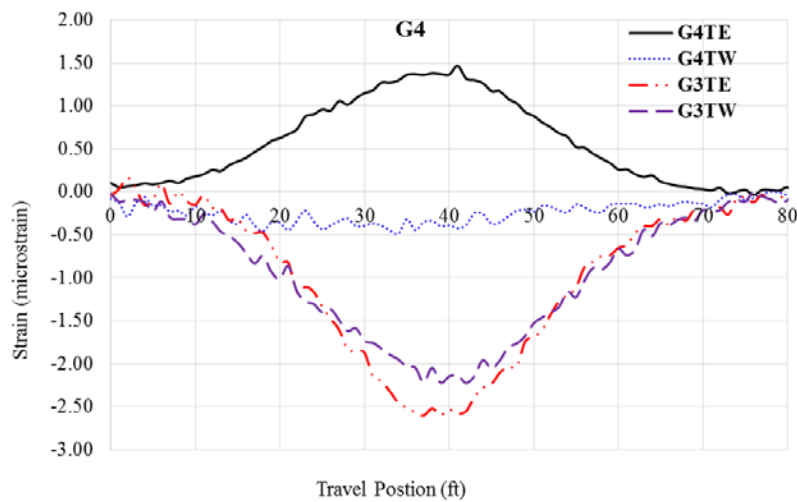
Figure 5.8. Strain response in girder bottom flanges for Load Path 1

The strain response in the girder top flanges for Load Path 1 was also plotted and is shown in Figure 5.8. Figure 5.8 indicates that the strains in the bottom flanges increase from the west to

east. This is mainly due to the shear lag effects of the box-beam cross-section and biaxial bending effects. Figure 5.9(a) indicates that strain spikes exist in the top flange strain gauges close to the truck loading.



(a) Girders 1 and 2

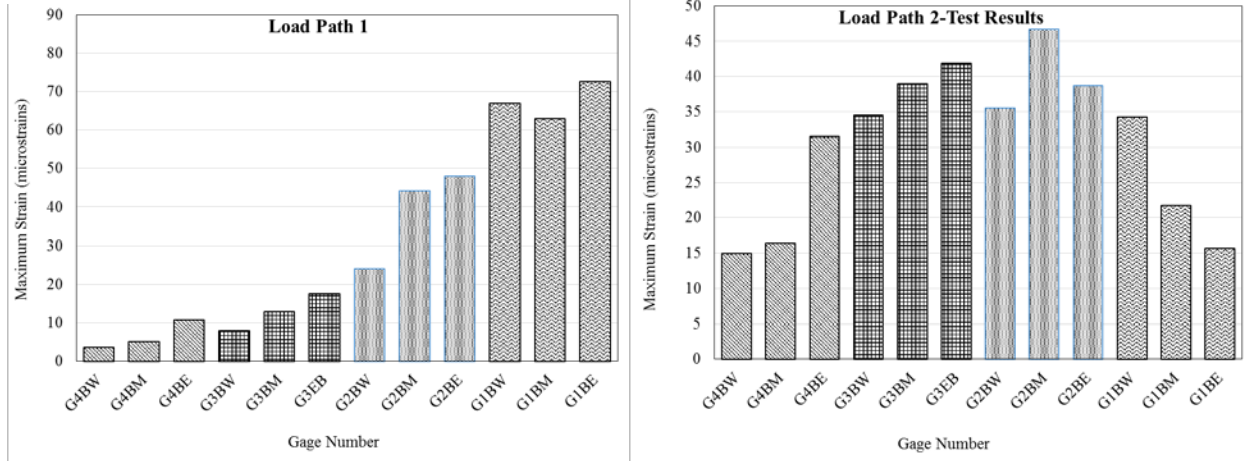


(b) Girders 3 and 4

Figure 5.9. Strain response in girder top flanges for Load Path 1

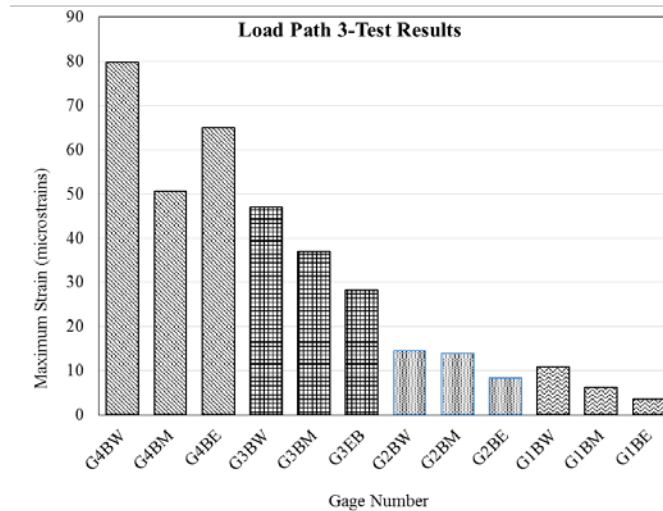
Note that the three spikes were caused by the three axles of the truck. Additionally, Figure 5.9 indicates that the strains in the top flange are small and can be greatly influenced by the localized effects of shear studs in the top flanges. Accordingly, the strains in the top flanges were excluded from further analysis.

The peak strains of all strain gauges on the bottom flanges were collected from different load paths and are illustrated in Figure 5.10.



(a) Load Path 1

(b) Load Path 2



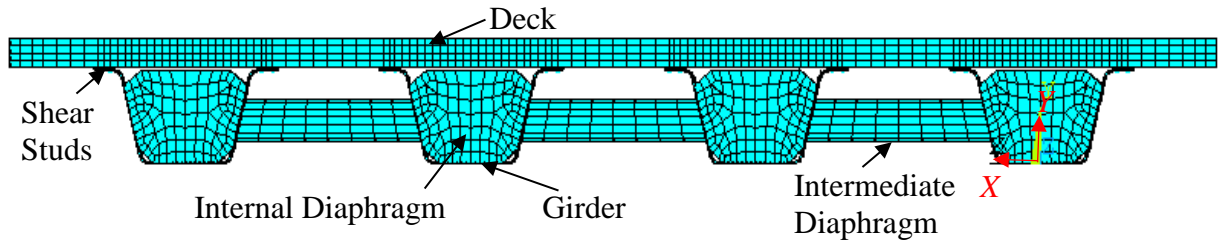
(c) Load Path 3

Figure 5.10. Peak strains in girder bottom flanges from all gauges at mid-span for three load paths – Test I

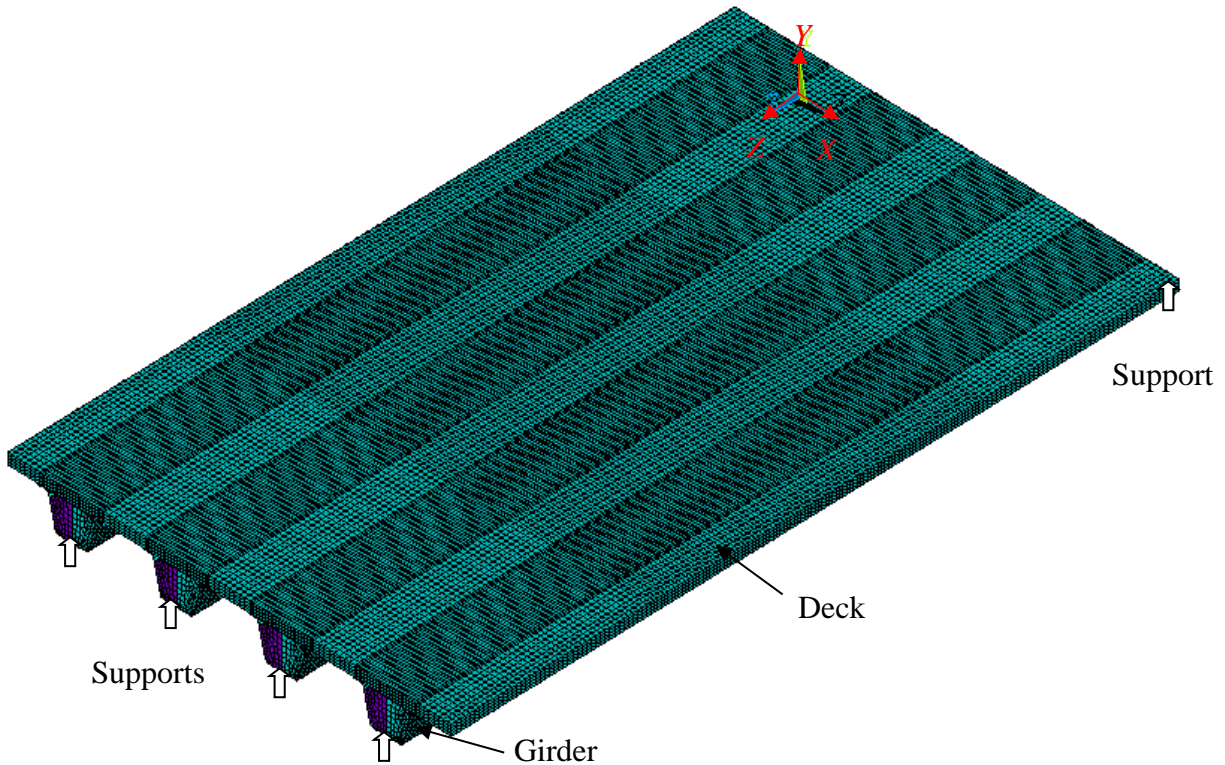
Figure 5.10(a) and Figure 5.10(c) indicate that, when the truck load is located on the east side of the bridge, the strain is higher on the east side of each girder, and, when the truck load is located on the west side of the bridge, the strain is higher on the west side of each girder. Figure 5.10(b) indicates that, for each girder, when the truck load is located in the middle region of the bridge, the strain is generally higher when the strain gauge is relatively closer to the bridge center. The magnitudes of the strain peaks among the four girders due to Load Path 1 have a reversed change pattern compared to those due to Load Path 3.

5.3 Details of FE Modeling

A full bridge model was established using the commercial software ANSYS to further study the behavior of the bridge under the load testing conditions. Cross-section and three-dimensional (3D) views of the FE model are shown in Figure 5.11(a) and Figure 5.11(b), respectively.



(a) Cross-section view



(b) 3D view

Figure 5.11. Full model of the bridge

The bridge model consisted of the deck, girders, shear studs, internal diaphragms, and intermediate diaphragms. The folded plate beam and diaphragms were both modeled using a four-noded SHELL181 element with six degrees of freedom at each node: translations in the x, y, and z directions, and rotations about the x, y, and z axes. An elastic–plastic uniaxial material model with bilinear kinematic hardening was used for the steel and the yield strength, elastic modulus, and Poisson’s ratio of the steel were set to 50 ksi (345 MPa), 29,000 ksi (200 GPa), and 0.3, respectively. The strain hardening modulus (also named tangent modulus) was set to 5% of the elastic modulus. The diaphragms were perfectly connected to the steel girder via shared common nodes, but were not connected with the concrete deck.

The concrete deck was modeled using an eight-noded SOLID65 element, which had three translational degrees of freedom at each node and incorporated cracking (in three orthogonal

directions) and crushing capabilities. The concrete material properties were also assigned with multi-linear isotropic hardening, in combination with the von Mises yield criterion. The stress-strain relationship of the normal-strength concrete proposed by Hognestad (1951) was utilized for the concrete constitutive model:

$$f_c = f'_c \left[2 \left(\frac{\varepsilon}{\varepsilon_o} \right) - \left(\frac{\varepsilon}{\varepsilon_o} \right)^2 \right] \quad (5.1)$$

where, f_c and ε are stress and strain on concrete respectively, and strain at peak stress (ε_o) is expressed as:

$$\varepsilon_o = 0.00078(f'_c)^{1/4} \quad (\text{in MPa}) \quad (5.2)$$

The smeared fixed crack model and Rankine maximum stress criterion were utilized to determine the initiation and development of concrete cracking. According to the AASHTO LRFD specifications for bridges (AAHSTO 2010), maximum concrete tensile strength can be derived by:

$$f_t = 0.24\sqrt{f'_c} \quad (\text{in ksi}) \quad (5.3)$$

For convergence purposes, shear transfer coefficients of 0.3 and 0.6 were used for an open crack and a closed crack, respectively. The smeared reinforcement capacity of the SOILD65 element was utilized to define the amount of reinforcement in the concrete deck. The volume ratios (i.e., the volume of steel bars divided by the total concrete element volume) were defined for both the transverse and longitudinal reinforcement.

The shear studs between the concrete deck and the folded plate beam were modeled using a COMBIN39 element. The COMBIN39 element is a unidirectional spring element that can incorporate a nonlinear generalized force-deflection relationship (ANSYS 2011). This element provides the horizontal shear transfer of the shear studs and was placed where the shear stud was located between the nodes of the deck element and the girder element. The COMBIN39 element was active along the slip direction, and the other two directions of the two nodes were coupled together. For simulation purposes, the shear force-slip relationship proposed by Ollgard et al. (1971) was incorporated in the COMBIN39 element to simulate the shear transfer mechanism of the shear studs at the interface. The adopted shear force-slip relationship of the shear studs was derived based on push-off testing results and can be expressed as:

$$Q = Q_n (1 - e^{-18s})^{\frac{2}{5}} \quad (5.4)$$

where, Q = shear force in a shear stud, s = slip at the weld point of the stud, and, according to AASHTO LRFD Bridge Design Specifications, nominal shear resistance, Q_n , is determined by:

$$Q_n = 0.5A_{sc}\sqrt{f'_cE_c} \leq F_uA_{sc} \quad (5.5)$$

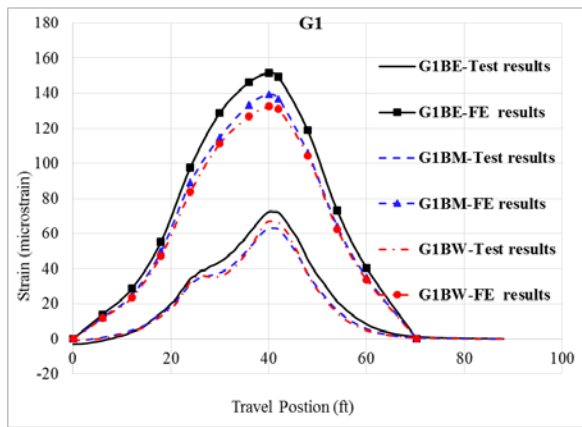
where, A_{sc} = cross-sectional area of the stud, f'_c = compressive strength of concrete, E_c = elastic modulus of the concrete, and F_u = minimum specified tensile strength of the stud (60 ksi).

The boundary conditions of the bridge (i.e., support restraint) were determined by comparing the predicted results with the measured data. The truck loads were applied to the bridge model for the three load paths. The square root sum of the squares (SRSS) and absolute value sum associated with convergence tolerances were utilized to set the convergence criteria for the displacement and force, respectively. To improve the computational convergence of the nonlinear problem, the following strategies were utilized to derive results from the FE model: (1) extra displacement shapes were suppressed and tensile stress relaxation after cracking was incorporated in the SOLID65 elements, (2) a trial-and-error process was performed to select the proper amount of load steps and sub-steps, and (3) auto-step and predictor were utilized to assist in solving the potential computational problem (Deng 2012, Deng and Morcouc 2013, Deng et al. 2013, and Deng et al. 2015).

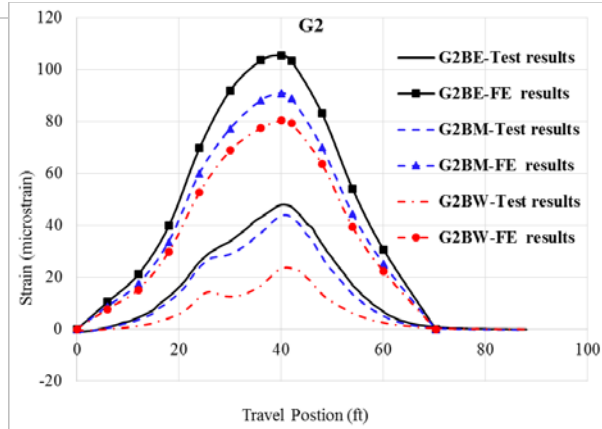
5.4 Comparisons and Discussions of Results

5.4.1 Comparisons of Measured and Predicted Strain Results

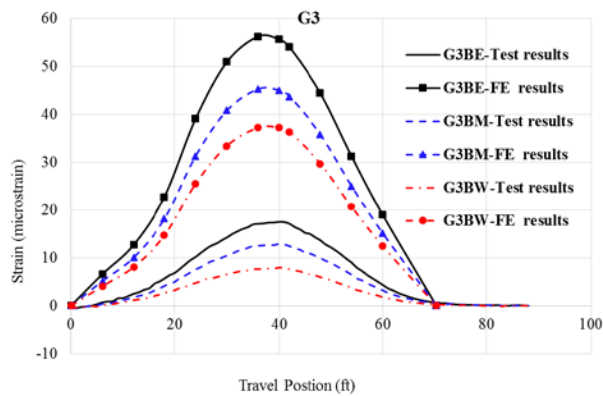
The simply supported boundary condition and the truck loads following Load Path 1 were initially applied to the bridge model. The predicted strain results for the bottom flanges were extracted from the FE model under different travel positions. For Test I, the strain responses in Girders 1, 2, 3, and 4 under Load Path 1 were predicted using the FE model and compared with the test results, as shown in Figure 5.12(a), Figure 5.12(b), Figure 5.12(c), and Figure 5.12 (d), respectively.



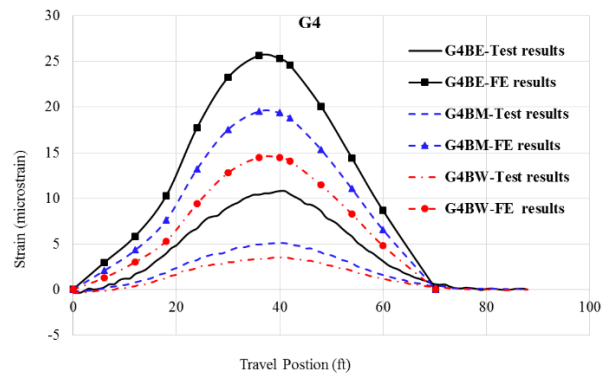
(a) Girder 1



(b) Girder 2



(c) Girder 3

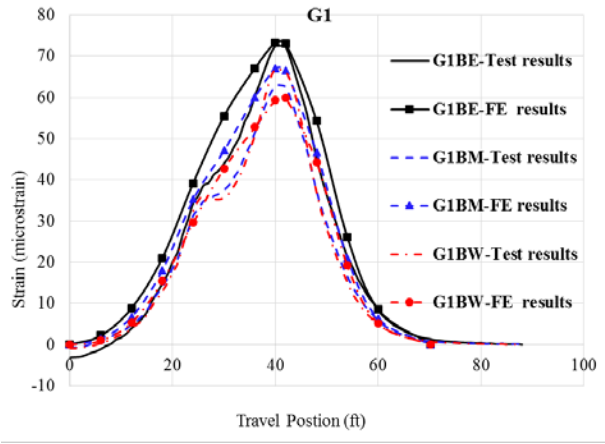


(d) Girder 4

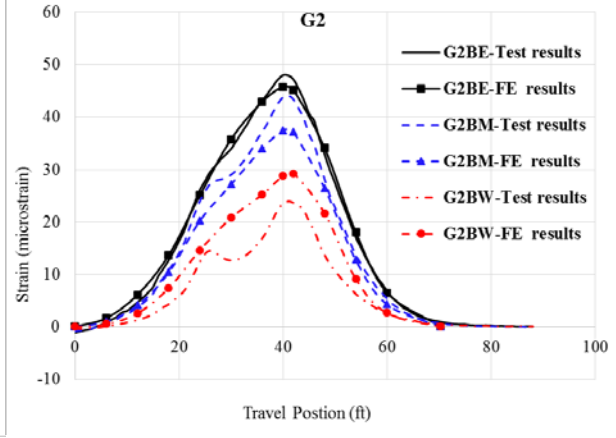
Figure 5.12. Comparisons of strain response in girder bottom flanges at mid-span for Load Path 1 of Test I - simply supported condition

Figure 5.12 indicates that the FE predictions are significantly larger than the test results for the four girders. This is mainly due to the fact that significant support restraint exists at the end supports of the bridge due to the synergetic action of the GRS-IBS, abutments, wing walls, deck, and girders as shown previously in Figure 5.3. Accordingly, the fixed boundary condition was applied to the bridge model to study the amount of girder end restraint.

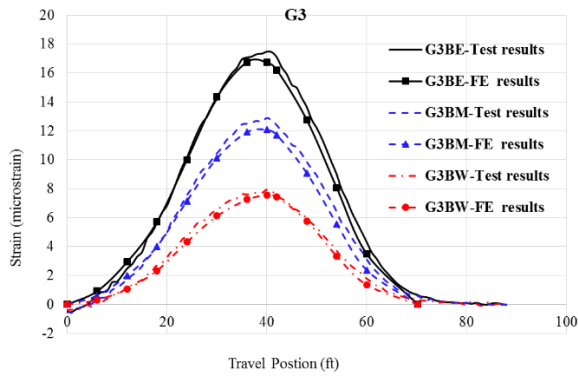
The strain responses in the girders under Load Paths 1, 2, and 3 from Test I were predicted using the FE model and compared with the test results, as shown in Figure 5.13, Figure 5.14, and Figure 5.15, respectively.



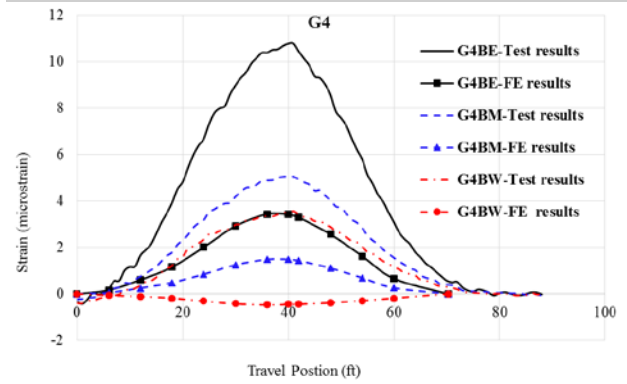
(a) Girder 1



(b) Girder 2

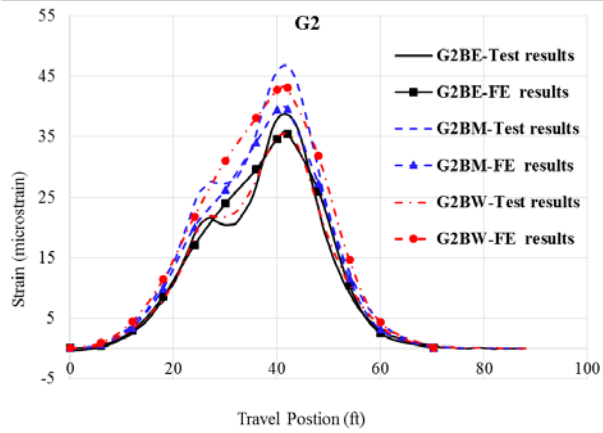


(c) Girder 3

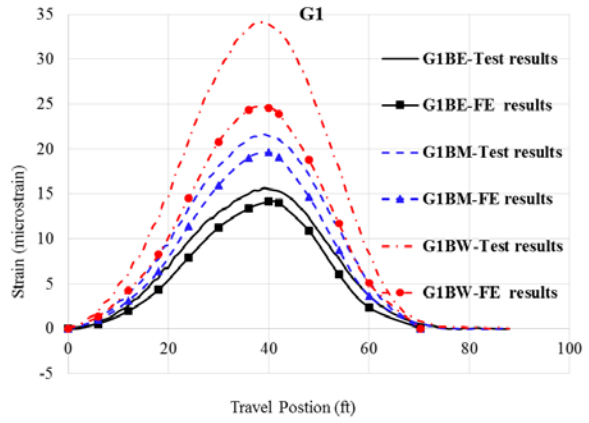


(d) Girder 4

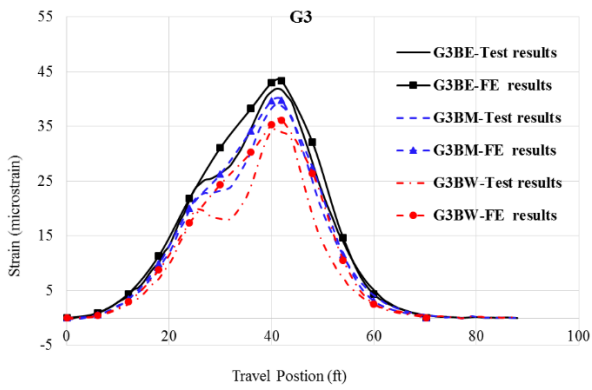
Figure 5.13. Comparisons of strain response in girder bottom flanges at mid-span for Load Path 1 of Test I – fixed support condition



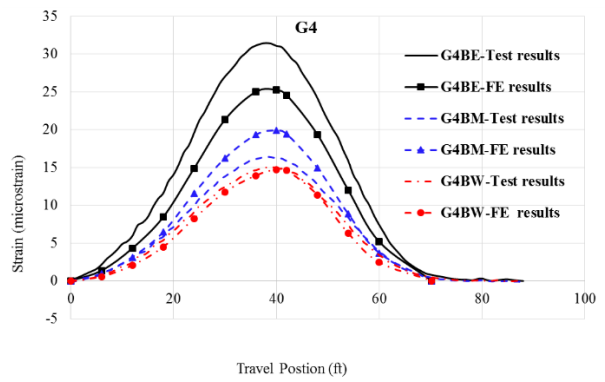
(a) Girder 1



(b) Girder 2



(c) Girder 3



(d) Girder 4

Figure 5.14. Comparisons of strain response in girder bottom flanges at mid-span for Load Path 2 of Test I – fixed support condition

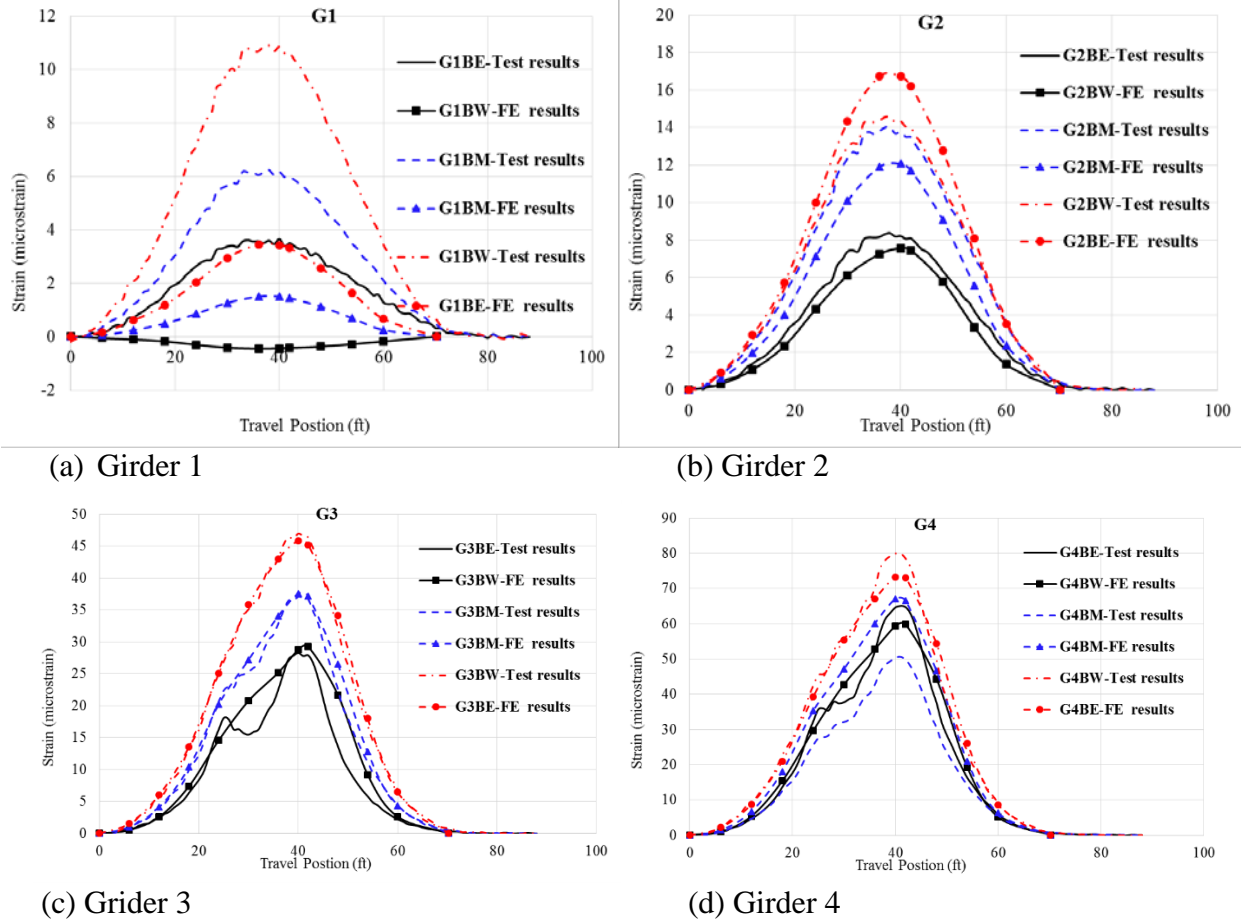
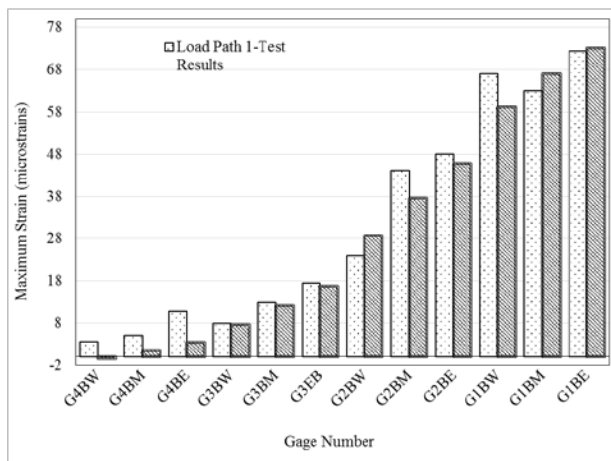
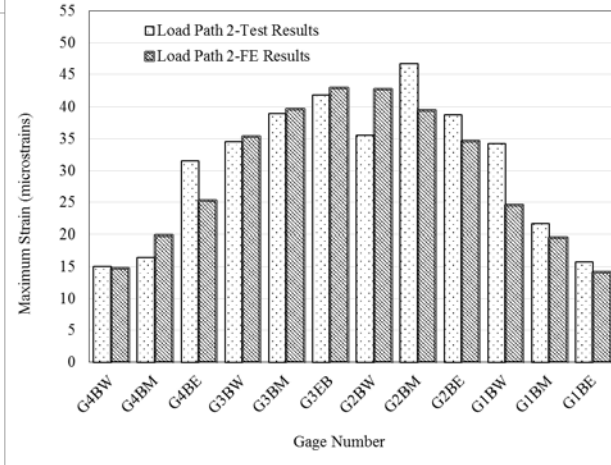


Figure 5.15. Comparisons of strain response in girder bottom flanges at mid-span for Load Path 3 of Test I – fixed support condition

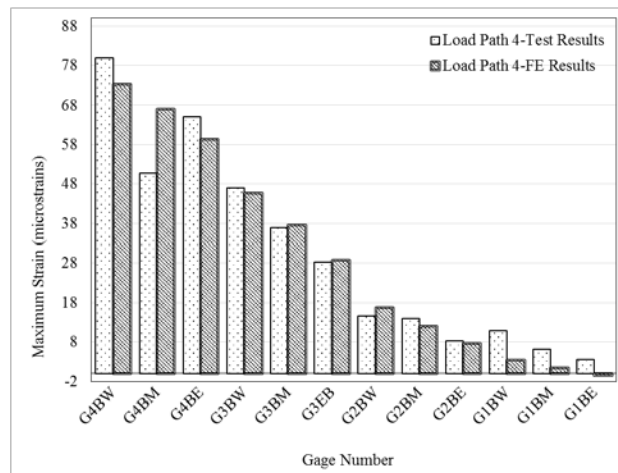
Figure 5.13 through Figure 5.15 indicate that the FE predictions are in good agreement with the test results for the four girders, which validates the assumption that significant support restraint exists in the end supports. The peak strains in all the strain gauges were always reached when the first axle of the truck was located at about 40 ft from the support. The peak strains from all strain gauges were further extracted from both the test and FE results for comparison purposes as shown in Figure 5.16.



(a) Load Path 1



(b) Load Path 2

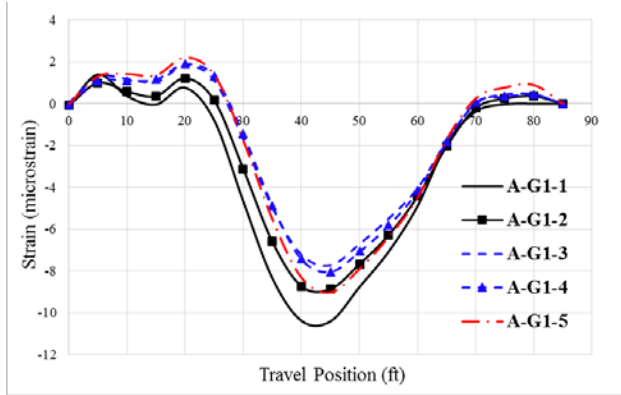


(c) Load Path 3

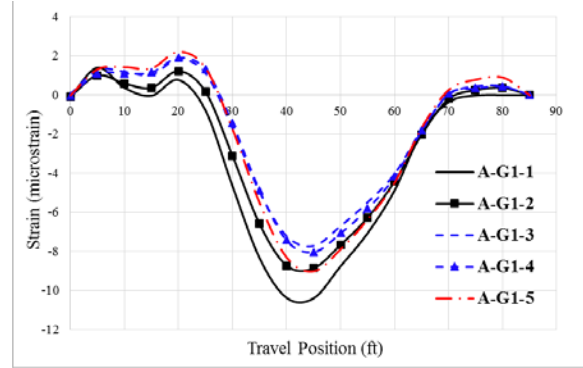
Figure 5.16. Comparisons of peak strains in girder bottom flanges at mid-span for three load paths of Test I – fixed support condition

This comparison indicates that the strain peaks were slightly under-estimated using the FE model compared with the test results. This is possibly due to the fact that the end supports are not fully under the fixed support condition (i.e., somewhere between the pinned and fixed support conditions).

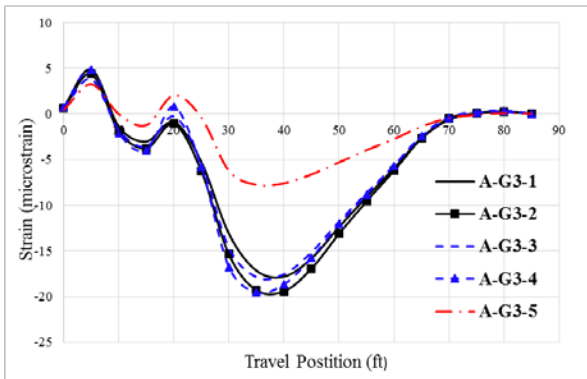
For Test II, the measured strain responses in the bottom flanges of the four girders at the abutment cross-section were plotted, as shown in Figure 5.17.



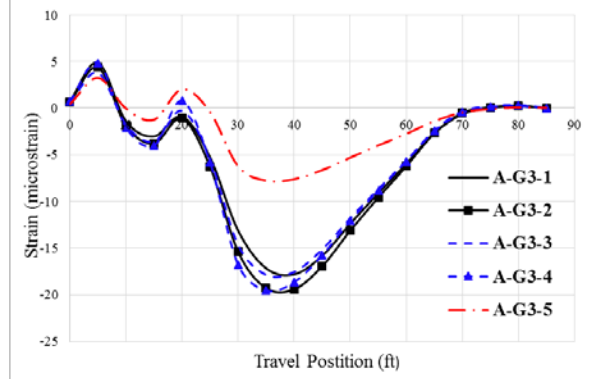
(a) Girder 1



(b) Girder 2



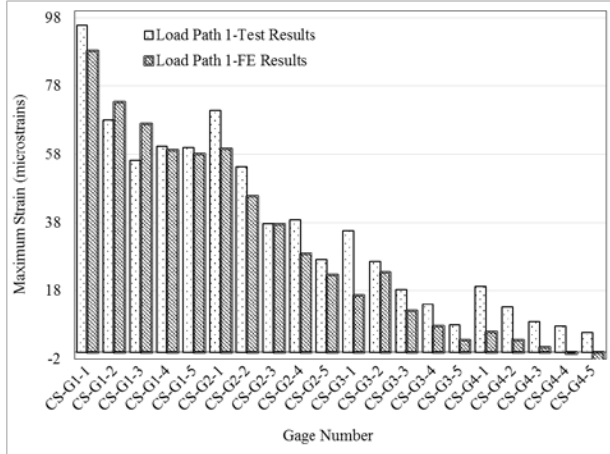
(c) Girder 3



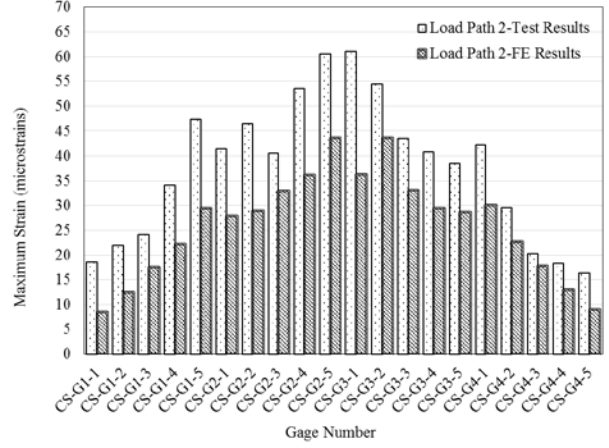
(d) Girder 4

Figure 5.17. Measured strain response in girder bottom flanges at abutment for Load Path 2 of Test II

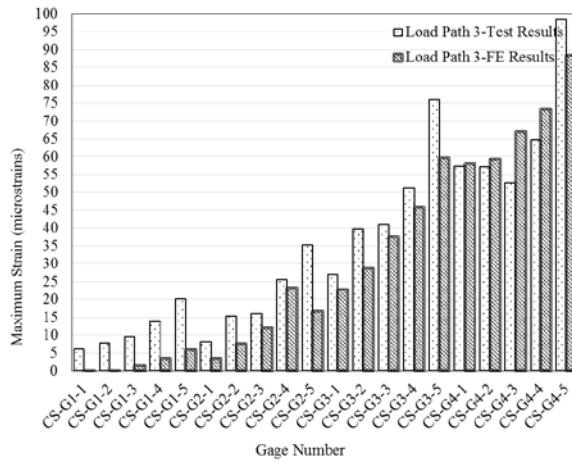
Figure 5.17 indicates that significant tensile strains were induced in the girder bottom flanges and that a negative moment was induced in each bridge end due to the restraint from the supports. The assumption that significant support restraint exists in the end supports is further confirmed. The peak strains from all strain gauges at the mid-span and abutment were further extracted from both the test and FE results for comparison purposes as shown in Figure 5.18 and Figure 5.19, respectively.



(a) Load Path 1

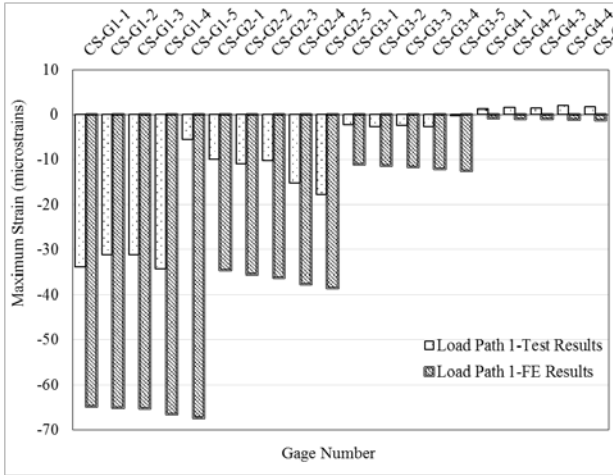


(b) Load Path 2

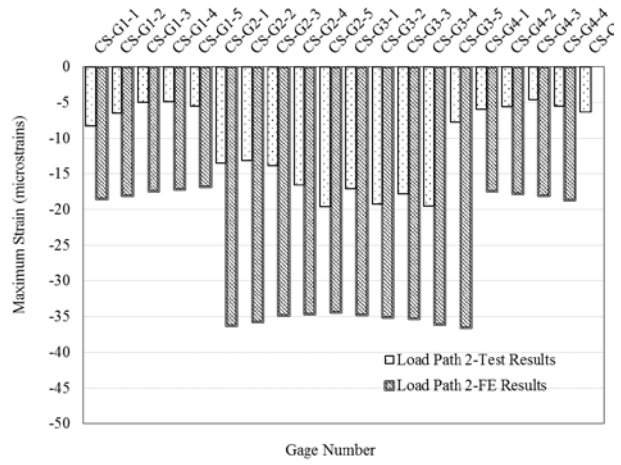


(c) Load Path 3

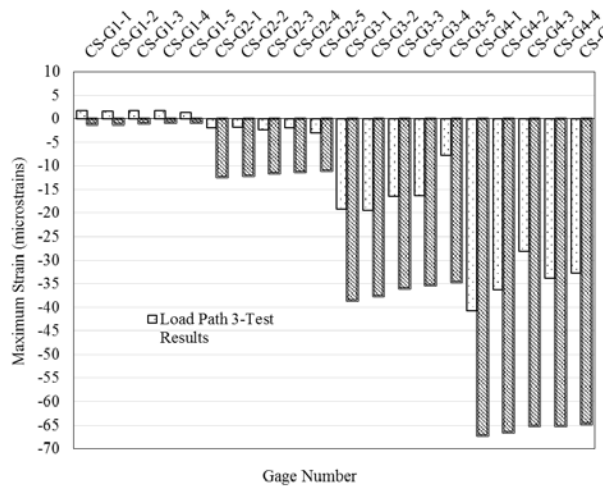
Figure 5.18. Comparisons of peak strains in girder bottom flanges at mid-span for three load paths of Test II



(a) Load Path 1



(b) Load Path 2



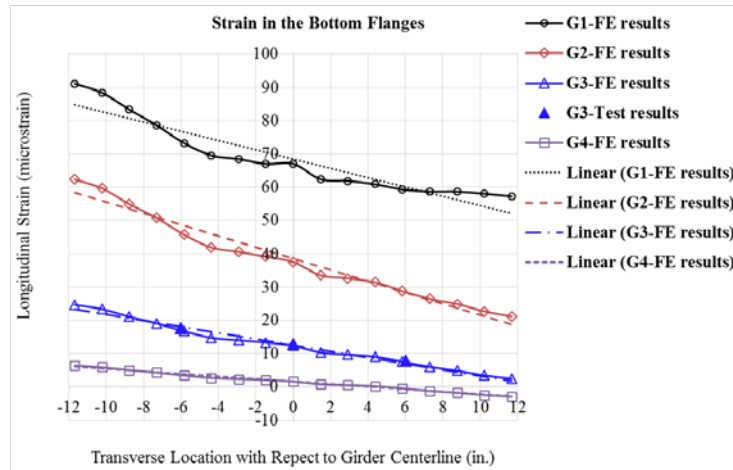
(c) Load Path 3

Figure 5.19. Comparisons of peak strains in girder bottom flanges at abutment for three load paths of Test II

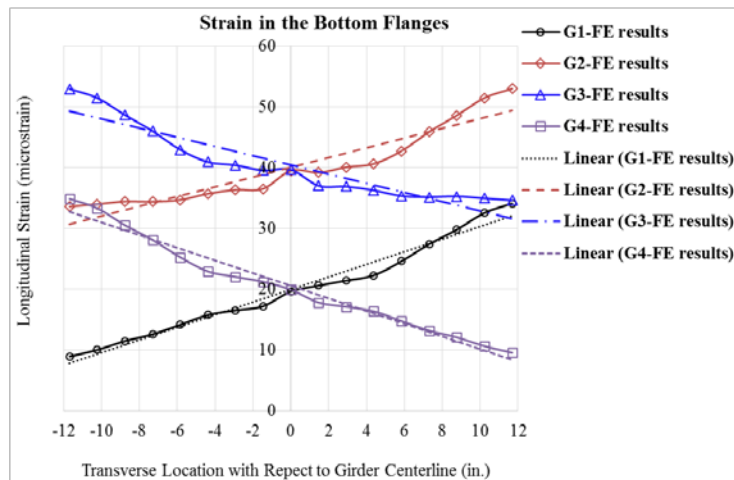
Figure 5.18 indicates that, for the mid-span cross-section, the strain peaks were slightly underestimated using the FE model compared with the test results; and Figure 5.19 indicates that, for the abutment cross-section, the strain peaks were over-estimated using the FE model compared with the test results. This further confirms that the end supports functioning between nominal pinned and fixed support conditions.

5.4.2 Strain Distribution in Bottom Flanges

Load Paths 1 and 2 of Test I were utilized to further investigate the strain distribution in the bottom flanges. The strains in different transverse locations with respect to the centerline of the bottom flanges due to Load Paths 1 and 2 are shown in Figure 5.20(a) and Figure 5.20(b), respectively.



(a) Load Path 1



(b) Load Path 2

Figure 5.20. Comparisons of strain response in girder bottom flanges of Test I for Load Paths 1 and 2

Figure 5.20 indicates that the strains in the bottom flanges almost linearly vary either from west to east or from east to west. However, the strains near the ends of the bottom flanges (i.e., the bottom corners of the cross-sections) are relatively higher than those predicted from the linear trend lines, as shown in Figure 5.20. This is mainly due to the shear lag effects in box girder cross-sections. The linear change trend in the strains is caused by the weak-axis bending. This phenomenon is further studied through extracting the forces and moments in the girders and bridges from the FE model as described subsequently.

Load Path 1 was further selected for the investigation of forces and moments in the bridge. The forces and moments in the bridge and different girders at the mid-span were extracted from the FE model and are summarized in Table 5.2.

Table 5.2. Forces and moments in bridge and girders at mid-span – Load Path 1

Forces	Bridge	G1	G2	G3	G4	Sum
FX (kips)	134	-143	111	151	15	134
FY (kips)	4734	2064	2619	49	3	4734
FZ (kips)	-506	-4971	616	3129	719	-506
MX (kip-ft)	237386	134496	76071	23738	3081	237386
MY (kip-ft)	160	29505	22220	13869	8003	73597
MZ (kip-ft)	-47847	-5061	-9512	-317	-131	-15020

F=force; M=moment; X, Y, and Z=coordinate directions

Note that forces in three dimensions (FX, FY, FZ) and the moment in the X-coordinate direction in the four girders were directly summed to derive the forces in the bridge as summarized in Table 5.2. The moments in the Y/Z-coordinate directions (MY, MZ) of the bridge were derived using Equations 5.7 and 5.8 from the forces and moments in the four girders as summarized in Table 5.3.

$$MX_{Bridge} = \sum_{i=1}^4 MX_i \quad (5.6)$$

$$MY_{Bridge} = \sum_{i=1}^4 (MY + FZ * X)_i \quad (5.7)$$

$$MZ_{Bridge} = \sum_{i=1}^4 (MZ + FY * X)_i \quad (5.8)$$

Table 5.3. Forces and moments in girders at mid-span in Y and Z coordinate directions – Load Path 1

Forces	G1	G2	G3	G4	Sum
FZ (kips)	-4,971	616	3,129	719	
X (ft)	11.3	3.8	-3.8	-11.3	
FZ×X (kip-ft)	-55,922	2,311	-11,734	-8,093	-73,437
MY+FY×X (kip-ft)	-26,417	24,531	2,136	-90	160
FY (kips)	2,064	2,619	49	3	
X (ft)	-11.3	-3.8	3.8	11.3	
FY×X (kip-ft)	-23,220	-9,819	183	29	-32,826
MZ+FY×X (kip-ft)	-28,281	-19,331	-133	-101	-47,847

F=force; M=moment; X, Y, and Z=coordinate directions

As shown in Table 5.2 and Table 5.3, the total forces and moments with respect to the bridge centerline derived from those in the four girders are equal to those in the bridge extracted from the FE model. The calculated results verify the accuracy of forces and moments in the bridge mid-span cross-section.

Table 5.2 indicates that the strong-axis bending moment greatly contributes to the stress/strain in the girders. Table 5.2 also indicates that the weak-axis bending moment is small in the bridge but large in individual girders. The weak-axis bending moments are the main causes of the linear changes in strains, as illustrated previously in Figure 5.20.

Additionally, Table 5.2 indicates that torsion exists in the full bridge cross-section and individual girders. The torsion is caused by the truck loads applied on the bridge side transversely for Load Path 1, which is a common phenomenon in box girder bridges. However, for Load Path 2, the loads were almost applied at the center region transversely, and the torsion is relatively small, as shown in Table 5.4.

Table 5.4. Forces and moments in bridge and girders at mid-span – Load Path 2

Forces	Bridge	G1	G2	G3	G4
FX (kips)	-1	-252	-165	158	257
FY (kips)	4,877	-22	2,493	2,444	-38
FZ (kips)	-316	2,540	-2,631	-2740	2,515
MX (kip-ft)	241,750	38,313	81,472	82,400	39,566
MY (kip-ft)	-12	-8,771	-9,817	9,262	8,637
MZ (kip-ft)	493	-5	2,048	-1,252	63

F=force; M=moment; X, Y, and Z=coordinate directions

5.4.3 Live Load Distribution Factor

The live LDF for each girder can be determined by:

$$LDF_i = \frac{L_i}{\sum_i L_i} \tag{5.9}$$

where, i = girder number, LDF_i = load distribution factor of girder I , and L_i = internal force (moment or shear) in girder i .

The transformed section properties of the folded plate girders with/without the deck were calculated as summarized in Table 5.5.

Table 5.5. Transformed section properties of folded plate girders of the tested bridge

Type of Section	Stiffness Ratio	Area (in²)	Moment of Inertia (in⁴)	Centroid Location (in.)	Section Modulus (in³)
Girder without deck	N/A	49.4	5,381	12.11	109
Interior girder with deck	6.5	167.1	19,853	26.12	760
Exterior girder with deck	6.5	176.9	20,232	26.45	765

Table 5.5 indicates that the section modulus of the interior girder with the deck is almost equal to that of the exterior girder with the deck. Accordingly, the moment LDF for each girder can also be determined by:

$$DF_i = \frac{\varepsilon_i}{\sum_i \varepsilon_i} \quad (5.10)$$

where, $\varepsilon_i [i = 1, 2, 3, 4]$ = longitudinal strain component.

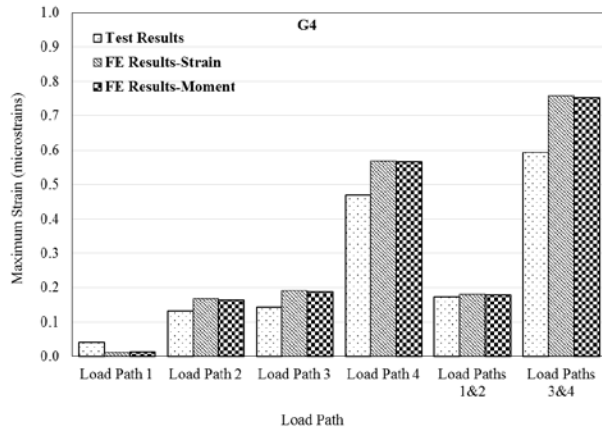
As mentioned previously, the strain in the bottom flange linearly varies from one side to the other due to the weak-axis bending. Accordingly, the longitudinal strain at the center of the bottom flange was utilized for moment LDF calculations. It should be noted that the moment LDFs using longitudinal strains were calculated based on the test data per Equation 5.10 and the moment LDFs using longitudinal strains and vertical bending moments were calculated based on the FE results per Equations 5.9 and 5.10, respectively.

For a concrete deck on multiple open steel box girders, the moment LDF of live loads for interior and exterior girders can be determined by (AASHTO 2010):

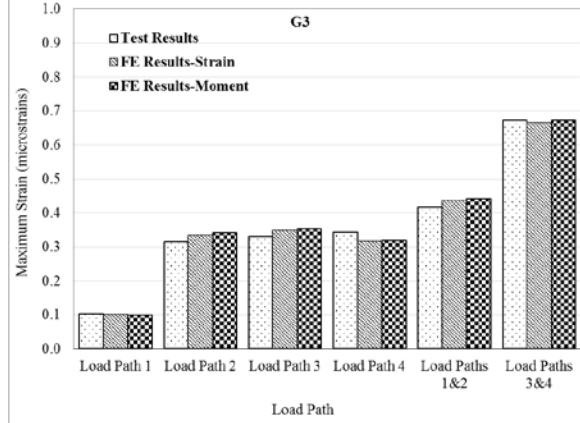
$$LDF = 0.05 + 0.85 \frac{N_L}{N_b} + \frac{0.425}{N_L} \quad (5.11)$$

where, N_L = number of lanes and N_b = number of girders.

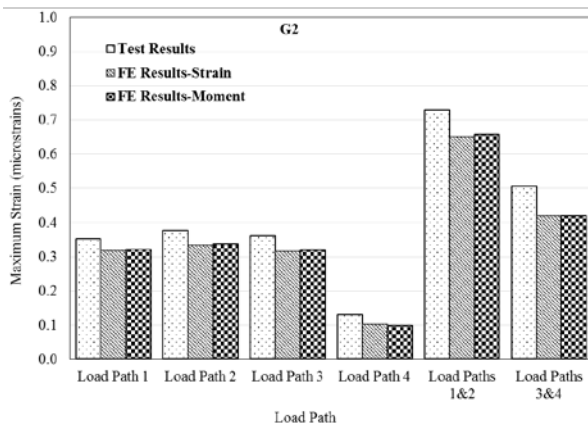
For Test I, moment LDFs derived based on the field testing and FE results for Load Paths 1–4, 1 and 2, and 3 and 4 and the four girders are illustrated in Figure 5.21.



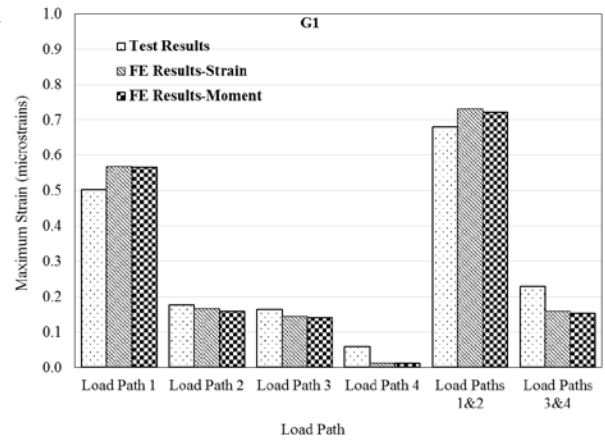
(a) Girder 4



(b) Girder 3



(c) Girder 2



(d) Girder 1

Figure 5.21. Comparisons of moment LDFs based on test and FE results – Test I

As shown in Figure 5.21, for Test I, the moment LDFs based on the strains from the FE model are almost identical to those based on moments from the FE model.

Accordingly, for Test II, moment LDFs were derived based only on the strain results (and not the moment results) from the FE models as shown in Figure 5.22.

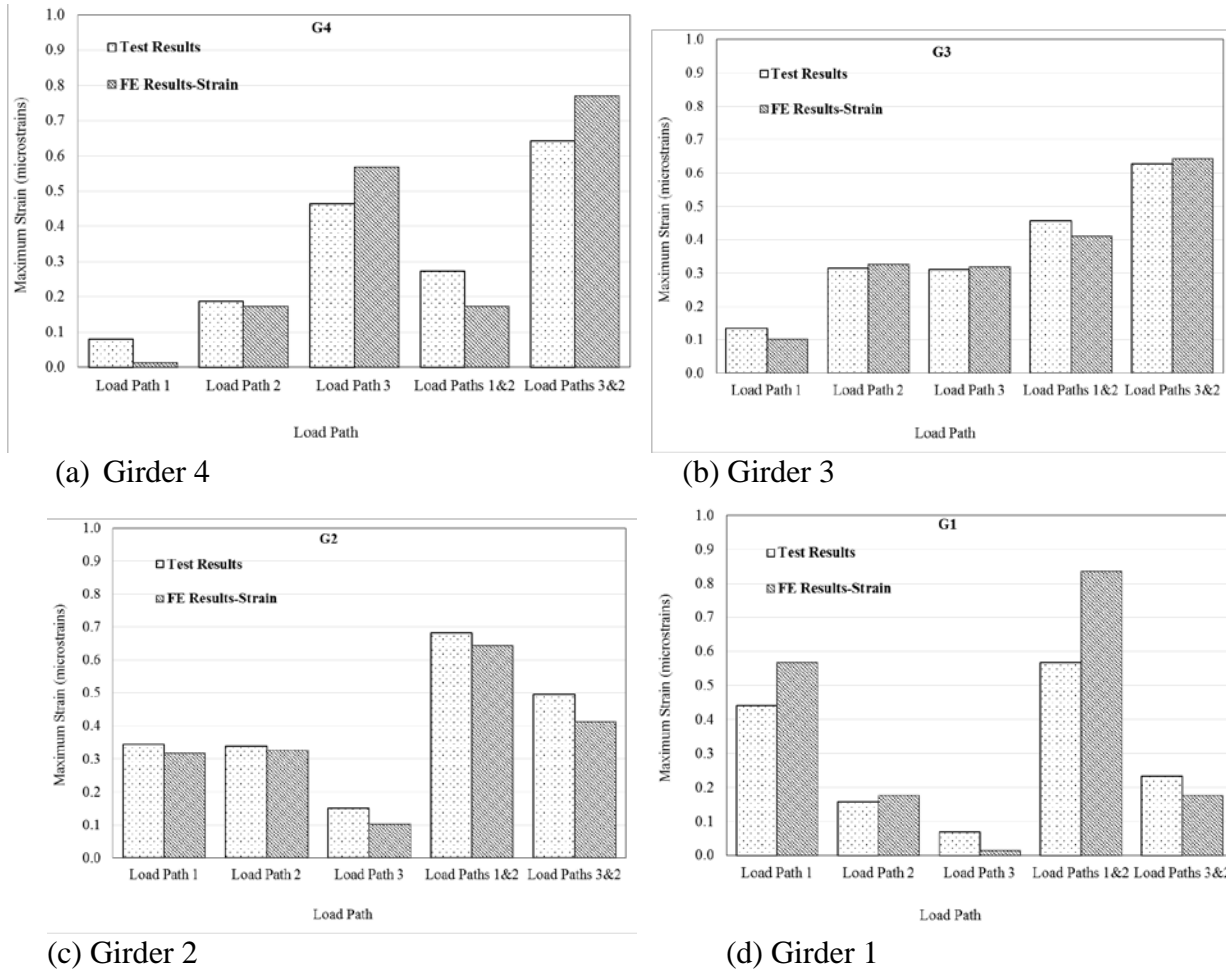
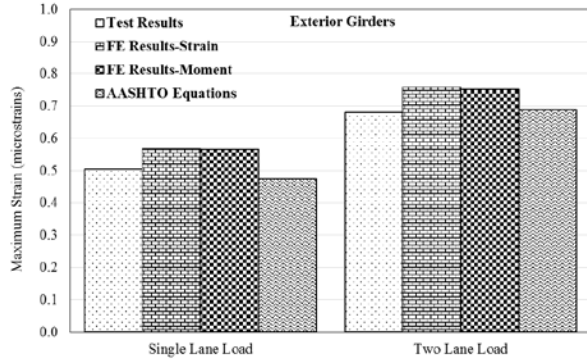
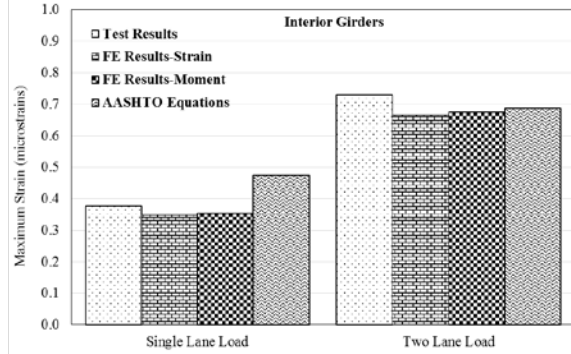


Figure 5.22. Comparisons of moment LDFs based on test and FE strain results – Test II

Figure 5.21 and Figure 5.22 indicate that the moment LDFs derived based on the FE results compare well with those calculated based on the test results. Furthermore, for Tests I and II, the moment LDFs for exterior and interior girders were summarized and compared with those calculated using the AASHTO equations, as illustrated in Figure 5.23 and Figure 5.24, respectively.

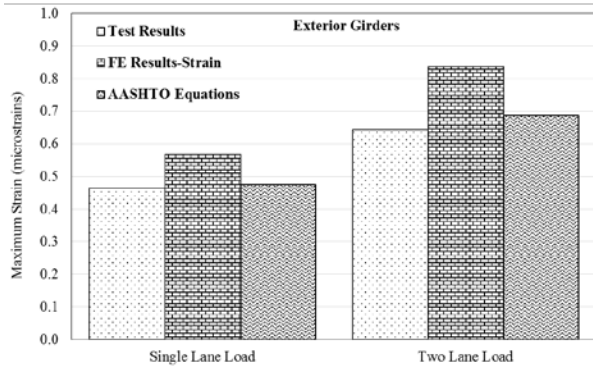


(a) Exterior girders

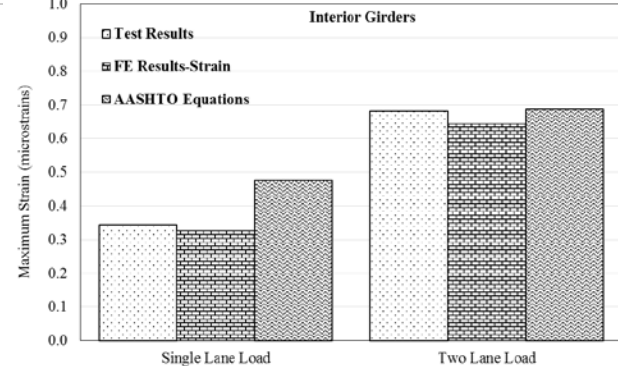


(b) Interior girders

Figure 5.23. Comparisons of calculated moment LDFs with those per AASHTO equations – Test I



(b) Exterior girders



(b) Interior girders

Figure 5.24. Comparisons of calculated moment LDFs with those per AASHTO equations – Test II

Figure 5.23 and Figure 5.24 indicate that AASHTO equations are either slightly conservative or un-conservative for single- and two-lane loading cases when compared with moment LDFs based on the test results. Figure 5.23 and Figure 5.24 also indicate that the AASHTO equations are either conservative or un-conservative for single- and two-lane loading cases when compared with moment LDFs that were derived based on the test results. When compared with moment LDFs derived from the FE results, AASHTO equations are un-conservative for the exterior girders and conservative for the interior girders as shown in Figure 5.23 and Figure 5.24. However, the differences between the moment LDFs per the test and FE results and those per the AASHTO equations are not significant, especially for the two-lane load case, which is the dominant case. In summary, the moment LDFs for the investigated bridge can be reasonably estimated using the AASHTO equations.

5.5 Field Test and Finite Element Modeling Summary and Conclusions

The researchers conducted two field tests on the Amish Sawmill Bridge, which was designed and constructed using four folded plate girders. Strains were measured on the folded plate girders during live load testing. In addition, full bridge FE models were established to interpret the field test results and further study the behavior of the bridge under the loading conditions tested.

The research team drew the following conclusions based on the field measured data and the predictions using the FE models:

- Due to the shear lag effects, the strains near the bottom corners of the bottom flanges are larger; due to the biaxial bending effects, strains in the bottom flanges vary from one side to the other.
- The GRS-IBS and abutments provide significant restraint to the girder ends. It was concluded that the end supports are under an intermediate support condition between the pinned and fixed support conditions.
- The strong-axis bending moment is the major contributor to the stress/strain in the girders. The weak-axis bending moment, which is small in the bridge but large in individual girders, causes the linear change trend of strains in the girder bottom flanges. Torsion exists in the full bridge cross-section and individual girders.
- Due to the biaxial bending moments in the folded plate girders, it is feasible to use the strain in the center of the girder bottom flanges to calculate LDFs.
- AASHTO equations were reasonably accurate at estimating the LDFs for interior and exterior girders of the investigated folded plate girder bridge.

CHAPTER 6 SUMMARY AND CONCLUSIONS

The Amish Sawmill Bridge was designed using folded plate girders and constructed on the secondary road system in Buchanan County, Iowa. This bridge utilizes a folded plate girder superstructure supported on GRS abutments. The researchers conducted laboratory and field testing with the goal of validating the adequacy of the folded plate girder for short-span bridge construction.

To evaluate the structural behavior of the folded plate girder, the researcher team conducted three laboratory tests on a folded plate girder specimen similar to the girders that were used on the completed bridge in Buchanan County.

For the first test (Test A – Constructability), the researchers tested a single folded plate girder under two-point bending to evaluate the behavior of the girder during construction prior to acting compositely with the deck. The girder was tested up to a moment that was equal to a moment that would be created by two times the girder's own self-weight.

For the second test (Test B – Flexure), a concrete deck was cast onto the folded plate girder that was used for Test A. The researchers then tested the specimen under two-point bending to determine the composite flexural behavior of the folded plate girder system in the elastic region.

For the last test (Test C – Shear), the research team tested the same folded plate girder with the CIP composite deck from Test B by loading the girder with a two-line load located close to one of the supports. This test was completed to study the shear behavior of the folded plate girder system and its ultimate capacity.

Laboratory testing results were as follows:

- For Test A, no noticeable, unwanted deformations or strain levels were found, and the strains and displacements were well predicted by the design calculations.
- For Test B, at the loads comparable to the design truck (HS-20) and the design truck (HS-20) plus lane load, no noticeable, unwanted deformations or strain levels were found, and measured strains and displacements were similar to the predictions from the design calculations. Strain in the girder bottom flange approached the yielding strain when the applied moment was much below the predicted yielding moment, and the measured displacements were much larger than the predictions.
- For Test C, the bent plate girder performed similarly to that of Test B in respect to predictions. In terms of the shear data, all of the shear strains for both the top and bottom gauge locations were much lower than predicted for the yield load. Due to the boundary conditions (the load points were relatively farther away from the support), the beam ultimately failed in flexure with the deck concrete crushing, which was consistent with the results based on hand calculations. Given this girder has two webs, and thus a large shear capacity, the shear strength of the folded plate girder when placed is not a point of concern with the bent plate girder's design.

The researchers conducted live load field tests immediately after completion of the bridge (Test I) and about one year after bridge construction (Test II) to evaluate the behavior of the bridge and its components. Strains were measured on the four folded plate girders during fielding testing. Full bridge FE models were established to interpret the test results and further study the behavior of the bridge under the loading conditions tested.

The researchers drew the following conclusions based on the field measured data and the predictions using the FE models:

- Due to the shear lag effects, the strains near the bottom corners of the bottom flanges are larger; due to the biaxial bending effects, strains in the bottom flanges vary from one side to the other.
- The GRS-IBS and abutments provide significant restraint to the girder ends. And, the end supports have restraint characteristics of an intermediate support condition, between the pinned and fixed support conditions.
- The strong-axis bending moment was the major contributor to the stress/strain in the girders. The weak-axis bending moment, which is small in the bridge but large in individual girders, causes a linear change in strains in the girder bottom flanges. Torsion exists in the full bridge cross-section and individual girders.
- Due to the biaxial bending moments in the folded plate girders, it is feasible to use the strain in the center of the girder bottom flanges to calculate live LDFs.
- AASHTO equations were reasonably accurate at estimating the LDFs for interior and exterior girders of the folded plate girder bridge.

In summary, based on the laboratory and field test results and FE simulation results, the researchers concluded that the folded plate girder is an effective alternative for construction of short-span bridges that are designed based on the AASHTO LRFD specifications for bridges.

REFERENCES

- AASHTO. 2012. *AASHTO LRFD Bridge Design Specifications* 6th Edition. American Association of State Highway and Transportation Officials, Washington, DC.
- AASHTO. 2010. *AASHTO LRFD Bridge Design Specifications*. 5th Edition, with 2010 interim revisions. American Association of State Highway and Transportation Officials, Washington, DC.
- ANSYS. 2011. *ANSYS FLUENT User's Guide*. Release 14.0, ANSYS, Inc., Canonsburg, PA.
- AISC. 2005. *Steel Construction Manual*, 13th Edition. American Institute of Steel Construction, Inc., Chicago, IL.
- Barth, K., J. Mash, G. Michaelson, M. Barker, and D. Snyder. 2013. Development of a Shallow Press-Brake Formed Tub Girder for Short-Span Steel Bridges. *Durability of Bridge Structures: Proceedings of the 7th New York City Bridge Conference*, August 26–27, New York, NY, pp. 87–98.
- Buchanan County, Iowa. No date. *Plans of Proposed Improvement on the Secondary Road System in Buchanan County: Folded Plate Steel Bridge*. Preliminary. FHWA # 84260. Iowa Department of Transportation Highway Division.
- Burgueño, R. and B. S. Pavlich. 2008. *Evaluation of Prefabricated Composite Steel Box Girder Systems for Rapid Bridge Construction*. Department of Civil and Environmental Engineering, Michigan State University, East Lansing, MI.
- Burner, K. 2010. Experimental Investigation of Folded Plate Girders and Slab Joints Used in Modular Construction, MS thesis. University of Nebraska, Lincoln, NE.
- Deng, Y. 2012. Efficient Prestressed Concrete-Steel Composite Girder for Medium-Span Bridges. PhD dissertation, University of Nebraska, Lincoln, NE.
- Deng, Y. and Morcouc, G. 2013. Efficient Prestressed Concrete-Steel Composite Girder for Medium-Span Bridges: II - Finite Element Analysis and Experimental Investigation. *Journal of Bridge Engineering*, Vol. 18, No.12, pp. 1358–1372.
- Deng, Y., T. R. Norton, and C. Y. Tuan. 2013. Numerical Analysis of Concrete-Filled Circular Steel Tubes. *Structures and Buildings*, Vol. 166, No. 1, pp. 3–14.
- Deng, Y., B. Phares, H. Dang, and J. Dahlberg. 2015. Impact of Concrete Deck Removal on Horizontal Shear Capacity of Shear Connections. *Journal of Bridge Engineering*, Vol. 21, No. 3.
- FHWA. 2016. Geosynthetic Reinforced Soil-Integrated Bridge System (GRS-IRS). Federal Highway Administration. www.fhwa.dot.gov/innovation/everydaycounts/edc-3/grs-ibs.cfm, last modified on January 29, 2016.
- Glaser, L. 2010. Constructability Testing of Folded Plate Girders. MS thesis. University of Nebraska, Lincoln, NE.
- Hognestad, E. 1951. *A Study of Combined Bending and Axial Load in Reinforced Concrete Members*. Bulletin Series No. 399, Bulletin No. 1, University of Illinois Engineering Experiment Station, University of Illinois, Urbana, Champaign, IL.
- Nakamura, S. 2002. Bending Behavior of Composite Girders with Cold Formed Steel U Section. *Journal of Structural Engineering*, Vol. 128, No. 2, pp. 1169–79.
- Ollgard, J. G., R. G. Slutter, and J. W. Fischer. 1971. Shear Strength of Stud Connectors in Lightweight and Normal Concrete. *AISC Engineering Journal*, Vol. 8, No. 2, pp. 55–64.
- Riley, W. F., L. D. Sturges., and D. H. Morris. 2007. *Mechanics of Materials, 6th Edition*. John Wiley and Sons, Inc., Hoboken, NJ.

Taly, N. and H. Gangarao. 1979. Prefabricated Press-Formed Steel T-Box Girder Bridge System.
Engineering Journal, Vol. 16, No. 3, pp. 75–83.